

# DEVELOPMENT OF A NOVEL MULTICHANNEL SEISMOCARDIOGRAPHY METHOD

by

Kim Munck Jeppesen



**AALBORG UNIVERSITY**  
STUDENT REPORT

Fall Semester 2016 and Spring semester 2017

**SIEMENS** | Fonden

# TITLE PAGE

**Department of Health  
Science and Technology**  
Aalborg University, Denmark  
<http://www.smh.aau.dk>



**AALBORG UNIVERSITY**  
STUDENT REPORT

**Title:**  
Development of a Novel Multichannel  
Seismocardiography Method

**Theme:**  
Applied biomedical  
engineering and informatics

**Project Period:**  
Fall Semester 2016 and Spring Semester 2017

**Project Group:**  
17gr10400

**Author:**  
Kim Munck Jeppesen

**Supervisors:**  
Samuel Emil Schmidt  
Johannes J Struijk  
Kasper Sørensen

**Date of Completion:**  
June 7, 2017

**Standard pages:**  
118 pages (2,400 characters incl. spaces).

© Copyright by Kim Munck Jeppesen

# DANSK RESUME

**Intro:** Ventrikel dyssynkroni er en abnormalitet i hjertets ventrikler, der gør at disse ikke kontraherer samtidigt. Denne forskudte kontraktion resulterer ofte i en nedsat pumpeevne, der leder til hjertesvigt. Man kan mindske dødeligheden ved hjertesvigtspatienter med ventrikel dyssynkroni ved at behandle med kardiell resynkroniseringsterapi (CRT), som involverer en biventrikulær pacemaker. De markører som i dag anvendes til identificering af hjertesvigt patienter, som ville gavne af behandlingen er i midlertidigt meget upræcise, med tilfælde på 30% hvor behandlingen ikke havde nogen effekt.

Seismokardiografi (SCG) er en målemetode som anvender accelerometer til at undersøge hvordan sammentrækningen af ventriklerne påvirker brystkassens bevægelser. Litteraturen har dog vist, at viden omkring placeringen af SCG's indflydelse på det målte signal er uvist. Denne tese foreslår derfor at udvikle, implementere og studere en ny metode til undersøgelse af multikanals seismokardiografi (mSCG) som en markør for ventrikel dyssynkroni hos hjertesvigtspatienter.

**Metode:** Den nye metode for mSCG blev designet og implementeret som et udstyr med 12 SCG kanaler, der kørte synkront med et ekg respirationsbælte, der overførte opsamlede målinger via tre programmerede mikrocontrollere til en computer, med et opsamlings program implementeret i projektet. Denne mSCG metode anvendte digitale MEMS accelerometer, som konverterede SCG signalet ved kilden og digitalt overførte målingerne via en BUS, i modsætning til andre SCG udstyr, som anvender analog MEMS accelerometer sammen med en fælles omformer.

Studiet inkluderede tre sunde forsøgspersoner som var lagt ned i en 10 minutter lang periode hvor mSCG, ekg og respiration blev opsamlet. De opsamlede mSCG blev filtreret i to bånd, for at kunne undersøge kræfterne tilstede på brystkassen, 0.5 Hz til 30 Hz, og hjertelyds energierne, 20 Hz til 250 Hz. Sammen med filtreringen blev en enkelt hjerte cyklus segmenteret, fra signalet og frem stillet ved at kortlægge signalet for mange tidspunkter i cyklussen. Kortlægningen blev udført med en 2D interpolation af kortene for at kunne fortolke dem. Kortene blev derefter opdelt i systolen og diastolen for og derefter blev mønstre identificeret mellem forsøgspersonerne.

**Resultat:** Indledende test af the implementerede metode til mSCG var udført. Her viste alle SCG kanaler at være synkron med en standard afvigelse på 140  $\mu$ s, og at være 8.9 ms forskudt fra ECG målingerne.

Ud fra kortene der beskrev kræfterne på brystkassen blev der fundet identiske mønstre for alle forsøgspersonerne som ikke kunne have været set uden mSCG. Disse mønstre involverede to modsat rettede kræfter som var til stede to gange under systolen og en gang under diastolen. Ved mønstre, som var tydelige på et traditionelt SCG, kunne mSCG desuden identificere lokationen af disse. Ud fra kortlægningen af hjertelydens energier, kunne disse lyde under nogle tilfælde adskilles, og for den første og anden hjertelyd blev det observeret, at den anden hjertelyd generelt lå højere end den første.

**Diskussion:** Kræfterne til stede på brystkassen, kan ud fra litteraturen spekuleres til at beskrive bestemte dele af hjertets bevægelse, men flere målinger med mSCG, der også involverer ekkokardiografi ville være nødvendige. Placeringen af anden hjertelyd i forhold til første hjertelyd, stemmer over ens med litteraturen. Yderligere signalbehandling kan blive foretaget på mSCG signaler, da for eksempel kun en af de 3-axes SCG signaler fra alle sensorer var anvendt i studiet. Desuden vil en tydeligere adskillelse af hjertelydende være mulig med multikanals komponentanalyse.

**Konklusion:** Denne 1-års tese inkluderer; ansøgning af midler, anmeldelse til etisk komité, udvikling og implementering af analoge samt digitale elementer i mSCG, udførelse af forsøg og signalbehandling som blandt andet involver avancerede præsentationsmetoder og identificering af mønstre.

Studiet ville ikke kunne besvare definitivt om hvor vidt metoden ville være en god markør for forudsigelse af CRT udfald, men mønstre i mSCG blev fundet som relaterede til ventrikelkontraktionen, og inkluderingen af CRT patienter vil muligvis vise værdien af mSCG som markør for ventrikel dyssynkroni.



# ACKNOWLEDGEMENTS

I would like to thank the Siemens foundation for granting the resources necessary to implement the novel method designed through this master thesis. I would also like to give special thanks to Jan Stavnsbøj, at Aalborg university at the Department of Health Science and Technology, for consultancy and assistance with the design and implementation of the equipment's electronics and 3D printing. Additional thanks are given to Knud Larsen, at Aalborg university at the Department of Health Science and Technology, for consultancy with programming the data acquisition software in LabView.



# TABLE OF CONTENTS

<b>CHAPTER 1. INTRODUCTION</b>	<b>10</b>
<b>CHAPTER 2. PROBLEM ANALYSIS</b>	<b>11</b>
2.1. VENTRICULAR DYSSYNCHRONY	12
2.1.1. TREATMENT	12
2.1.2. EXISTING MARKERS	13
2.2. SEISMOCARDIOGRAPHY	14
2.2.1. PAST	14
2.2.2. PRESENT	14
2.2.3. FUTURE	17
2.1. WHERE TO MEASURE	18
2.1.1. AUSCULTATORY AREAS	18
2.1.2. MEASURING SITES OF SCG	19
2.1.3. MULTIPLE MEASURING SITES	20
<b>CHAPTER 3. AIM</b>	<b>23</b>
3.1. PROBLEM FORMULATION	23
<b>CHAPTER 4. METHOD</b>	<b>24</b>
<b>CHAPTER 5. PILOT STUDY</b>	<b>25</b>
5.1. SPECTRAL CONTENT	25
5.2. SIGNAL NOISE	27
5.3. SIGNAL AMPLITUDES	29
5.4. RESULTS FROM THE PILOT STUDY	32
<b>CHAPTER 6. SYSTEM REQUIREMENTS</b>	<b>33</b>
6.1. STUDY SYSTEM REQUIREMENT	33
6.2. PATIENT/SUBJECT POINT OF VIEW	33
6.3. DATA ANALYST POINT OF VIEW	34
6.4. OPERATOR POINT OF VIEW	35
6.5. DOCTOR/PHYSICIAN POINT OF VIEW	35
6.6. PRIORITY OF SYSTEM SPECIFICATIONS	35
<b>CHAPTER 7. DESIGN</b>	<b>37</b>
7.1. SENSORS	38
7.1.1. CHOICE OF ACCELEROMETER	38
7.1.2. SYNCHRONOUS SAMPLING	40

7.1.3. COMMUNICATION	41
7.1.4. NOISE	43
7.1.5. MECHANICS OF SENSOR	44
7.1.6. DEBUGGING	45
<b>7.2. ELETROCARDIOGRAM</b>	<b>45</b>
<b>7.3. MICRO CONTROLLER</b>	<b>46</b>
<b>7.4. ACQUISITION SOFTWARE</b>	<b>48</b>
<b>CHAPTER 8. IMPLEMENTATION</b>	<b>49</b>
<b>8.1. IMPLEMENTATION OF SENSOR DESIGN</b>	<b>50</b>
8.1.1. DRAWING ELECTRICAL CIRCUITS	50
8.1.2. DRAWING THE PCB	53
8.1.3. ORDERING PCB PANELS AND SOLDER COMPONENTS	54
8.1.4. DRAWING AND ORDERING 3D PRINTED CASING	54
8.1.5. PROGRAMMING THE SENSOR	55
<b>8.1. IMPEMANTATION OF CENTRAL UNIT</b>	<b>56</b>
8.1.1. MASTER UNIT	58
8.1.2. $\mu$ C ELECTRICAL IMPLEMENTATION	59
8.1.3. USB HUB IMPLEMENTATION	60
8.1.4. IMPLEMENTATION OF THE ADS1298ECGFE-PDK	60
8.1.5. IMPLEMENTATION OF SUPPORT CIRCUITS	61
<b>8.2. IMPLEMENTATION OF THE <math>\mu</math>C PROGRAM</b>	<b>62</b>
<b>8.3. IMPLEMENTATION OF THE ACQUISITION SOFTWARE</b>	<b>67</b>
<b>CHAPTER 9. TEST PROTOCOL</b>	<b>70</b>
<b>9.1. SYNCHRONIZATION EXPERIMENT</b>	<b>70</b>
<b>9.2. SIGNAL CHARACTERISTICS INVESTIGATION</b>	<b>71</b>
<b>CHAPTER 10. STUDY DESIGN</b>	<b>72</b>
<b>10.1. PURPOSE</b>	<b>72</b>
<b>10.2. SUBJECTS</b>	<b>72</b>
<b>10.3. DESIGN AND METHODS</b>	<b>72</b>
<b>CHAPTER 11. DATA PROCESSING</b>	<b>74</b>
<b>11.1. ENERGY MAPPING</b>	<b>75</b>
<b>11.2. FORCE MAPPING</b>	<b>75</b>
<b>CHAPTER 12. RESULTS</b>	<b>76</b>
<b>12.1. RESULTS FROM THE SYNCHRONIZATION EXPERIMENT</b>	<b>76</b>
<b>12.1. RESULT FROM SIGNAL CHARACTERISTICS INVESTIGATION</b>	<b>77</b>
<b>12.2. HEART SOUND SIGNALS</b>	<b>78</b>

12.2.1. ENERGY MAPPING DURING SYSTOLE	79
12.2.2. ENERGY MAPPING DURING DIASTOLE	81
<b>12.3. SCG SIGNALS</b>	<b>83</b>
12.3.1. FORCE MAPPING DURING SYSTOLE	84
12.3.2. FORCE MAPPING DURING DIASTOLE	87
<b>CHAPTER 13. DISCUSSION</b>	<b>89</b>
<hr/>	
<b>CHAPTER 14. CONCLUSION</b>	<b>91</b>
<hr/>	
<b>APPENDICE</b>	<b>95</b>
<hr/>	

# CHAPTER 1. INTRODUCTION

The number of heart failure patients in the western world has been increasing the past three centuries. It is estimated that in Denmark alone, there are 60,000 patients with chronic heart failure and a similar number with reduced cardiac function without the clinical symptoms of heart failure. Moreover, it is estimated that 20,000 new heart failure cases occur yearly in Denmark. The high incidence of chronic heart failure is mainly due to a combination of an aging population and an improvement to the survival rates for acute myocardial infarction, where heart failure is one of the known sequela. Danish numbers show a 1-year mortality rate of 20%, after the heart failure diagnose. (Dansk Cardiologisk Selskab 2007)

Ventricular dyssynchrony is a heart condition where the timing of the contractions of the ventricles are delayed and lacks synchrony. Ventricular dyssynchrony often leads to reduced cardiac efficiency that can be caused by large differences in the timing of the contractions. This reduced cardiac efficiency may lead to heart failure symptoms. (Nagueh 2008)

Treatment of heart failure should, according to ACC/AHA, be treated by pharmaceuticals or Cardiac Resynchronizations Therapy (CRT), depending on the presence of ventricular dyssynchrony (American Heart Association 2014). There are different types of markers which are used for estimating which treatment will have the best prognosis (American Heart Association 2014).

To predict the CRT response, markers such as Left Ventricular Ejection Fraction (LVEF), QRS interval and the New York Heart Association (NYHA) Functional Classification are used. However, studies have shown that the QRS interval has proven to be a poor indicator to predict the CRT response (Bleeker et al. 2004; Yu et al. 2003). These studies have shown that 20 to 30 percent of patients, that were treated according to the markers, did not benefit from the CRT, and that some patients without all the markers did benefit from a CRT treatment (DeMaria & Blanchard 2008).

New markers have proven useful in diagnosing ventricular dyssynchrony. These markers include advanced echocardiographic techniques, such as Tissue Doppler Imaging (TDI), and conductance catheter techniques. TDI is an echocardiography technic that can be used to measure the movements of the two ventricle walls, and the conductance catheter technique is an invasive method to measure the ventricular volume accurately. (Bleeker et al. 2006)

Seismocardiography (SCG) is an inexpensive, non-invasive method used to investigate how the forces of the heart is projected onto the chest surface by the use of accelerometers (Inan et al. 2015). We propose that these forces measured by the SCG could be a suited and inexpensive marker to determine the timing of the ventricles mechanical contractions. This could potentially make the SCG method useful when detecting ventricular dyssynchrony and predicting the CRT response.

## **Initiating problem:**

How can seismocardiography be a useful marker for ventricular dyssynchrony?

## CHAPTER 2. PROBLEM ANALYSIS

The problem analysis was composed of four sections.

The first section further investigated the problem related to ventricular dyssynchrony in relation to diagnosis, treatment, and pathological behavior.

The second section investigated seismocardiography (SCG) by dividing the analysis into a past, present and future focusses, derived from the literature.

As an outcome of the analyses related to ventricular dyssynchrony and seismocardiography, the third section focus on which measuring sites SCG would be most suited for the studying ventricular dyssynchrony.

## 2.1. VENTRICULAR DYSSYNCHRONY

Ventricular dyssynchrony is caused by irregular electrical impulses that results in the ventricles contracting out of sync. This limits the ventricles from properly emptying with blood to achieve cardiac efficiency, and causes the heart to dysfunction. This condition is a common cause of heart failure. Ventricular dyssynchrony is often caused by Left Bundle Branch Block (LBBB), but can also be caused by dilated cardiomyopathy.

As illustrated by Figure 1, a LBBB would affect the QRS duration, due to the delayed action potential from the bundle branch to the left ventricle. This delayed contraction of the left ventricle would over longer periods lead to myocardium remodeling, which would worsen the ventricular dyssynchrony, and cause a vicious cycle if not treated correctly.

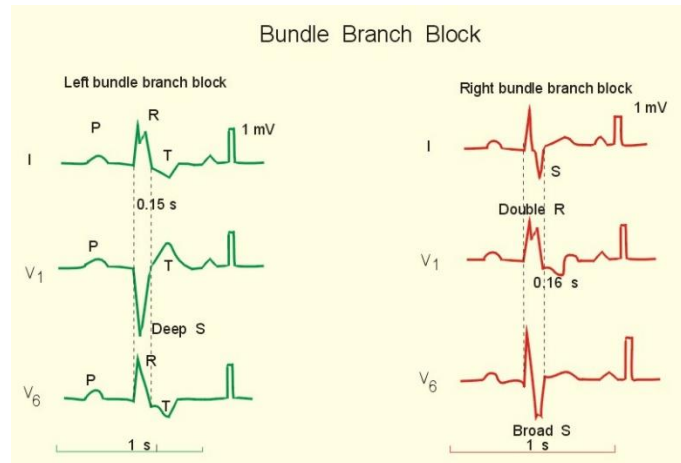


Figure 1 Illustration of how bundle branch block effects the ECG and the QRS duration. Illustration is from (Paulev & Zubieta-Calleja 2017)

### 2.1.1. TREATMENT

According to three larger randomized studies, the treatment of heart failure patient with CRT, that meets the marker guidelines set by the ACC/AHA, still received a significantly better symptoms improvement and reduction in their morbidity rate (Abraham et al. 2002; Erdmann et al. 2005; Krueger et al. 2004).

When the markers are meet a CRT is implanted as illustrated by Figure 2. The initial CRT units was a combination of biventricular pacing with a right atrial lead for both pacing and sensing. The CRT would pace both ventricles the achieve synchronicity for every heartbeat. The pacing is controlled by the sensing atrial lead and the delay between sensing and pacing is adjusted based on echocardiography or on the patient's PR interval on the ECG. (Gottdiener 2004)

Optimal programming of the CRT however, requires expertise to achieve optimal function and god response for the CRT (Burri et al. 2006).As mentioned before bad response of the CRT have been proven to be related to the QRS duration being used as a marker for ventricular dyssynchrony.

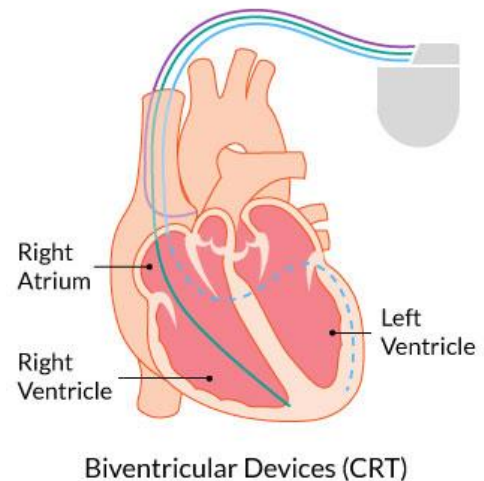


Figure 2 Illustration of a how a Cardiac Resynchronization Therapy unit would be implanted in a patient. Illustration is from Ted Rogers Centre for Heart Research 2017

### 2.1.2. EXISTING MARKERS

Current markers approved by ACC/AHA are subjects that stay in the NYHA III or IV regardless of an optimal medical treatment, QRS duration  $> 120$  ms, and LVEF  $< 35\%$  (American Heart Association 2014). However, the QRS duration has been proven to be a poor marker for predicting the CRT response (DeMaria & Blanchard 2008).

Other markers have been investigated using echocardiography techniques, such as TDI which measures the mechanical movement of the left ventricular wall and the septum. Figure 3 illustrates this. Here the velocity measurements of the septal and lateral-wall are charted to investigate the synchronicity of the walls. (Bleeker et al. 2005)

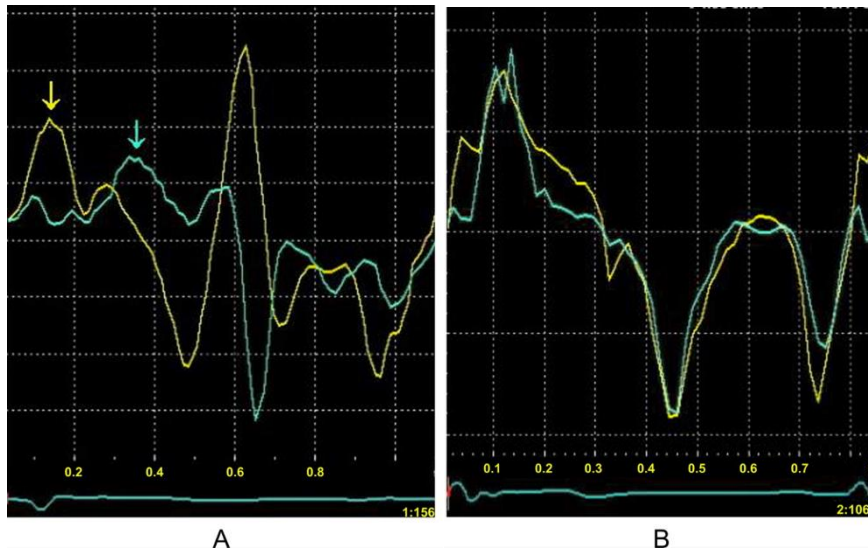


Figure 3 Illustration of the Tissue Doppler Imaging where velocity measurement was shown from the septum (yellow curve) and the lateral left ventricle wall (green curve). The bottom graph is the ECG II lead. Time is on the x-axis, relative to the R-peak, and the velocity of the walls are in the y-axis. Panel A is from a patient with dilated cardiomyopathy, where the septal-to-lateral delay is 250 ms with indicate ventricular dyssynchrony. Panel B is from a healthy subject without ventricular dyssynchrony. Illustration were from (Bleeker et al. 2005)

Chung et al. 2008 investigate how well 12 echocardiographic parameters of dyssynchrony might predict CRT outcomes better than current standards on 498 patients with CRT. According to this study the sensitivity and specificity did not change significantly, enough to recommend changing the guidelines. Efforts that may reduce the variabilities associated with interpretation and operator factors may improve the prediction abilities. (Chung et al. 2008)

## **2.2. SEISMOCARDIOGRAPHY**

This section will be separated into three minor sections; the Past will investigate what SCG is and where it originates from; the Present will investigate how the measuring technics of SCG have changed and what the literature knows of how to interpret SCG; and the future will investigate what the literature suggest future works should focus further on in the fields of SCG.

### **2.2.1. PAST**

SCG was first mentioned in 1961 (BOZHENKO 1961) where researchers started investigating this new method by looking at vibrations produced by the heart. SCG is a method where accelerometers are used to measure how the chest move as a reaction to the forces applied by the heart. The only accelerometers available where piezoelectric accelerometers that weighed more than 1 kilogram and was relatively expensive.

SCG is measurements of the chest vibrations coming from the contraction and ejection of blood by the ventricles (Inan et al. 2015). According to Zanetti & Tavakolian 2013 the primary cause of the SCG is due to the interaction between the epicardium and the thorax.

The terms of measuring on these low frequency movements of the chest area have been given many descriptions dependent on their quantity (acceleration, velocity or displacement) and the measuring sites (Inan et al. 2015). Some of the terms used for these low-frequency signals are seismocardiography (SCG), apexcardiography, kinectocardiography, cardiokymocardiography and ballistocardiography (BCG). (Castiglioni et al. 2007)

### **2.2.2. PRESENT**

Different from the pioneers on modern SCG (Salerno et al. 1991; BOZHENKO 1961), which used some heavy and bulky accelerometers, recent research has been based on using lighter accelerometers with similar performance characteristics. These sensors are called Micro Electro-Mechanical Systems (MEMS) accelerometers. (Zanetti & Tavakolian 2013)

These new types of sensors made it possible for average researchers to get involved and to study how different positions of the body or the sensors would affect the measurements, due to them being relatively inexpensive and low weight (Di Rienzo et al. 2013).

In the literature, different types of MEMS accelerometers have been used when capturing SCG, as listed by Table 1.

*Table 1 List of the literature found that used MEMS accelerometers for measuring seismocardiography, along with the relevant specification of the used accelerometers*

Study	Accelerometer model	Frequency response [Hz]	Range [g]	Noise [ $\frac{\mu g}{\sqrt{Hz}}$ ]	Axis
(Paukkunen et al. 2016)	SCA610-C21H1 A	20 to 70 (true DC)	$\pm 1$ g	30	Z
(Wick et al. 2012)	ADXL327	0.5 to 550	$\pm 2$ g	250	XYZ
(Di Rienzo et al. 2013)	LIS3LV02DL	? to 640	$\pm 2$ g / $\pm 6$ g		XYZ
(Pandia et al. 2012)	LIS3L02AL	0 to 1500	$\pm 2$ g	50	XYZ
(Nguyen et al. 2012; Jafari Tadi et al. 2014b)	MMA8451Q	1.56 to 400	$\pm 2$ g / $\pm 4$ g / $\pm 8$ g	126	XYZ
(Schmidt et al. 2014)	1521L-002	0 to 400	$\pm 2$ g	5	Z
(Ramos-castro et al. 2012)	ADXL330	0.5 to 550	$\pm 3$ g	350	XYZ

Based on the literature research on accelerometers, both analog MEMS and digital MEMS has been implemented. Typically ranges of  $\pm 1$  g to  $\pm 3$  g is used. The most common frequency response is below 1.5 Hz and higher than 400 Hz, and single axis MEMS is typically more noise suppressing.

From the review, it was found that the SCG acquisition setup had a resolution varying from 2 mg/LSB down to 70  $\mu$ g/LSB and that the temporal resolution was between 200 Hz to 10 kHz.

When relating the knowledge about the frequency responses and signals obtainable from the chest it is revealed that the accelerometer would be able to acquire very low frequency signals without disrupting the signal, but would not be suited for measuring the higher frequency signals dependent on the type of MEMS accelerometer.

The 0 Hz signal from all three axes contains information about the orientation of the accelerometer in relation to the earth. The frequency component below 5 Hz contains information about the respiration (Jafari Tadi et al. 2014a; Pandia et al. 2012)

The interval from 0.6 Hz to 20 Hz contains the SCG signal that contains information about the contraction of the ventricles (Castiglioni et al. 2007). The sound produced when the heart valve closes can be heard from 20 Hz to 120 Hz (Castiglioni et al. 2007). Murmurs, caused by blood flow irregularities in the heart, could also potentially be collected with accelerometers in a frequency band below 1 kHz.

How the literature denotes the SCG signals is illustrated by Figure 4, in a modified Wiggers diagram to relate the signal to other modalities. A positive SCG signal would indicate that a force in the anterior direction is being applied to the chest by the heart, and a negative SCG signal would indicate a force in the posterior direction.

A SCG signal is composed of several reoccurring waveforms that have distinct systolic and diastolic components (Paukkunen 2014). Some of these components occurs with other modalities distinct features, and the SCG signal could then be described as follows:

Starting from the P wave of the ECG lead II and SCG signal would have a positive wave followed by a negative wave during the QR interval. Shortly after the R-peak the S1 heart sound could be heard on a phonocardiogram (PCG) at the same time as the SCG signal would have a positive peak. This was interpreted as the mitral valve closing. Then the SCG signal would have a high positive peak, which would be interpreted as the aortic valve opening. Then the ventricles would empty until shortly after the T wave where the aortic valve would close, and the second heart sound would appear on the PCG. (Paukkunen 2014)

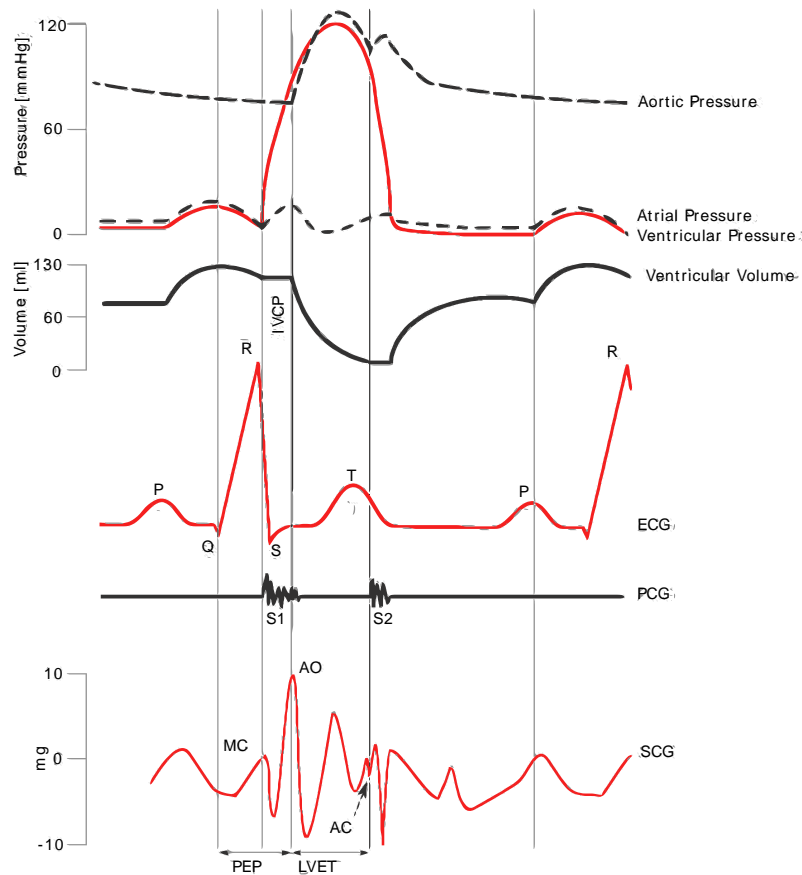


Figure 4 Wiggers Diagram Amended with SCG (Zanetti & Tavakolian 2013). A Wiggers Diagram consist of alignment of different modalities for cardiac activity. Here an example of a healthy subject is illustrated with the modalities of; pressure in the aortic, atrial and ventricles, volume of ventricle, electrocardiogram (ECG), phonocardiography and seismocardiography (SCG). The figure is denoted with the pre-ejection period (PEP), the isovolumic contraction period (IVCP), and the left ventricular ejection time (LVET). The SCG is denoted with the mitral valve closure (MC), aortic valve opening, and aortic valve closing.

### 2.2.3. FUTURE

Some of the leading researchers have in their recent publications discussed future work that would be useful for any further work with SCG:

Inan et al. 2015 lists the open issues found in the SCG and BCG literature. There is a need for further standardization of; how SCG and BCG signals are defined and how they are different, what nomenclature use for defining peaks and valleys, and how measuring site, sensor characteristics and sensor orientations are denoted by the literature for comparison across studies. Apart from the standardization issues, a list of six open issues that may improve understanding of SCG and BCG (Inan et al. 2015):

1. The biological meaning and clinical relevance of deflections in SCG and BCG
2. Common features of the SCG and BCG
3. Parameters derivable from the SCG 3D curvature and BCG
4. How respiration, posture, right ventricle, and sensor adherence effect the signal quality
5. SCG and BCG in relation to clinical practice
6. Reference values for healthy and diseased subjects for SCG and BCG, and for a different body types and ages

Apart from the open issues some areas for future work was specified. SCG and BCG show potential for out-of-hospital monitoring due to it being simple and inexpensive. However, the physiological origin of SCG and BCG must be studied further. By mapping SCG and BCG to each measurement modality, through mechanical and cardiovascular modeling, different measuring technics can be compared. An open database of SCG and BCG signals, along with processing tools, and microprocessor code needs to be made available to expand the amount of researcher working on this field and to develop SCG and BCG into an established technique, useful in clinical practice. (Inan et al. 2015)

Zanetti & Tavakolian 2013 have discussed the strength and weaknesses of SCG. Some of the strengths of SCG is the low-cost, that it is easily accessible, easy to reproduce, the possibility of automated analysis system like that of ECG diagnostics, had potential for integration with 12-lead ECG to provide additional knowledge and the potential for a new imaging modality based on SCG measurements from different sites to map the acceleration of the chest. Some of the weaknesses is the SCG signal is difficult to interpret visually, the technology had a long history making it an already old technology, and was still in the early development stages. (Zanetti & Tavakolian 2013)

Wick et al. 2012 also discusses the implementation of multiple SCG signals to permit the evaluation of a 3D motion of the heart.

Schmidt et al. 2014 discussed that work on defining a robust and standardized method for placing the accelerometers. The study also stated the 3D curvature measurements needed to have its clinical relevance investigated further.

Paukkunen 2014 also discussed that SCG was useful with out-of-hospital monitoring. Investigating what new information the SCG contributes with to the ECG signal might also be of interest, as reported by Kaminska et al. 2007. Further studies should be done on 3-D axis SCG and the difference of the signal in relation to supine and sitting, and the additional knowledge the extra axis contributes with. Studying the inter-subject variation of SCG would be necessary for better understanding of the physiology behind the variation. (Paukkunen 2014)

## 2.1. WHERE TO MEASURE

From the analysis of ventricular dyssynchrony it was found that a change in the timing of the ventricles contraction timing would result in a reduced cardiac efficiency and thereby heart failure.

From the analysis of seismocardiography it was found by the literature that there was a relation between features of the SCG signal and the contraction of the ventricles. However, the literature states a further understanding of the measuring sites was needed, both, to better understand the behavior of the SCG signal, but also in relation to information obtainable about the ventricle contractions.

This section then investigates the literatures understanding of measuring any type of movements of the chest caused by the heart, in three minor sections. The first minor section analysis the medical determined knowledge, followed by investigating what sites were used for SCG measuring seen in the literature, and in the last minor section, an investigating of how other studies had used multiple measuring sites to measure the movement of the chest.

### 2.1.1. AUSCULTATORY AREAS

When doctors and physicians use a stethoscope to listen for the vibrations from the heart valves closing, they use the established auscultatory areas. The auscultatory areas is where the heart sound belonging to the individual valves are best separated from each other, as illustrated by *Figure 5*. (Pelech 2004)

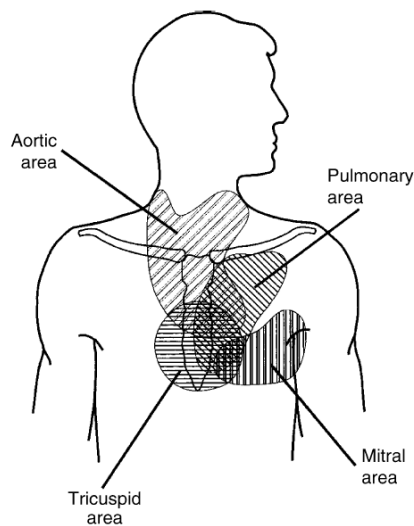


*Figure 5 The four primary auscultatory areas when listening for heart sounds and murmurs. The areas are defined as where sounds related to the four valves are best heard and defined (Pelech 2004)*

### 2.1.2. MEASURING SITES OF SCG

Investigating where the literature places the SCG sensors when measuring, might reveal what attributes the different sites have.

Studies that have investigated SCG have obtained the signals by placing accelerometers on different locations of the chest area, as illustrated by Figure 7. Commonly the accelerometer is placed on the xiphoid process due to the older type of accelerometers was heavy and could only be placed there for practical reasons (Inan et al. 2015). With the smaller and lighter MEMS accelerometers, a larger selection of placement sites is possible and are therefore selected dependent on the purpose of the acquired SCG signal. Studies have shown that by placing the accelerometer on the left side of the sternum, grants a SCG signal with better information about the S2 heart sound (Jain et al. 2016), which fits with the knowledge about the auscultation area.

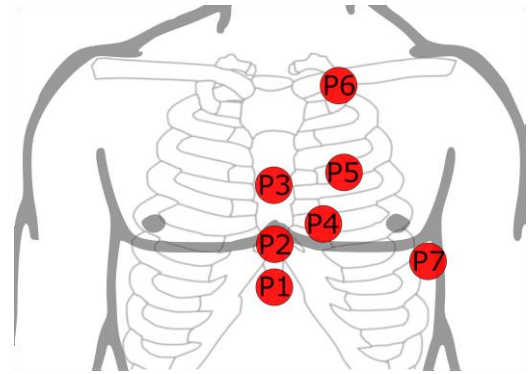


Figure 6 Placement of SCG measurements done by various studies from the found literature

During acquisition of the SCG signal in the reviewed studies, different positions of the subjects also have been investigated, due to how this changes the hearts sound and noise conditions of the accelerometers. Most studies measure on subjects in a supine position. The studies, that also included other positions, found out that additional motion artefact was added.

Table 2 Studies from the literature review of studies that measured seismocardiography with MEMS accelerometers along with the orientation of the subjects, number of subjects participated and the measuring sites of the SCG signal with Figure 6 as reference.

Study	Measuring sites	Subject orientation	Number of subjects
(Laurin et al. 2016)	P1	Supine	18
(Paukkunen et al. 2016)	P2	Supine	13
(Jain et al. 2016)	P4	Standing	5
(Wick et al. 2015)	P1	Supine	7
(Di Rienzo et al. 2013)	P1	Standing Supine	1
(Jafari Tadi et al. 2014b)	P2	Supine	10
(Tavakolian et al. 2013)	P1	Supine	142
(Pandia et al. 2012)	P5	Sitting	18
(Wick et al. 2012)	P7	Sitting	2
(Ramos-castro et al. 2012)	P3	Supine	12
(Nguyen et al. 2012)	P5	Supine	1
(Castiglioni et al. 2007)	P6	Standing Supine	1

### 2.1.3. MULTIPLE MEASURING SITES

Over the years different measuring technics have been used to measure the movement of the chest, which have had different advantages and disadvantages, then the SCG method with accelerometers.

However, some of these technics have been used to measure on multiple sites for better understanding the movements of the complete chest area. By considering what these studies found, better understanding of how the SCG behaves would be possible.

Some studies focus on only measuring from the front while others include measurements from the back. These studies use different technologies for measuring the vibrations and different measuring sites. A list of these studies conducting multiple sites measurements of chest movements are listed in *Table 3*.

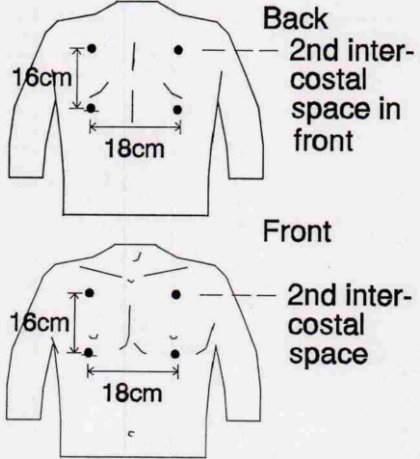
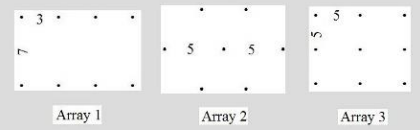
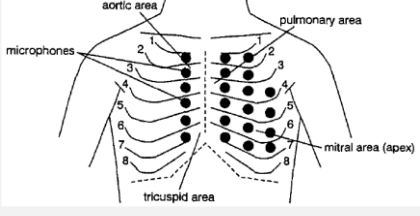
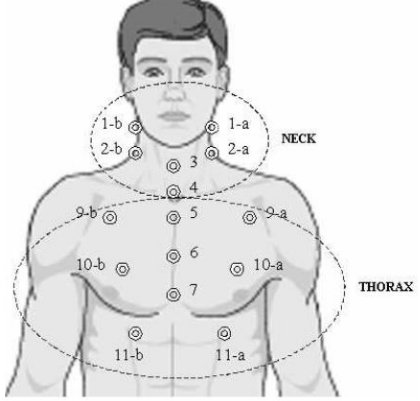
*Table 3 List of studies conducting multiple site measurements along with notation on their measuring technology, number of measuring sites used, if it was measured on front or back, if a reference sensor was used for noise reduction, and the aim of the study*

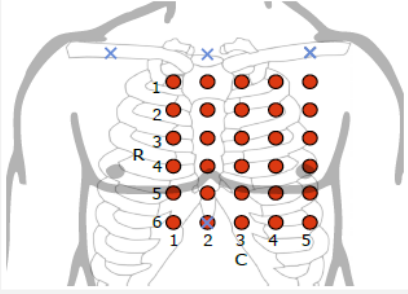
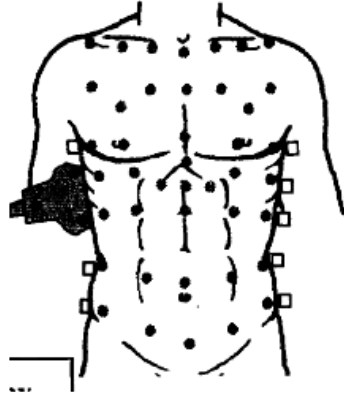
Study	Measuring technologies	Number of sites	Front or Back	Ref. for noise reduction	Aim
Kompis & Pasterkamp 2001	Microphones	8-16	Both	Yes	3D model of respiration and heart sounds.
Kajbaf & Ghassemian 2009	Microphones	18	Both	No	A novel method for acoustic image of heart sounds
Cozic et al. 1998	Microphones	22	Front	Yes	Designing equipment for heart sound mapping
Rendón et al. 2007	Piezoelectric accelerometer	8 pairs	Front	No	Find the best site for single accelerometer measuring of snoring and heart sounds.
(Munck et al. 2016; Struijk et al. 2016)	Laser Doppler vibrometer	30	Front	No	Map the movement of the chest caused by the heart and the heart sound energies
Aliverti et al. 1998	Optoelectronic motion analysis	89	Front	No	Investigate movement of the internal/external movement of the chest caused by respiration.

Most studies focus on the heart sounds or respiration, due to their limitation of measuring technologies. However, studies that did investigate the lower frequency movement showed there was a time difference between peaks of signals measured at different sites. The same studies also concluded that better alignment of measuring sites signals would be necessary for better understanding of the signal.

The acquisition of these signals was done with different approaches. Some measure all sites simultaneously while other measure one or two points at a time and then segments and aligns the signals with other biological signal markers such as ECG R-peaks. *Table 4* shows the sites of measuring for the studies in *Table 3*.

*Table 4* List of found studies that use different technologies to measure a movement of the chest at multiple sites. The table also includes the measuring technology used and which sites the measurements where conducted

Study	Measuring technologies	Aim
Kompis & Pasterkamp 2001	Microphones	 <p>Back 2nd intercostal space in front</p> <p>16cm 18cm</p> <p>Front 2nd intercostal space</p> <p>16cm 18cm</p>
Kajbaf & Ghassemian 2009	Microphones	 <p>Array 1      Array 2      Array 3</p>
Cozic et al. 1998	Microphones	 <p>aortic area / pulmonary area</p> <p>microphones</p> <p>2 3 4 5 6 7 8</p> <p>mitral area (apex)</p> <p>tricuspid area</p>
Rendón et al. 2007	Piezoelectric accelerometer	 <p>1-b 1-a NECK</p> <p>2-b 2-a</p> <p>3</p> <p>4</p> <p>5</p> <p>6</p> <p>7</p> <p>8-b 8-a</p> <p>9-b 9-a</p> <p>10-b 10-a THORAX</p> <p>11-b 11-a</p>

(Munck et al. 2016; Struijk et al. 2016)	Laser Doppler vibrometer	
Aliverti et al. 1998	Optoelectronic motion analysis	

According to the literature, only a few studies have investigated the mapping of lower frequency movements of the chest, and those that had were missing some proper temporal alignment of the measuring sites.

Studies that had investigated to higher frequency movement of the chest, as the heart sounds, speculated that such mapping technics could be useful for detecting heart valve diseases (Cozic et al. 1998; Kompis & Pasterkamp 2001; Kajbaf & Ghassemian 2009).

## CHAPTER 3. AIM

Based on the problem analysis there is a need for a marker related to heart failure patients that would benefit from CRT due to them having ventricular dyssynchrony. Other types of more complex markers utilizing echocardiography, MRI or CT have been proposed, but these solutions are expensive, requires higher levels of trained personal, and are to inconsistent due to the interpretation and technical factors. The currently used markers were based on the electrical activity of the heart, while the newer techniques focuses on investigating the mechanical activity.

Based on the analysis of seismocardiography, this technique had promising results in regards of measuring contraction of the ventricles. This indicates that it may be used as a marker for the predicting the CRT response, while still being a cheaper and more consistent alternative to other proposed techniques. However, some of the leading authors in SCG states that further understanding of measuring sites are necessary.

An analysis, of how measuring the movement of the chest at multiple sites would contribute with additional information, was conducted. According to the analysis no conclusive studies were found that could explain how the low frequency movement for the complete chest was behaving. However, studies investigating heart sounds speculated that such mapping techniques could be used for detecting heart valve diseases.

The analysis was conducted due to the lack of literature in the seismocardiography analysis that could explain how measuring sites would affect the signal, but also due to the knowledge of ventricular dyssynchrony analysis about how this condition affect the timing of mechanical actions caused by the ventricles located at different sites relative to the chest.

The analysis of where to measure lead to a further interest in investigating the potential of measuring on multiple locations for gaining knowledge about an additional marker for ventricular dyssynchrony in heart failure patients.

### 3.1. PROBLEM FORMULATION

To develop, implement, and study a novel method for investigating multichannel seismocardiography as a marker for ventricular dyssynchrony in heart failure patients.

## CHAPTER 4. METHOD

To forefeel the problem formulation the following 7 faces administered:

### **Pilot study**

For the system specification, some prior knowledge of the signal needed to be assessed. Among these requirements were knowledge about the signal specification. For the assessment of the signal specifications, a database of SCG measurements from a control group and Cardiac Resynchronization Therapy (CRT) subjects group (Jensen et al. 2014). The control group consist of data from 39 subjects performing different tasks. The CRT group consist of 15 subjects with their CRT turned on, off and on different settings (Jensen et al. 2014). Based on prior knowledge gathered from other studies, and the data from the database, the signal specification were investigated.

### **System specification**

The system specification was based on to study protocols, found in Appendix C. From the study design, a general requirement of the system was specified. Based on the study design to involved roles were analyzed and their individual perspective was used to describe the requirements in a prioritized order.

### **Design**

From the system specifications deriving from the perspectives of the parties involved in the study, a design was made. Through this design, larger decisions, such as choice of accelerometer,  $\mu$ C, block diagrams, acquisition software etc., was taken. Many of the design decisions rely on the choice of accelerometer.

### **Implementation**

With funding from “Siemens Fonden” it is possible to implement the mSCG method based on the system specifications and design. A grant from “Siemens Fonden” of 27,500 DDK and the Aalborg University of 4,500 DDK made the implementation possible. The design choices were implemented when manufacturing the electronic circuits of sensors and data acquisition tool, along with the programming of the microcontrollers and implementation of the data acquisition software. Assembling, 3D printing boxes, and programming of the  $\mu$ C and user interface is also described in this chapter.

### **Test protocol**

Before the study begins the system had to pass some test to ensure stability of the acquisition and to ensure that there would not be any unforeseen bias in the study. A system test protocol was constructed and conducted in order to investigate the behavior of the system and specifically of the SCG sensors.

### **Study of subjects**

To investigate the mSCG in relation to healthy subject, a study was performed, where 3 male volunteers were included. The study was conducted on basis of the study protocol in Appendix C, that was approved by The North Denmark Region Committee on Health Research Ethics 28 of March 2017 (N-20170008).

### **Data processing**

After data acquisition, the mSCG had to be constructed into maps and then further analyzed by extracting features and identifiers. Both the forces applied by the heart onto the chest and the heart sound energies were of interest for this study.

# CHAPTER 5. PILOT STUDY

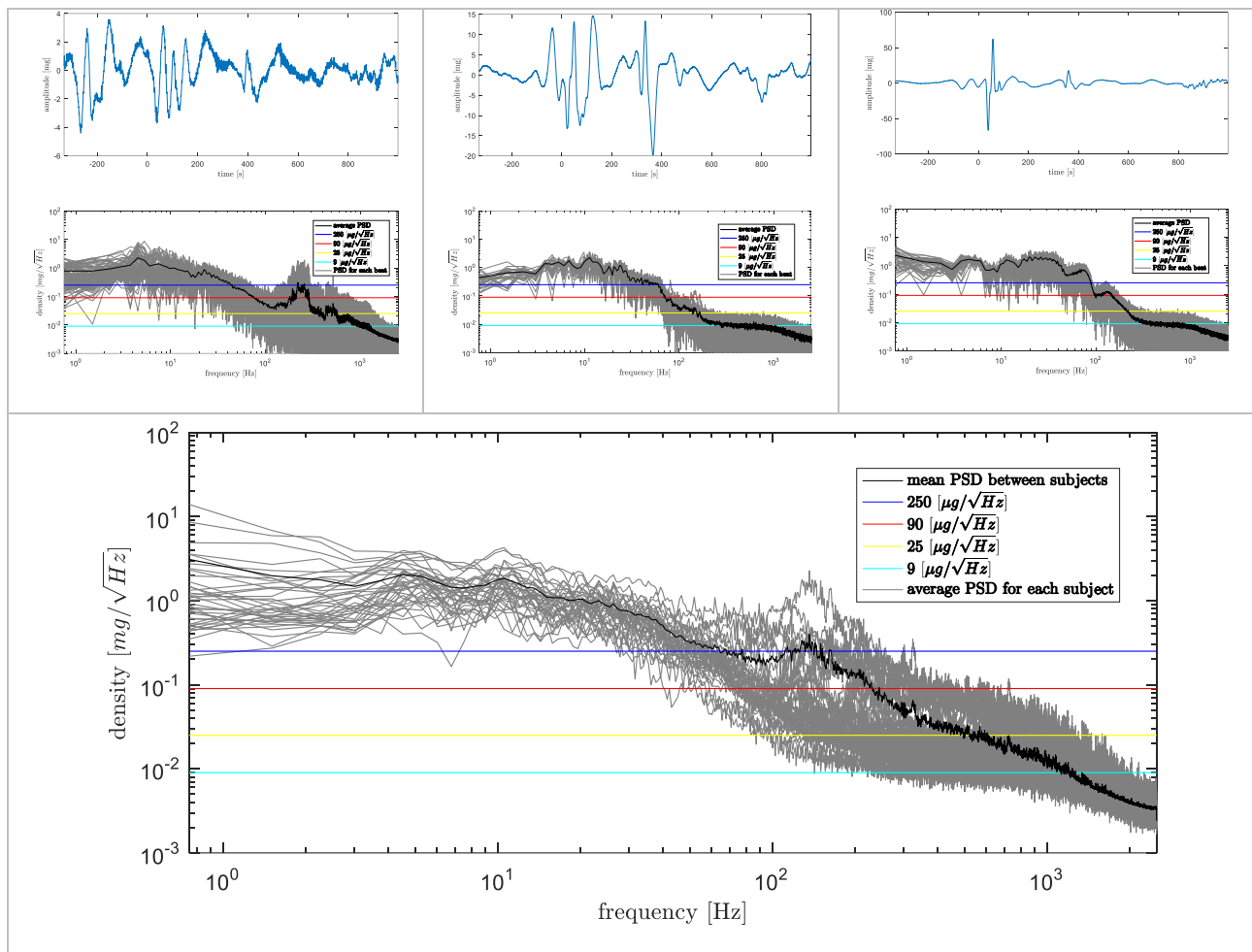
For better understanding the requirements of a system that would measure SCG, the specification of SCG signals were investigated through a pilot study. Data used in this pilot study were previously collected with one channel SCG from 38 healthy volunteers and 12 patient that had their CRT turned off during a measurement period. The aim with this pilot study was to add supporting knowledge about certain specifications of the SCG signals to develop a system able to measure these signals.

The SCG signal specifications investigated were divided into three main focuses; their spectral content, signal energy and signal amplitudes. Each specification was investigated in relation to typical MEMS accelerometer specification notations and in relation to both the low frequency SCG and heart sounds contents.

## 5.1. SPECTRAL CONTENT

The spectral content of an SCG signal was described by segmenting multiple heart cycles of SCG signals, and calculating both the average beat and the average Power Spectrum Density for all the beats, in order to reveal a more accurate representation. These results were presented for the control and CRT groups in Table 5 and Table 6, respectively.

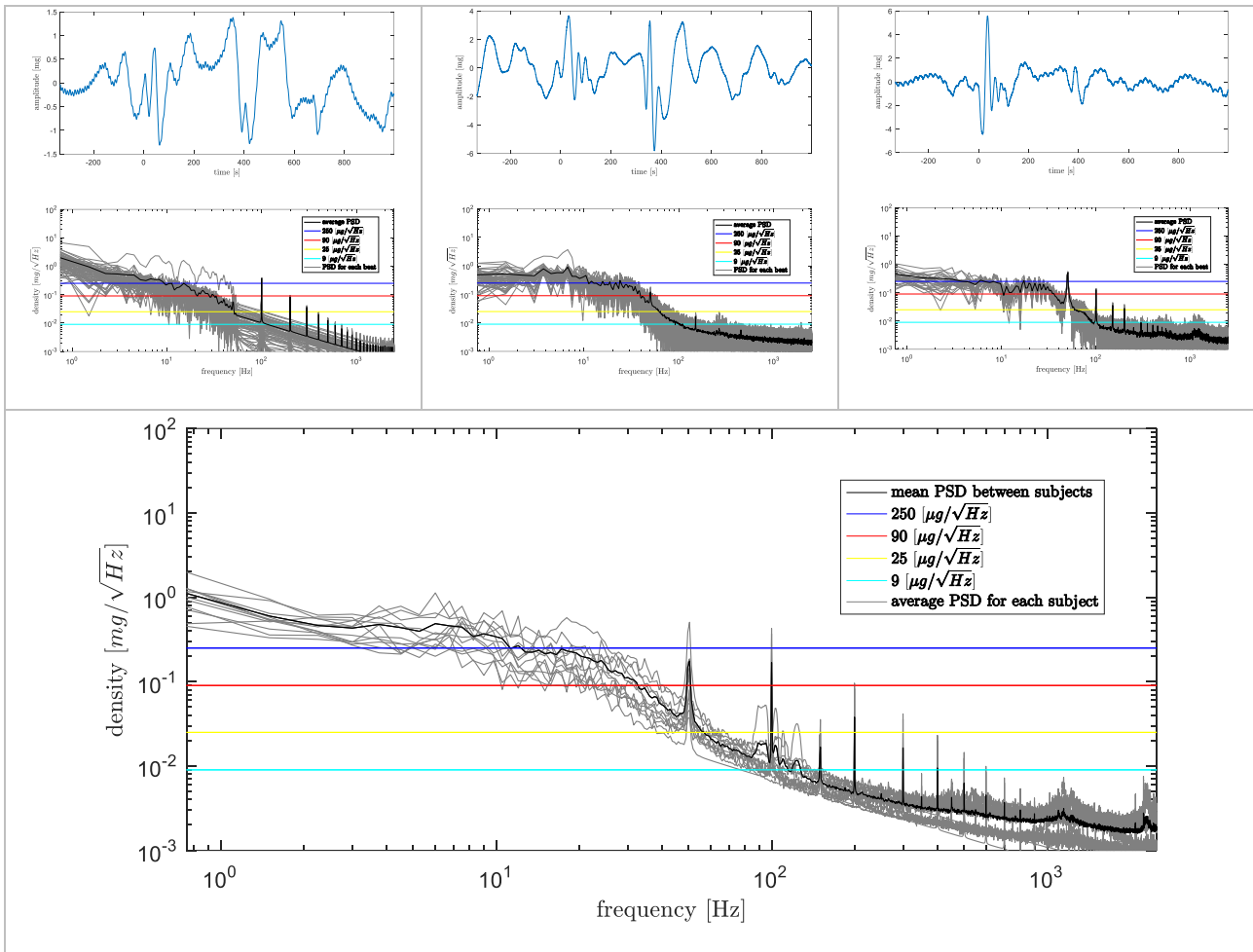
*Table 5 Representation of the average heart beat and the average Power Spectrum Density (PSD) of three handpicked subjects from the control group of 38 subjects, along with the mean PSD between all subjects in the last row. On the figures was also marked four levels of noise, commonly found with MEMS accelerometers for comparison*



When investigating the SCG signals, amplitudes varying from  $\pm 4$  mg to  $\pm 60$  mg was apparent. Investigating the SCG signals average PSD reveals a noise floor in most cases close to the  $9 \mu\text{g}/\sqrt{\text{Hz}}$  that was expected by this setup. Investigations also reveal that PSD above 300 Hz is in most cases at the noise floor and would therefore not contribute with any information.

In some of the cases the signal could be divided into two spectral sections. This is because the PSD falls in magnitude until it reaches another rise near 100 Hz, and then it typically falls again. This could be related to the heart sounds

Table 6 Representation of the average heart beat and the average Power Spectrum Density (PSD) of three handpicked subjects from the CRT group of 12 subjects, along with the mean PSD between all subjects in the last row. On the figures was also marked four levels of noise, commonly found with MEMS accelerometers for comparison



By comparing the SCG signals from the control group with the SCG signal from the CRT group, it becomes clear that the amplitudes were much smaller, ranging from  $\pm 1.5$  mg to  $\pm 6$  mg. Similar trends are visible in their PSD they typically were below the  $250 \mu\text{g}/\sqrt{\text{Hz}}$  marker, at the lower frequencies. However, the background noise was much lower with these SCG sensors since the noise floor where typically well below the  $9 \mu\text{g}/\sqrt{\text{Hz}}$  marker. But then close to half of the SCG signals were contaminated by some artifacts at specific frequencies that also had their harmonics through the higher bands.

Similar to the control group it was clear that at a spectrum higher than 300 Hz the signals would not contribute with any additional information.

## 5.2. SIGNAL NOISE

To better understand the importance of the noise and signal attributes, noise was added to the signals and a Signal to Noise Ratio (SNR) was calculated for the control and CRT group in Table 7 and Table 8. Each of the tables investigates the SNR at the lower frequency band of 0.5 to 300 Hz and the higher frequency heart sounds at 20 to 300 Hz, respectively. The two bands were selected based on the literature found in the Problem analysis and the initial findings of this pilot study. The tables present cases where noise is added for both the worst and the best-case examples.

Four levels of noise were added, and the levels were selected after an analysis of common noise levels of MEMS accelerometers. In the last rows of the tables were presented the mean SNR and standard deviation across subjects of the respected group.

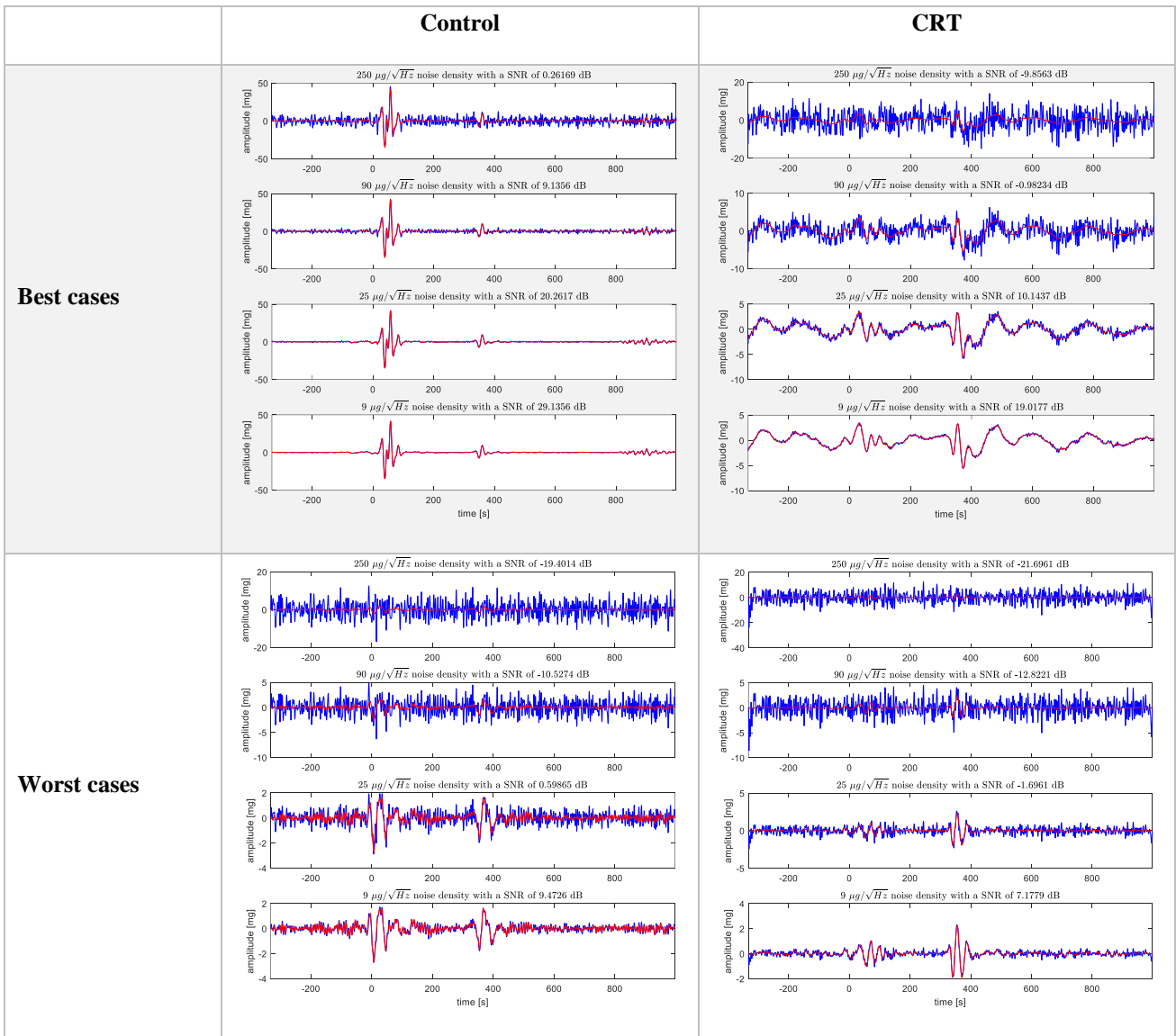
*Table 7 Investigation of the Signal to Noise Ratio (SNR) of the mean SCG beat from subjects in the control and CRT group, when adding different amounts of noise. The mean beats were filtered at 0.5 to 300 Hz to investigate the SNR effect on the lower frequency content of a SCG signal*

	Control	CRT
<b>Best cases</b>	<p>250 <math>\mu\text{g}/\sqrt{\text{Hz}}</math> noise density with a SNR of 4.8233 dB</p>	<p>250 <math>\mu\text{g}/\sqrt{\text{Hz}}</math> noise density with a SNR of -17.5464 dB</p>
	<p>90 <math>\mu\text{g}/\sqrt{\text{Hz}}</math> noise density with a SNR of 13.6973 dB</p>	<p>90 <math>\mu\text{g}/\sqrt{\text{Hz}}</math> noise density with a SNR of -8.6725 dB</p>
	<p>25 <math>\mu\text{g}/\sqrt{\text{Hz}}</math> noise density with a SNR of 24.8233 dB</p>	<p>25 <math>\mu\text{g}/\sqrt{\text{Hz}}</math> noise density with a SNR of 2.4536 dB</p>
	<p>9 <math>\mu\text{g}/\sqrt{\text{Hz}}</math> noise density with a SNR of 33.6973 dB</p>	<p>9 <math>\mu\text{g}/\sqrt{\text{Hz}}</math> noise density with a SNR of 11.3275 dB</p>
<b>Worst cases</b>	<p>250 <math>\mu\text{g}/\sqrt{\text{Hz}}</math> noise density with a SNR of -5.9123 dB</p>	<p>250 <math>\mu\text{g}/\sqrt{\text{Hz}}</math> noise density with a SNR of -34.8686 dB</p>
	<p>90 <math>\mu\text{g}/\sqrt{\text{Hz}}</math> noise density with a SNR of 2.9617 dB</p>	<p>90 <math>\mu\text{g}/\sqrt{\text{Hz}}</math> noise density with a SNR of -25.9946 dB</p>
	<p>25 <math>\mu\text{g}/\sqrt{\text{Hz}}</math> noise density with a SNR of 14.0877 dB</p>	<p>25 <math>\mu\text{g}/\sqrt{\text{Hz}}</math> noise density with a SNR of -14.8686 dB</p>
	<p>9 <math>\mu\text{g}/\sqrt{\text{Hz}}</math> noise density with a SNR of 22.9617 dB</p>	<p>9 <math>\mu\text{g}/\sqrt{\text{Hz}}</math> noise density with a SNR of -5.9946 dB</p>
<b>SNR [dB]</b> <b>250 <math>\mu\text{g}/\sqrt{\text{Hz}}</math></b>	<b>-1.4±3.1</b>	<b>-14.6±3.6</b>

<b>SNR [dB]</b> <b>90 <math>\mu\text{g}/\sqrt{\text{Hz}}</math></b>	7.4±3.1	-5.7±3.6
<b>SNR [dB]</b> <b>25 <math>\mu\text{g}/\sqrt{\text{Hz}}</math></b>	18.5±3.1	5.4±3.6
<b>SNR [dB]</b> <b>9 <math>\mu\text{g}/\sqrt{\text{Hz}}</math></b>	27.4±3.1	14.3±3.6

By setting a limit of the SNR to be 3 dB at least, the results reveal that for SCG signals bandpass filtered at 0.5 to 300 Hz, the control group would require acquisition tool with less than 90  $\mu\text{g}/\sqrt{\text{Hz}}$  for the control group and less than 25  $\mu\text{g}/\sqrt{\text{Hz}}$  for the CRT group. For signals bandpass filtered at 20 to 300 Hz, the noise would have to be below 25  $\mu\text{g}/\sqrt{\text{Hz}}$  for the control group and below 9  $\mu\text{g}/\sqrt{\text{Hz}}$  for the CRT group.

*Table 8 Investigation of the Signal to Noise Ratio (SNR) of the mean SCG beat from subjects in the control and CRT group, when adding different amounts of noise. The mean beats were filtered at 20 to 300 Hz to investigate the SNR effect on the higher frequency content of a SCG signal, related to the heart sounds*



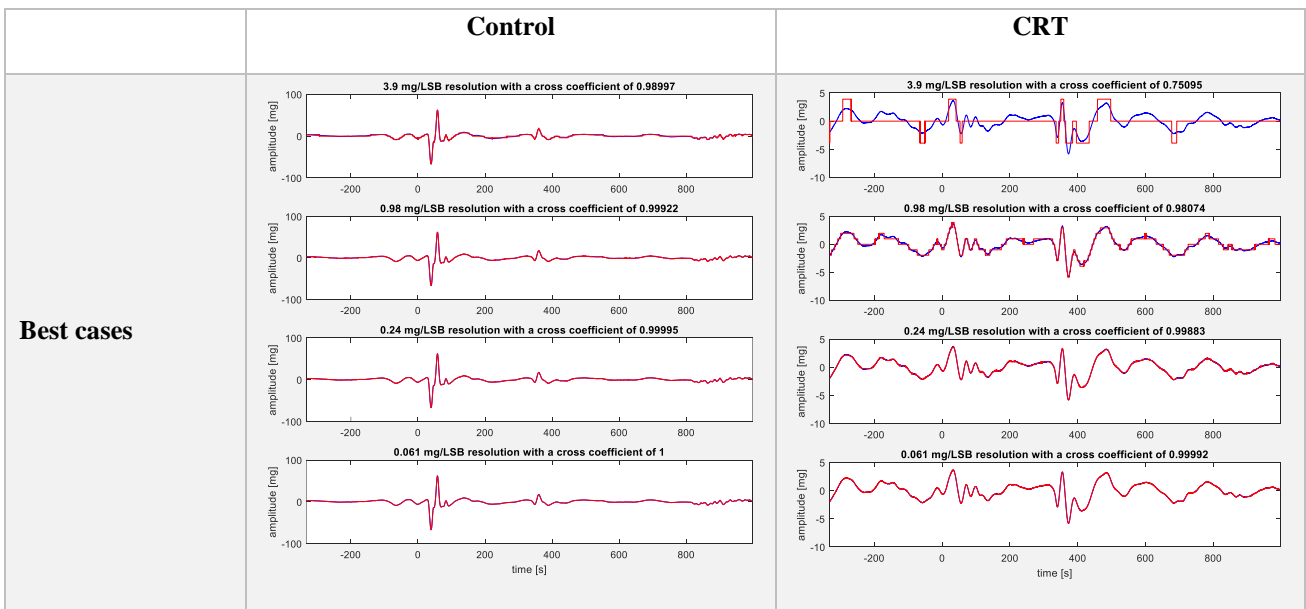
<b>SNR [dB]</b> <b>250 <math>\mu\text{g}/\sqrt{\text{Hz}}</math></b>	-10.8±4.3	-31.4±5.4
<b>SNR [dB]</b> <b>90 <math>\mu\text{g}/\sqrt{\text{Hz}}</math></b>	-1.9±4.3	-21.5±5.4
<b>SNR [dB]</b> <b>25 <math>\mu\text{g}/\sqrt{\text{Hz}}</math></b>	9.2±4.3	-10.4±5.4
<b>SNR [dB]</b> <b>9 <math>\mu\text{g}/\sqrt{\text{Hz}}</math></b>	18.1±4.3	-1.5±5.4

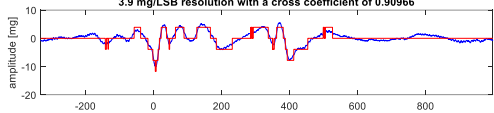
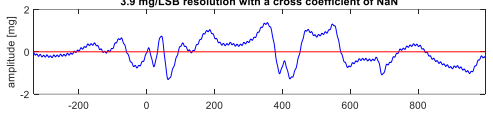
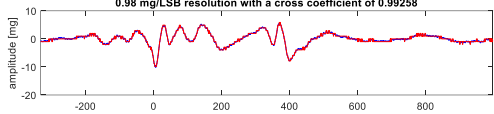
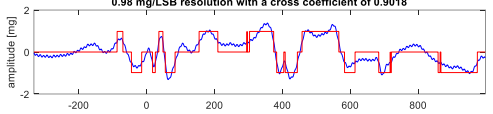
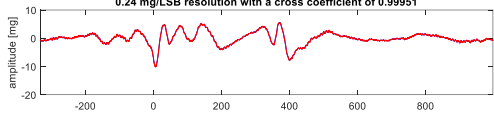
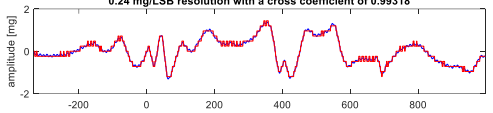
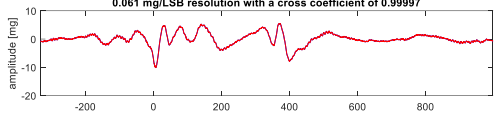
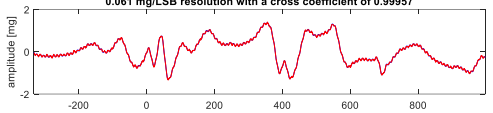
### 5.3. SIGNAL AMPLITUDES

To better understand the importance of the spatial resolution and signal attributes, the SCG signals resolution was changed and the cross-correlation coefficient was used to compare the original signal with the changed, for the control and CRT group in Table 9 and Table 10. Each of the tables investigates the spatial resolution at the lower frequency band of 0.5 to 250 Hz and the higher frequency heart sounds at 20 to 300 Hz, respectively. The two bands were selected based on the literature found in the Problem analysis and on the initial findings of this pilot study. The tables present cases where spatial resolution was changed for both the worst and the best-case examples.

Four levels of spatial resolution were selected, and the levels were selected after an analysis of common spatial resolutions of digital MEMS accelerometers. In the last rows of the tables were presented the cross-correlation coefficient and standard deviation across subjects of the respected group.

*Table 9 Investigation of the signal cross correlation-coefficient of the mean SCG beat from subjects in the control and CRT group, changing the spatial resolution. The mean beats were filtered at 0.5 to 300 Hz to investigate the SNR effect on the higher frequency content of a SCG signal, related to the heart sounds*



<b>Worst cases</b>	 <p>3.9 mg/LSB resolution with a cross coefficient of 0.90966</p>	 <p>3.9 mg/LSB resolution with a cross coefficient of NaN</p>
	 <p>0.98 mg/LSB resolution with a cross coefficient of 0.99258</p>	 <p>0.98 mg/LSB resolution with a cross coefficient of 0.9018</p>
	 <p>0.24 mg/LSB resolution with a cross coefficient of 0.99951</p>	 <p>0.24 mg/LSB resolution with a cross coefficient of 0.99318</p>
	 <p>0.061 mg/LSB resolution with a cross coefficient of 0.99997</p>	 <p>0.061 mg/LSB resolution with a cross coefficient of 0.99957</p>
<b>Cross Correlation Coefficient [%] 3.9 mg/LSB</b>	0.96±0.39	0.69±0.33
<b>Correlation Coefficient [%] 0.98 mg/LSB</b>	0.99±0.04	0.95±0.05
<b>Correlation Coefficient [%] 0.24 mg/LSB</b>	1±0.00	0.996±0.004
<b>Correlation Coefficient [%] 0.061 mg/LSB</b>	1±0.00	1±0.00

By setting a limit of the cross-correlation coefficient to be at least 0.95, the results reveal that for SCG signals bandpass filtered at 0.5 to 250 Hz, the control group would require acquisition tool with a lower spatial resolution than 0.24 mg/LSB for the control and CRT-group. For signals bandpass filtered at 20 to 300 Hz, the spatial resolution would have to be lower than 0.24 mg/LSB for the control group and lower than 0.061 mg/LSB for the CRT group.

Table 10 Investigation of the signal cross correlation-coefficient of the mean SCG beat from subjects in the control and CRT group, changing the spatial resolution. The mean beats were filtered at 20 to 300 Hz to investigate the SNR effect on the higher frequency content of a SCG signal, related to the heart sounds

	Control	CRT
<b>Best cases</b>		
<b>Worst cases</b>		
<b>Cross Correlation Coefficient [%] 3.9 mg/LSB</b>	0.81±0.21	0.58±0.41
<b>Correlation Coefficient [%] 0.98 mg/LSB</b>	0.96±0.04	0.79±0.34
<b>Correlation Coefficient [%] 0.24 mg/LSB</b>	0.997±0.004	0.95
<b>Correlation Coefficient [%] 0.061 mg/LSB</b>	1±0.00	0.99±0.01

#### 5.4. RESULTS FROM THE PILOT STUDY

This section summarizes the results from the pilot study to define the specification of a mSCG system useful for capturing SCG signals from healthy subject and patients with a CRT.

With respect to the spectral content analysis, frequencies higher than 300 Hz would not add additional information to the SCG signal.

With respect to the signal noise analysis, noise levels at  $25 \mu\text{g}/\sqrt{\text{Hz}}$  or lower would be necessary to capture the low frequency signals of the SCG in both the control and CRT-group, along with the high frequency heart sounds for the control group. To properly capture hearts sounds from the CRT group the noise would have to be  $9 \mu\text{g}/\sqrt{\text{Hz}}$  or lower.

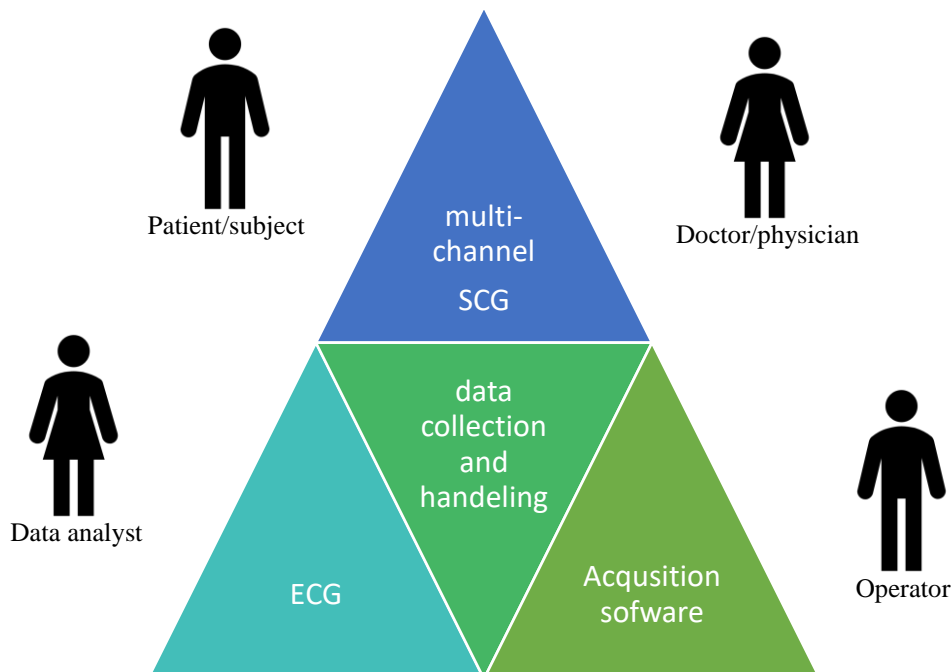
With respect to the signal amplitude analysis, a spatial resolution lower than 0.24 mg/LSB or lower would be necessary to capture the low frequency signals of the SCG in both the control and CRT-group, along with the high frequency heart sounds for the control group. To properly capture hearts sounds from the CRT group the spatial resolution would have to be 0.061 mg/LSB or lower.

## CHAPTER 6. SYSTEM REQUIREMENTS

The system requirements were used for the design of the mSCG equipment, but also for designing the study protocol in Chapter 10 and Appendix C. Therefore, when figuring out the system requirements, the study was put in focus along with its actor's individual points of view. By the end of this chapter all the system requirements were scored according to the MoSCoW method and collected in Table 11.

### 6.1. STUDY SYSTEM REQUIREMENT

A system to collect mSCG would be composed of multiple sensors that would contain MEMS accelerometers. Along with the sensors there would also be a need to collect an ECG signal along with the mSCG signals. All signals would have to be quantified such that the measurements could be stored on a computer to generate the BSKM and the further process the acquired data. Both the sensor and the ECG would require a power source.



### 6.2. PATIENT/SUBJECT POINT OF VIEW

When a study protocol is reported to the ethics committee it is important to consider the risks, side effects and disadvantages for the patient and to minimize these factors. When measuring an ECG, it is important to minimize the risk electrical shock by limiting any fault current to XX mA. For the SCG measurements there is no need for any direct contact with the subject and that is why the SCG sensors needs to be electrically isolated from the subject.

- Electrical insulation
  - SCG
  - ECG
- Minimization of wires
- Mounting methods

### 6.3. DATA ANALYST POINT OF VIEW

Based on the literature, problem analysis and the pilot study characteristics about the measured ECG and SCG signals defines the requirements of the acquisition tool.

#### SCG

In the pilot study, four main characteristics was investigated based on the problem analysis and MEMS accelerometer chapter:

- Noise
- Resolution
- Frequency
- Spatial resolution

The measured signal does not come from one source but from multiple sites of the chest. By measuring on multiple sites, it is possible to separate or detect the individual sources. However, each SCG measurements need to be sampled synchronous, meaning that that there is no time lag between the measurements and their sampling frequency are precisely the same.

- Noise requirements
  - Calculate the SNR of added different levels of noise to the mean beat of multiple SCG signals (control & CRT)
- ADC bit requirements
  - Reduce the amplitude resolution of mean beat
  - ADC precision
- Frequency requirements
  - Analysis of control and CRT
  - Flat frequency response
- Spatial resolution requirements
  - Measure with multiple accelerometers horizontal and vertical
- Synchronous sampling
  - How synchronous and why
  - Reasons
    - So that the ecg and sensors signals after longer periods would not need realignment
    - So that when mapping the mSCG signals, the timing of different events are true and movement of waves can be detected (Schmidt et al. 2016)

Synchronous sampling of the multiple accelerometer measurements was important for further data analysis when source separation is desired. It is also important that the sampling frequency is at the same frequency, in order to make it possible for at proper alignment of the data.

- Signal drift?
  - Temperature

#### ECG

- Simple solution compatible with the SCG solution
- Noise requirements
- Leak current 83  $\mu$ A (John G. Webster 2010)
- ADC bit requirements
- Frequency requirements
- Synchronous sampling
- 3-lead Einthoven's triangle

## 6.4. OPERATOR POINT OF VIEW

- Cost
- Flexible solution
- Digital accelerometer
- Standard communication protocols (minimum modifications)
- Communication protocols
  - Buffer
  - Speed limits
- Power consumption
- Equipment protection
  - Peak acceleration
  - Noise robustness
  - User fault protection
- Cable spaghetti syndrome

## 6.5. DOCTOR/PHYSICIAN POINT OF VIEW

The doctor would have to be able to make echocardiography measures, while the mSCG would be acquired. To make this possible number of wires on the subjects chest would have to be minimized and the placement of the SCG sensors would have to be discussed with the doctor.

The echocardiograph would have to be able to be aligned with the mSCG signals and therefore a typical approach is to measure ECG with both equipment.

## 6.6. PRIORITY OF SYSTEM SPECIFICATIONS

Table 11 End system requirements scored according to the MoSCoW method and divided into belonging actors point of view

Group:	Patient/Subject	Data analyst	Operator	Doctor/physician
<b>Main focus:</b>	<ul style="list-style-type: none"> <li>• Safety</li> <li>• Stigma</li> </ul>	<ul style="list-style-type: none"> <li>• Signal characteristics</li> <li>• Synchronization</li> <li>• Cable influence on signal</li> <li>• Placement of SCG</li> </ul>	<ul style="list-style-type: none"> <li>• Setup of measurements</li> <li>• Robustness</li> <li>• Ease of use</li> </ul>	<ul style="list-style-type: none"> <li>• Multiple ECG tools</li> <li>• Room for ultrasound probe</li> <li>• Patient safety</li> </ul>
<b>MUST HAVE:</b>	<ul style="list-style-type: none"> <li>• Electrical isolation of SCG</li> <li>• Limiting faulty leakage current on ECG to 83 <math>\mu</math>A</li> </ul>	<ul style="list-style-type: none"> <li>• Z-axis measurements</li> <li>• Frequency band</li> <li>• Signal to noise ratio</li> <li>• Acceleration resolution</li> <li>• Sampling frequency</li> <li>• Spatial resolution</li> <li>• 12 SCG sites</li> <li>• Zero data loss (fast transfer)</li> </ul>	<ul style="list-style-type: none"> <li>• Save data to Matlab</li> <li>• Low cost (relative to other SCG equipment)</li> </ul>	<ul style="list-style-type: none"> <li>• Able to end experiment at any time</li> </ul>
<b>SHOULD HAVE:</b>	<ul style="list-style-type: none"> <li>• Reduced number of wires</li> </ul>	<ul style="list-style-type: none"> <li>• 3 Lead ECG</li> <li>• Respiration measurements</li> </ul>	<ul style="list-style-type: none"> <li>• Plot SCG measures</li> </ul>	<ul style="list-style-type: none"> <li>• Use same ECG electrodes for monitoring health</li> </ul>

	<ul style="list-style-type: none"> <li>• Skin friendly placement method</li> </ul>		<ul style="list-style-type: none"> <li>• Plot ECG measures</li> <li>• Data traffic monitoring</li> </ul>	<ul style="list-style-type: none"> <li>• Reduced number of wires</li> </ul>
<b>COULD HAVE:</b>		<ul style="list-style-type: none"> <li>• 3-axis measurements</li> </ul>	<ul style="list-style-type: none"> <li>• Method for placing SCG and ECG</li> </ul>	<ul style="list-style-type: none"> <li>• Relation between probe sites and SCG placement</li> </ul>
<b>WANT TO HAVE:</b>		<ul style="list-style-type: none"> <li>• 17 SCG sites</li> <li>• 12 Lead ECG</li> </ul>	<ul style="list-style-type: none"> <li>• Wires that don't break under use</li> <li>• Turn plots on/off</li> <li>• Debug features</li> </ul>	

## CHAPTER 7. DESIGN

The design was based on the system requirements and research into existing solutions of the individual problem within the system. As the block diagram in Figure 7 illustrates the system consist of four types of blocks. The block types present were; sensors, microcontrollers ( $\mu\text{C}$ ), computer, electrodes, and ECG acquisition. Special for the sensors blocks was its high complexity and therefore it consists of six additional blocks.

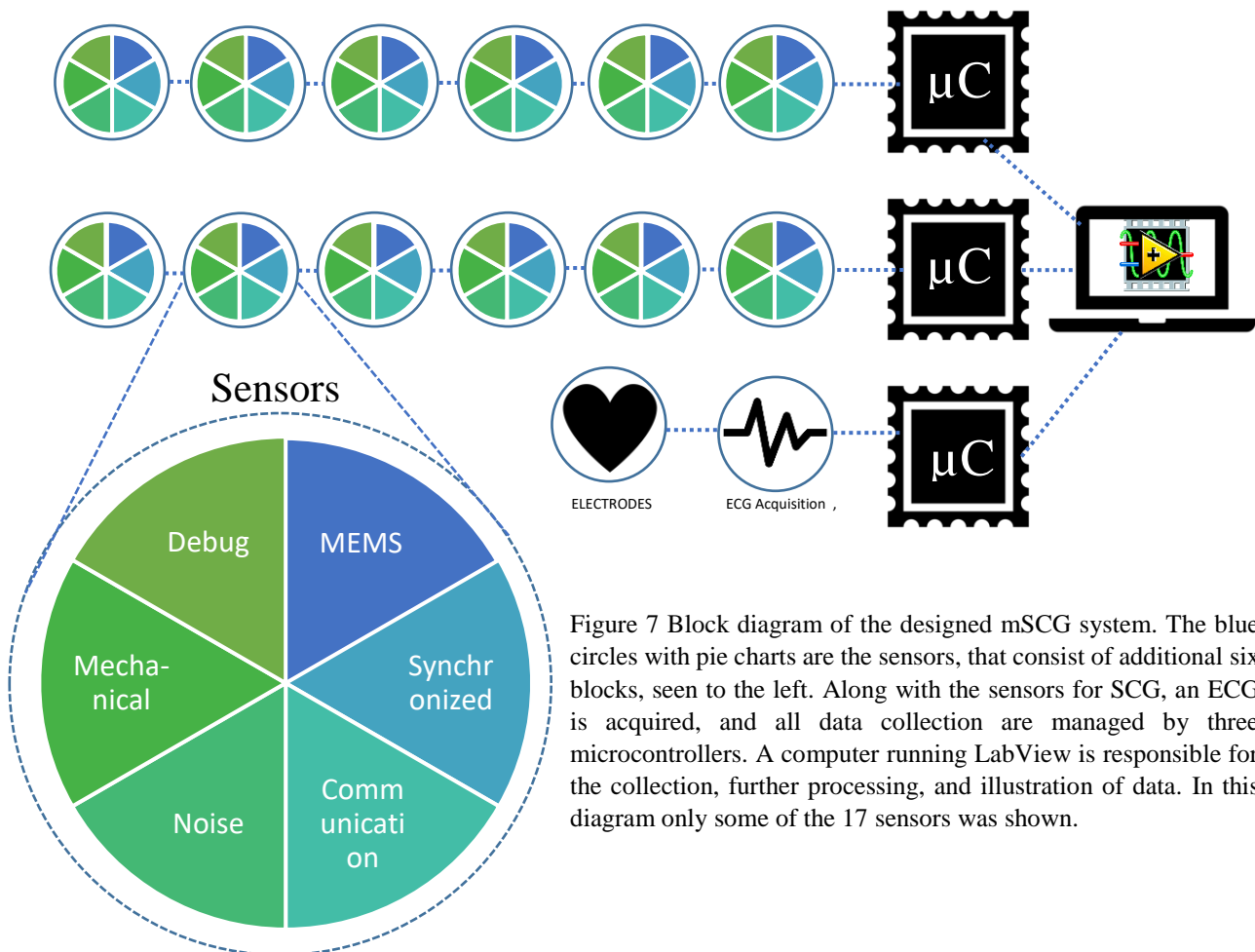
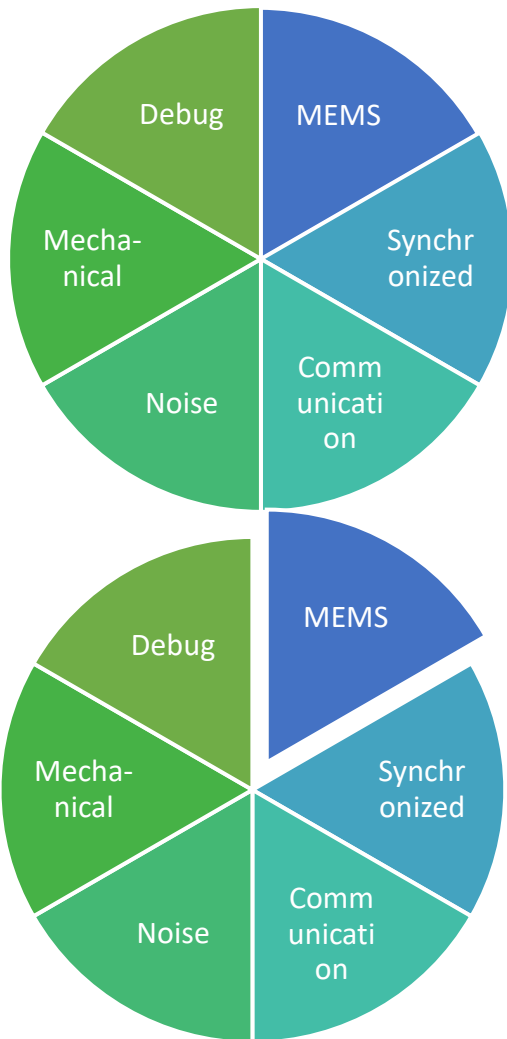


Figure 7 Block diagram of the designed mSCG system. The blue circles with pie charts are the sensors, that consist of additional six blocks, seen to the left. Along with the sensors for SCG, an ECG is acquired, and all data collection are managed by three microcontrollers. A computer running LabView is responsible for the collection, further processing, and illustration of data. In this diagram only some of the 17 sensors was shown.

Through the Design chapter each block has been further described on how they meet with the system requirements, how they were designed, and with what purpose and evidence the different design features where made.

## 7.1. SENSORS

At the center of the mSCG system was the sensors to measure the acceleration of the chest. By the system requirements different specifications of the accelerometer was addressed which was used for selecting a suited candidate for commercial available MEMS accelerometers. From the choice of MEMS accelerometers additional supporting part needed to be specified and designed.



### 7.1.1. CHOICE OF ACCELEROMETER

By looking at all the commercial manufactures of digital MEMS accelerometers and iNEMO (combinations of MEMS accelerometer and gyroscopes or magnetometers), we found two digital MEMS accelerometers that had a build-in synchronization feature for ensuring simultaneous sampling. Analog Devices manufactured both accelerometers that are listed by Table 12.

*Table 12 List of all investigated commercial digital MEMS accelerometers which has a method for synchronized sampling. Specifications of the devices are from the corresponding datasheets (Analog Devices 2016a; Analog Devices 2016b)*

Model	Range [g]	Sensitivity [ $\mu\text{g} / \text{LSB}$ ]	Noise [ $\mu\text{g} / \sqrt{\text{Hz}}$ ]	FIFO [samples]	Frequency band [Hz]	Sampling frequency [Hz]	Output protocol	Price range
ADXL362	$\pm 2$	61	175	32	200	12.5 to 400	SPI	35 DKK
ADXL355	$\pm 2.048$	3.9	20	32	1,000	4 to 4000	SPI/I2C	300 DKK

The ADXL362 specifications meets the requirements for acquiring SCG signals both in relation to range, sensitivity, noise, and frequency band. However, the ADXL355 additionally meets the requirements for acquiring the heart sounds, that would add additional knowledge about the source. Apart from meeting with the requirements specified in the System requirements chapter the ADXL355 also measures acceleration in 3 axes. The ADXL355 was a digital MEMS accelerometer designed in accordance with the block diagram in Figure 8.

For the ADXL355 a selection of options was available, where settings such as sampling frequency, filters etc. would be set in registers through the digital communications protocol. Based on these settings of the ADXL355 the sub section Signal pathway was described.

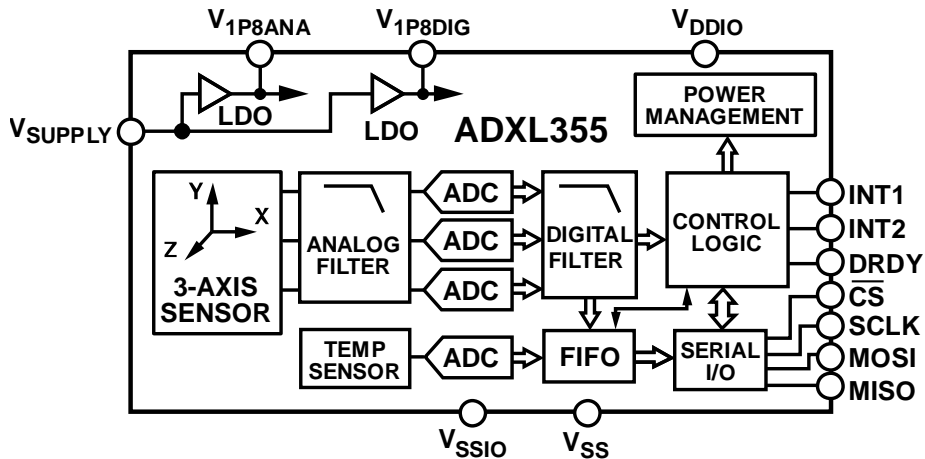


Figure 8 Blockdiagram of the ADXL355 MEMS accelerometer from Analog Devices. Illustration is from (Analog Devices 2016b)

**Signal pathway**

The ADXL355 measures the acceleration as described by Appendix A, where the demodulator generates a voltage directly proportional to the acceleration measured by the MEMS. This voltage signal is then antialiasing filtered before it is quantified by the build in ADC. The signal pathway of the acceleration signal within the ADXL355 is illustrated by Figure 9. The frequency response of multiple ADXL355 units analog antialiasing filter is illustrated by Figure 10.

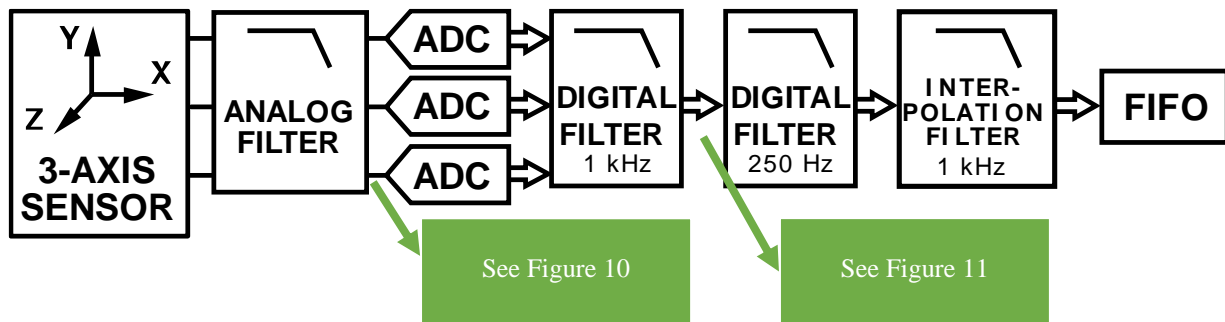


Figure 9 Illustration of the signal pathway for the 3-axis MEMS accelerometer signal, through an antialiasing filter, sampled by the ADC (Analog to Digital Converter), further filtered and downsampled and by the end stored in a FIFO (First In Last Out) memory. Illustration is modified from (Analog Devices 2016b)

The ADXL355 MEMS has a resonant frequency at 2.4 kHz and the antialiasing filter suppresses this with a cutoff frequency at 1.5 kHz. The analog antialiasing filter is a sinc3 filter which is a type of comp filter in 3<sup>th</sup> order. After the accelerometer signal, have been sampled by the build-in ADC, the signal is filtered with a digital LP-filter with a cutoff frequency at 1 kHz. The frequency response of the 1 kHz digital LP-filter is illustrated for multiple ADXL355 units by Figure 11.

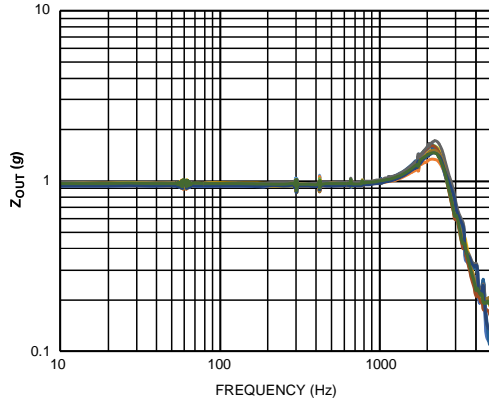


Figure 10 Frequency response of the ADXL355 for its Z-axis after the analog antialiasing filter. Illustration is from (Analog Devices 2016b)

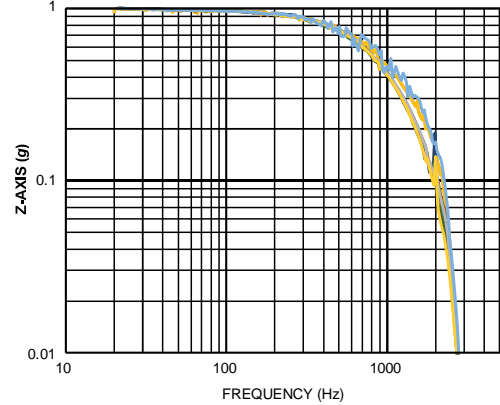


Figure 11 Frequency response of the ADXL355 for its Z-axis after the analog antialiasing filter and with a 1 kHz digital LP-filter. Illustration is from (Analog Devices 2016b)

Dependent on the programmed sampling frequency the accelerometer signal is passed through an additional digital LP-filter that has a cutoff frequency at 1/4 of the sampling frequency. Meaning that if the sampling frequency was 1 kHz the cutoff frequency would be at 250 Hz. At last the 3-axis digital acceleration signal is down sampled to the desired sampling frequency and save onto the FIFO memory, ready to be empty by the communication port.

### 7.1.2. SYNCHRONOUS SAMPLING

As described by the System requirements a synchronous sampled signal is important for proper alignment of the signals and for the signals not to experience a temporal drift due to different sampling rates. The ADXL355 sampling frequency may vary dependent on the unit as illustrated by Figure 12.

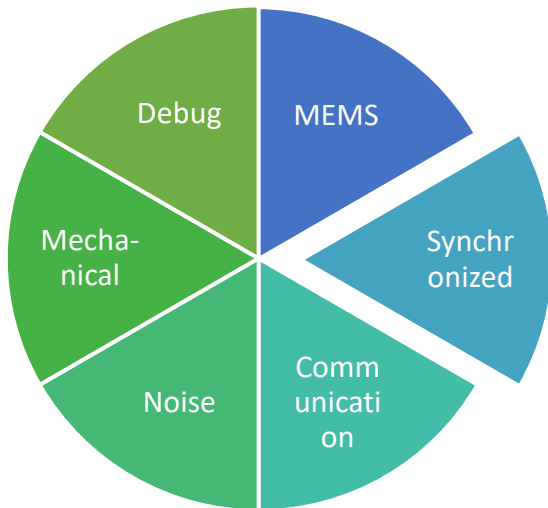
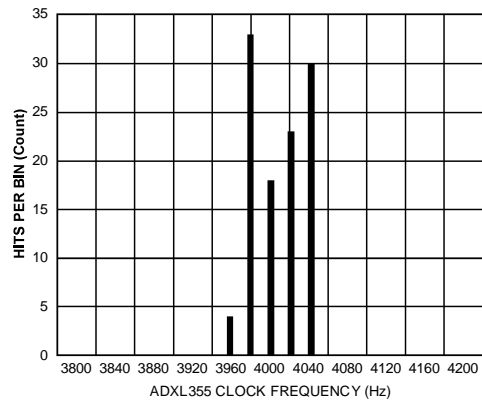


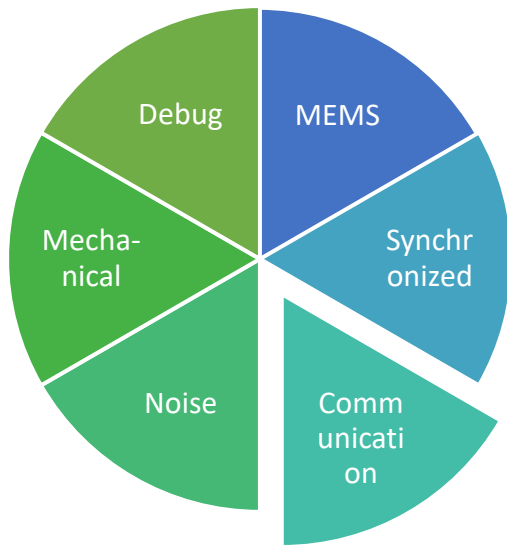
Figure 12 ADXL355 Internal Clock Frequency Histogram. Illustration is from (Analog Devices 2016b)



This would mean that two accelerometers with each extreme cases of internal clock frequencies would after a minute of measuring experience a temporal drift of 14.25 seconds between the two measurements, when sampling the signal at 4 kHz, as calculated by equation (1).

$$\frac{4040 \cdot 60 - 3960 \cdot 60}{4000} = 14.25 \frac{\text{seconds}}{\text{minute}} \quad (1)$$

### 7.1.3. COMMUNICATION



The ADXL355 can communicate with a 4-wire SPI protocol of clock rates at 100 kHz to 10 MHz, or the I2C protocol at 400 kHz and up to 3.4 MHz. Both protocols were not designed for of board communications but both were designed for bus communications.

For the I2C protocols bus function to work properly, each device on the bus needs to have their own address. The ADXL355 has a selection between 2 individual addresses. Circuits exist that may grand an additional selection of addresses of the devices. However, these circuits also limit the communication speeds to 400 kHz, which in turn reduces that purpose of the bus.

The SPI protocol uses chip select (CS) lines for selecting each individual device during communications. This means that each device had a need for their own CS line. These lines

however could be encoded for a reduced number of line on the bus. Apart from the CS line there are also the source clock (SCLK), master in slave out (MISO) data line, and master out slave in (MOSI) data line. The two data lines were used for transferring data each direction and the SCLK was used for triggering the read and write on the data lines. An example of a data read are illustrated by Figure 13.

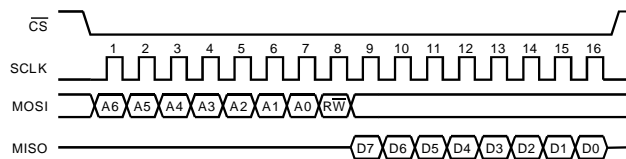


Figure 13 An example of a data read command to the ADXL355 with the SPI communication protocol. A6-A0 is the address to be read from, R/W is wether or not to read or write and the D7-D0 is one read byte. Illustration is from (Analog Devices 2016b)

To reduce line count on the bus, reduce noise and make the SPI protocol able to transmit over longer distances the LTC6820 isoSPI unit, from Linear Technology, was included in the design as illustrated by Figure 14.

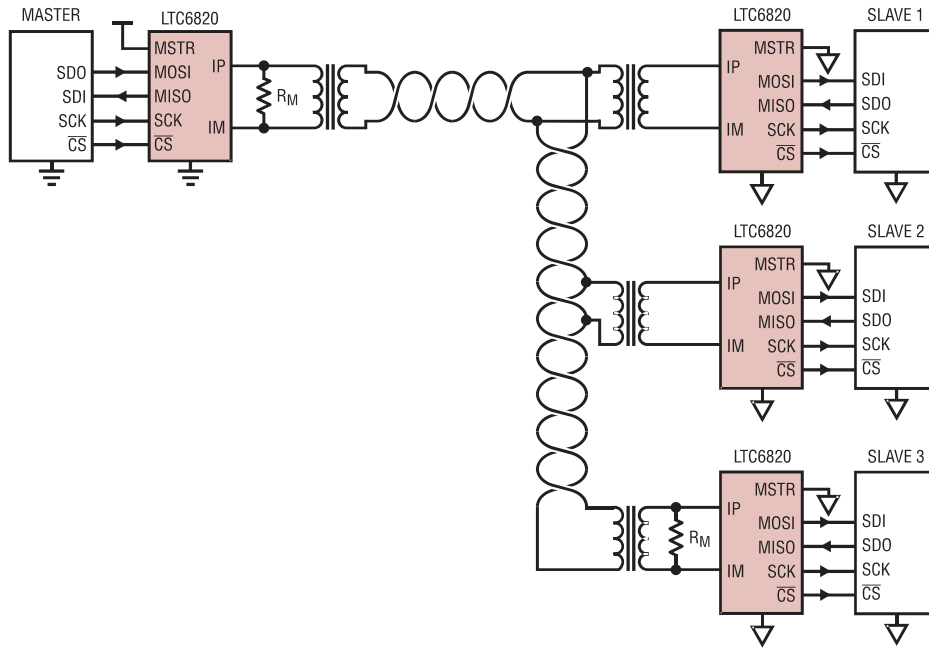


Figure 14 Bus configuration of the LTC6820 with isoSPI. Master is the  $\mu$ C and slave are the Sensors. Diagram is from the LTC6820 datasheet (Linear Technology Corporation 2012)

Due to limitations of the LTC6820 and the fact that if the path of the source clock from the master unit and back gets too long, the source clock and MISO signal gets out of sync, the data transfer rate cannot exceed 1 MHz. At cable length, larger the 10 meters the data rate needs to be reduced for the SCLK and MISO to be in sync, as illustrated by Figure 15.

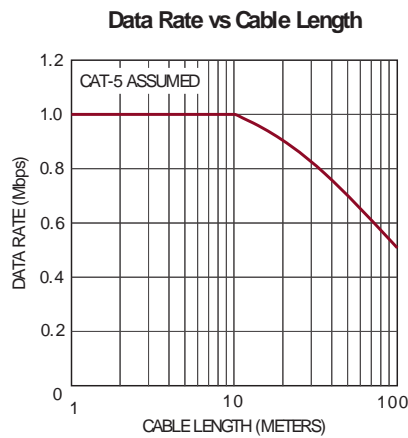


Figure 15 Relationship between the data rate and cable length when implementing the LTC6820 as described by the datasheet. The graf is from LTC6820 datasheet (Linear Technology Corporation 2012)

The relationship between the data rate of the bus, the sampling frequency of the ADXL355 and estimated number of accelerometers on the bus is shown by Table 13.

Table 13 The table illustrates how the settings of the ADXL355 sampling frequency relates to the digital low pass filter, needed data rate of the bus for one Sensor, needed data rate of the bus for 18 Sensors, and the number of Sensors possible on the 1 MHz designed SPI bus. The selected sampling frequency for this design is marked with the arrow

Sampling frequency	250 Hz	500 Hz	1 kHz	2 kHz	4 kHz
Low pass filter	62.5 Hz	125 Hz	250 Hz	500 Hz	1 kHz

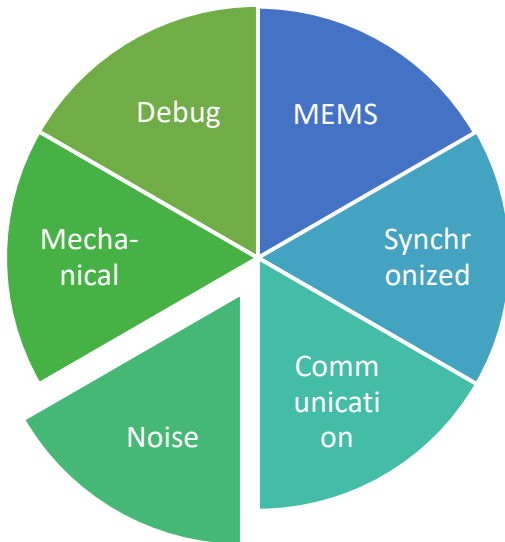
<b>Data rate per Sensor</b>	18 kbps	36 kbps	72 kbps	144 kbps	288 kbps
<b>Data rate of 9 Sensor</b>	162 kbps	324 kbps	648 kbps	1.3 Mbps	2.6 Mbps
<b>Data rate of 12 Sensor</b>	216 kbps	432 kbps	864 kbps	1.7 Mbps	3.5 Mbps
<b>Data rate of 17 Sensor</b>	0.3 Mbps	0.6 Mbps	1.3 Mbps	2.6 Mbps	5.2 Mbps
<b>Accelerometers on bus at 1 MHz</b>	55	27	13	6	3



For the LTC8620 setup illustrated by Figure 14 to function two criteria needs to be met by the sensors.

The first criteria was that the ADXL355 must be addressable. In order to fix this the CS line from the LTC6820 to the ADXL355 is detoured through an addressable switch as illustrated by Figure 24. Each sensor is then coded with a specific address and selected with a binary encoded 4-line connection. This makes it possible to address 16 sensors on the same bus.

**7.1.4. NOISE**



The ADXL355 has four different supplies as illustrated by

Figure 16. The supply is in this design set to 3.3V, and the built in LDO controls the 1.8 individual power supplies for the analog built in circuits and for the digital blocks. The VDDIO is also connected to the 3.3V supply to match the communication levels between the ADXL355 and the LTC6820.

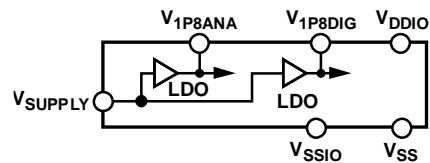


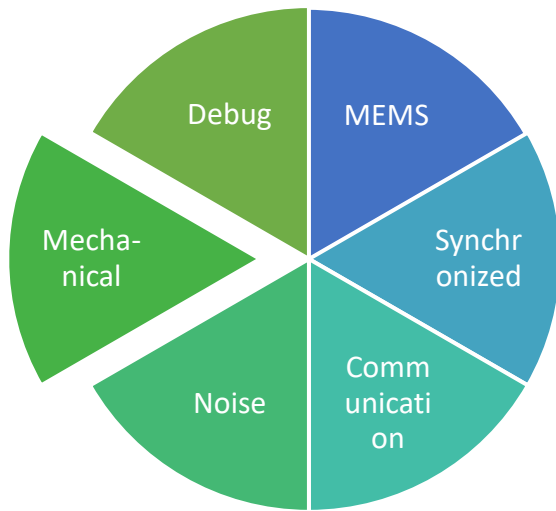
Figure 16 The power supply elements of the ADXL355 block diagram. Illustration is modified from (Analog Devices 2016b)

### 7.1.5. MECHANICS OF SENSOR

Each of the sensors was mounted within a custom 3D printed housing. The purpose of the housing was:

- Electrical insulation between subject and sensors
- High g protection
- Secure cable fixturing
- Direction markers
- Smooth mounting surface between sensor and subject

Besides the housing protecting subjects against faulty currents it also gives provides some overrange protection of the accelerometer against high g shocks over the absolute maximum ratings of 5,000 g for 100  $\mu$ s, that may occur during handling of the sensors. The accelerometer also has a build-in overrange protection for when the acceleration exceeds 8 g.



The 3D printed housing was designed as illustrated by Figure 17, where the housing was a two-part component. The bottom/container was designed to hold the Sensor board in place and the top/lid was designed to secure the ribbon cable when the housing was closed.

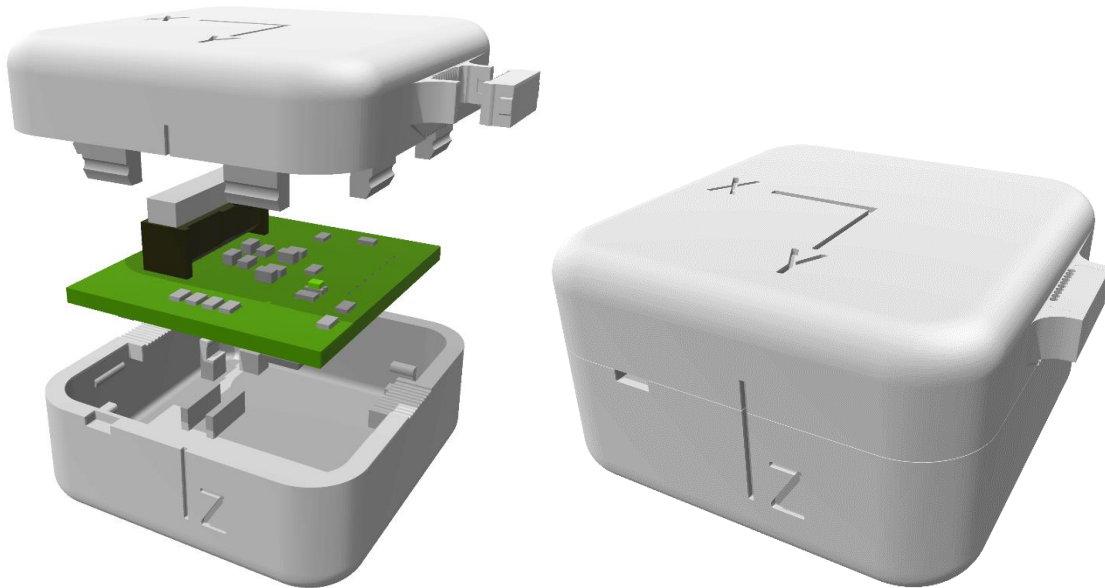
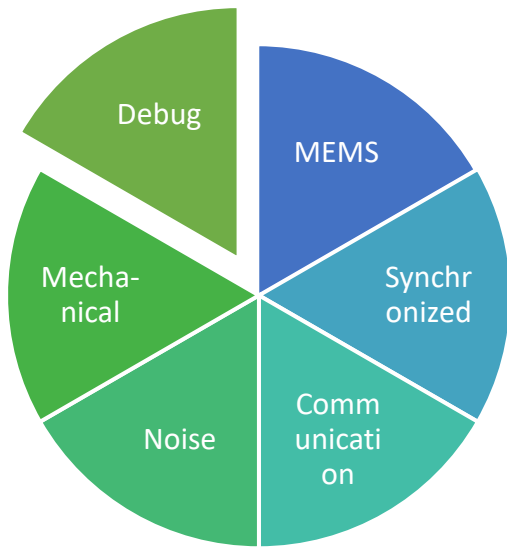


*Figure 17 3D model of the printed housing for the sensors*

The material and printing process Selective Laser Sintering (SLS) Nylon was chosen for its high precision, smooth surface abilities and electrical insulation.

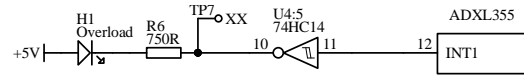
### 7.1.6. DEBUGGING



Z-axis.

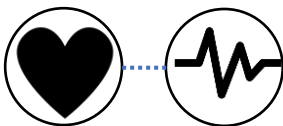
Accelerometer process indication

Test points



The ADXL355 has an incorporated self-test feature that test the mechanical and electronic systems of the ADXL355. The feature works by applying an electrostatic force on each of the axis when the SELF\_TEST register is set to 0x03. The force applied is specific to each axis and the self-test feature is independent to any external applied acceleration. The force applied to each axis would result in an acceleration output change of 0.3 g for the X-axis and Y-axis, and 1.5 g for the

### 7.2. ELETROCARDIOGRAM

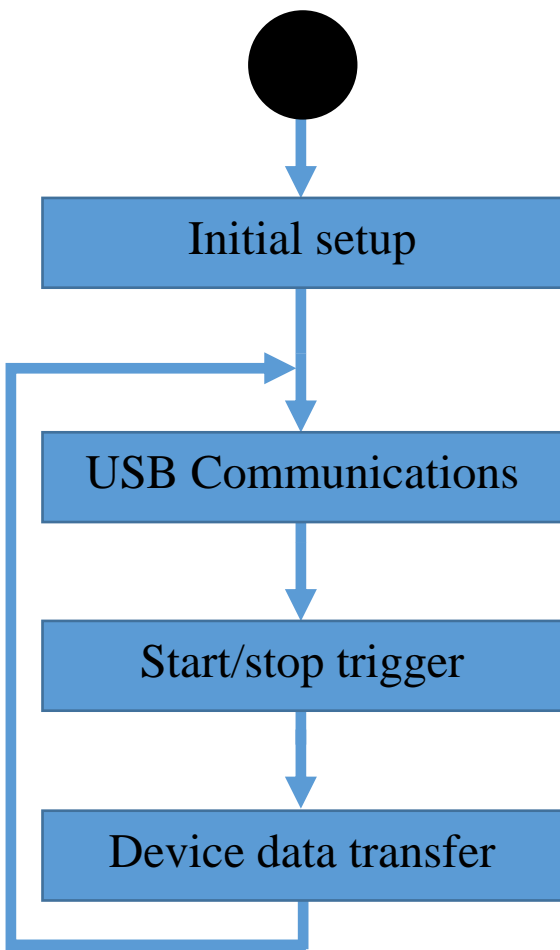


Since the collection of the SCG signals was done through the SPI protocol it would be best with a similar solution for collecting a simultaneous ECG signal with the SCG. From Texas Instrument was the ADS1298, which was a 24-bit, 8-Ch, ADC for ECG acquisition. This chip was also based on collecting data through the SPI protocol. The ADS1298 also came as a developer solution for easy connecting and programming the system the collect a 3-lead ECG at the 2 kHz with 24-bit resolution and adjustable preamplifiers. The developer solution ADS1298ECGFE-PDK from Texas Instrument are illustrated by Figure 18.



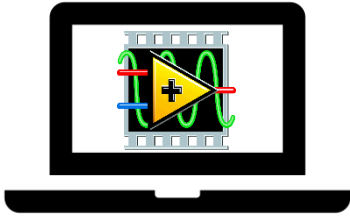
Figure 18 The ADS12398ECGFE-PDK from Texas Instrument used to collect a 3-lead ECG simultaneously with SCG signals.





<ul style="list-style-type: none"> <li>• Set initial variables</li> <li>• IOMUX (connecting port to sockets)</li> <li>• Setup USB protocols</li> <li>• Setup SPI protocols</li> <li>• Setup SPI devices</li> </ul>	
<ul style="list-style-type: none"> <li>• Establish USB connection</li> <li>• React to SPCI commands               <ul style="list-style-type: none"> <li>• *MEAS:# (Send Buffered data)</li> <li>• *START (Set global start signal)</li> <li>• *STOP (Set global stop signal)</li> </ul> </li> </ul>	
<ul style="list-style-type: none"> <li>• start/stop SCG measuring</li> <li>• Clear buffers</li> <li>• Set starting values</li> </ul>	
<p>SCG:</p> <ul style="list-style-type: none"> <li>• On DMA not running</li> <li>• Select a CS address</li> <li>• Check available buffer size on <math>\mu</math>C</li> <li>• Check buffered amount on SCG</li> <li>• Read buffer from SCG (with the DMA)</li> <li>• Write data to buffer</li> </ul>	<p>ECG:</p> <ul style="list-style-type: none"> <li>• On DRDY trigger</li> <li>• Read data from ECG</li> <li>• Check available buffer size on <math>\mu</math>C</li> <li>• Write data to buffer</li> </ul>

## 7.4. ACQUISITION SOFTWARE



Plan for the programming procedure

1. Program the  $\mu\text{C}$  with demo software
2. Transfer ADC measurements with the LabVIEW
3. Transfer ECG measurements
4. Setup UI with ECG in LabVIEW
5. Transfer SCG from ADXL355-EVAL
6. Transfer SCG via master boards from ADXL355-EVAL
7. Transfer SCG via master from one sensor
8. Update UI with multiple measurements and sensor setup
9. Transfer SCG via master from multiple sensors

## CHAPTER 8. IMPLEMENTATION

The novel mSCG design was then implemented, as illustrated by Figure 21.

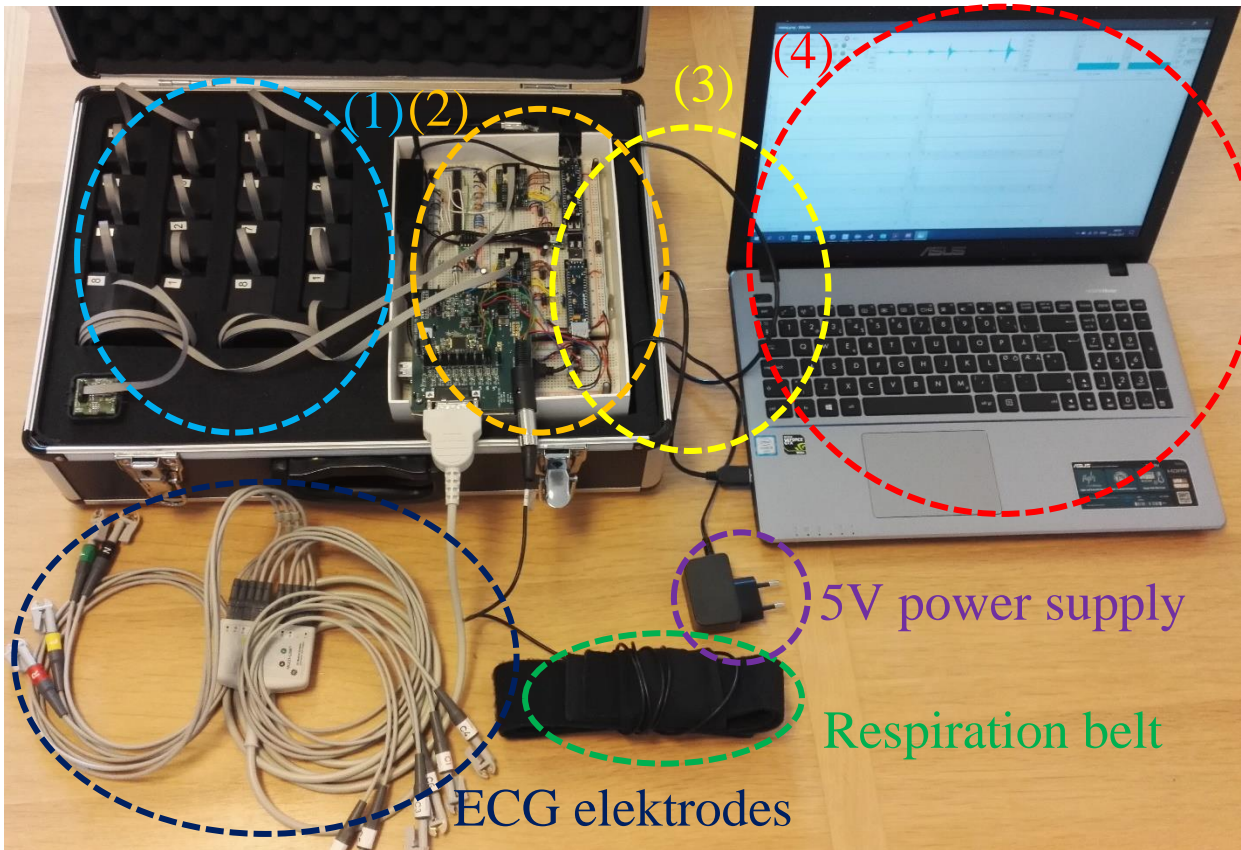


Figure 21 Illustrates the implemented mSCG method. (1) is the SCG sensors, (2) is the central unit, (3) is the microcontroller programming transferring data from the central unit to the acquisition software, and (4) is the computer running the acquisition software in LabVIEW. Connected to the equipment was also the ECG electrodes, respiration belt and an external 5 V supply

The following section will describe how point 1 to 4, from Figure 21, was implemented.

### 8.1. IMPLEMENTATION OF SENSOR DESIGN

Based on the design the sensors were fabricated by 5 processes:



#### 8.1.1. DRAWING ELECTRICAL CIRCUITS

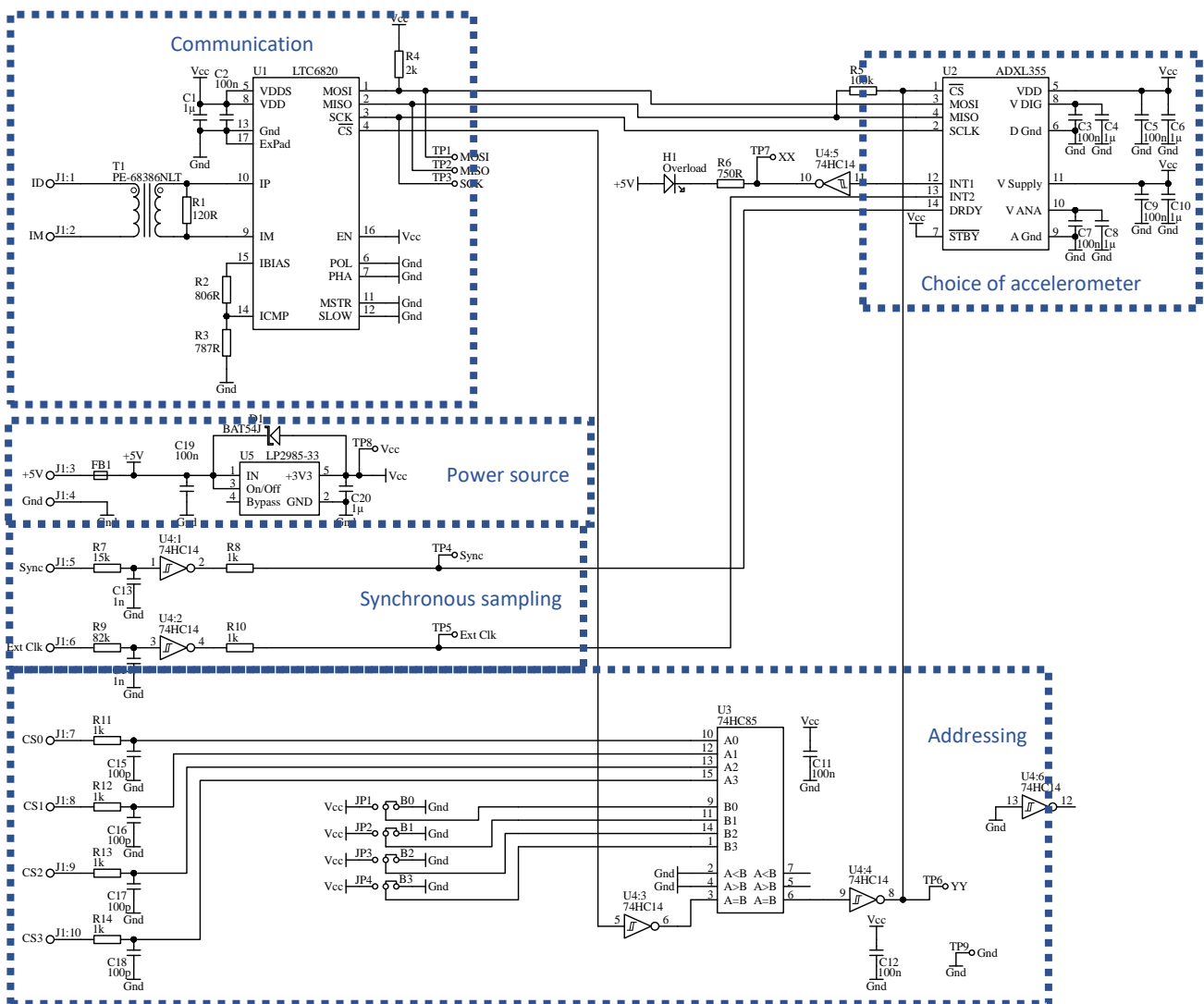


Figure 22 Electrical circuit diagram of the designed sensor

#### Communication

The electrical circuit diagram in Figure 23 illustrates how the LTC6820 was implemented along with the ADXL355 and a signal transformer PE-68386NLT from Pulse. For the data rate of the bus to reach 1 Mbps a pull-up resistor of 2kΩ on

the MOSI is needed for a good enough slew rate. As illustrated by Figure 14, only the last Sensors need a 120Ω at the signal transformer. The 806Ω and 787Ω resistors are there to set the ??? current.

(maximum 1 MHz and minimum a CS to sclk delay of 5 clk pulses)

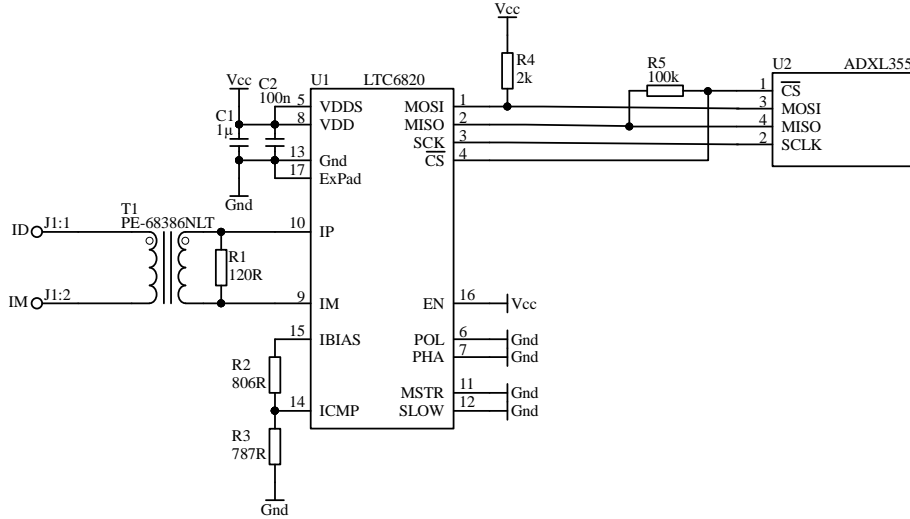


Figure 23 Illustration of how the LTC6820 was implemented in the design of the sensors, in relation to the ADXL355

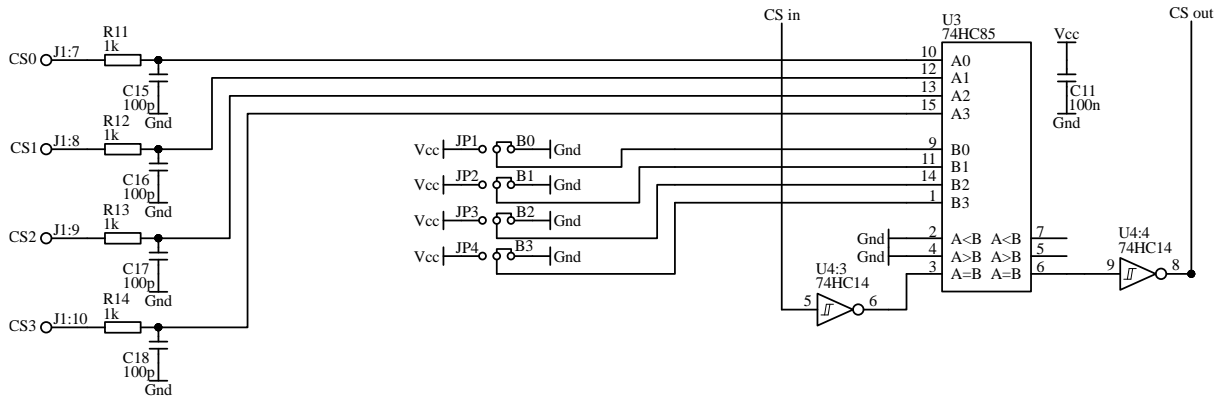
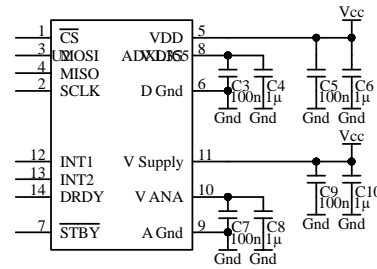


Figure 24 Electrical circuits of the designed addressable chip select circuit. The specific Sensor is addressed by the CS0-CS3 lines and the address is coded by the JP1-JP3. The 74HC85 magnitude comparator compares the code address of the Sensor and the addressed address so that the chip select only gets low when the correct address is selected and the CS in is low

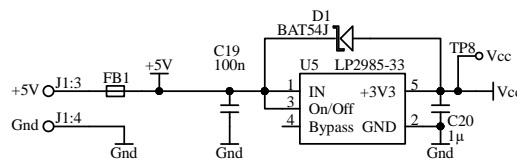
The second criteria were that the MISO line is kept high when the Sensors is not active on the bus. Since the MISO is high impedance on the ADXL355 when it is not chip selected, a resistor of 100k between the CS line and the MISO line. When the ADXL355 is chip selected the MISO line is pulled down but with a very low current.

## POWER

Each of the four power supplies of the ADXL355 was also decoupled by 100nF and 1μF capacitors to reduce noise as specified by the datasheet.



The 3.3V power source for the Sensor comes from the 5V power source that is transferred from the Master unit. By using a higher voltage as the source and regulating the voltage close to the recipient, the noise is reduced. A BAT54J diode is included in the design for the LDO to regulate the voltage faster. Along with a ferrite bead and some decoupling capacitors the noise on the 3.3V power source is reduced significantly.



If the power supply would be faulty and deliver the +5V supply from the cables instead of the desired +3.3V, the absolute maximum ratings of 5.4V would not be surpassed and the ADXL355 would not be damage under short use.

**Synchronization**

The ADXL355 has several methods for using an external clock for the synchronous sampling and for ensuring identical sampling rate of all Sensors. The method most suited for synchronizing multiple ADXL355 units would be the feature utilizing both an external clock (EXT\_CLK) and a sampling clock (SYNC). The way this method works is illustrated by Figure 25.

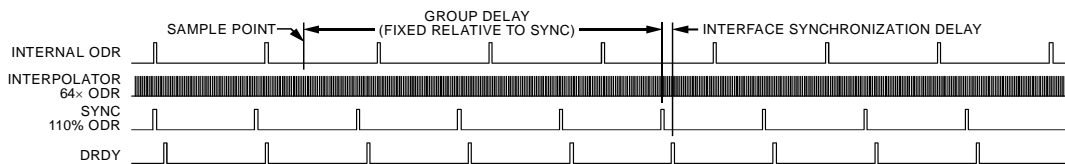


Figure 25 How the ADXL355 external synchronisation function works with an external sync and external clock. Data ready (DRDY) represent when a sample is stored to the FIFO memory and is not an actual output with this setup.

The EXT\_CLK is exactly 256 times faster than the SYNC, and drives the internal logic of the ADXL355. The SYNC is used to align the internal ODR and all samples before the alignment was discarded. This requires that the SYNC pulse is minimum 4 EXT\_CLK periods long.

When a SYNC pulse is detected the sample quantified by the ADC a curtain group delay ago would be store in the FIFO memory. The group delay of the digital low-pass filters when sampling at 1 kHz was listed to be 1.78 ODR cycles or 1.78 ms(Analog Devices 2016b). Since this setup has the digital high-pass filter deactivated the only group delay effecting the sampled signal is the 1.78 ms delay.

To ensure a stable a low noise interfered synchronous sampling both the EXT\_CLK and SYNC were passed through a high pass filter with a cutoff frequency at 1.6 MHz and 10 kHz, respectively. Also, a Schmidt trigger was used to reduce any low amplitude noise from tampering with the synchronization clocks, as illustrated by Figure 26.

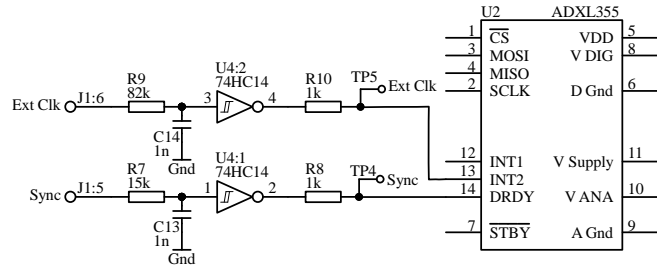
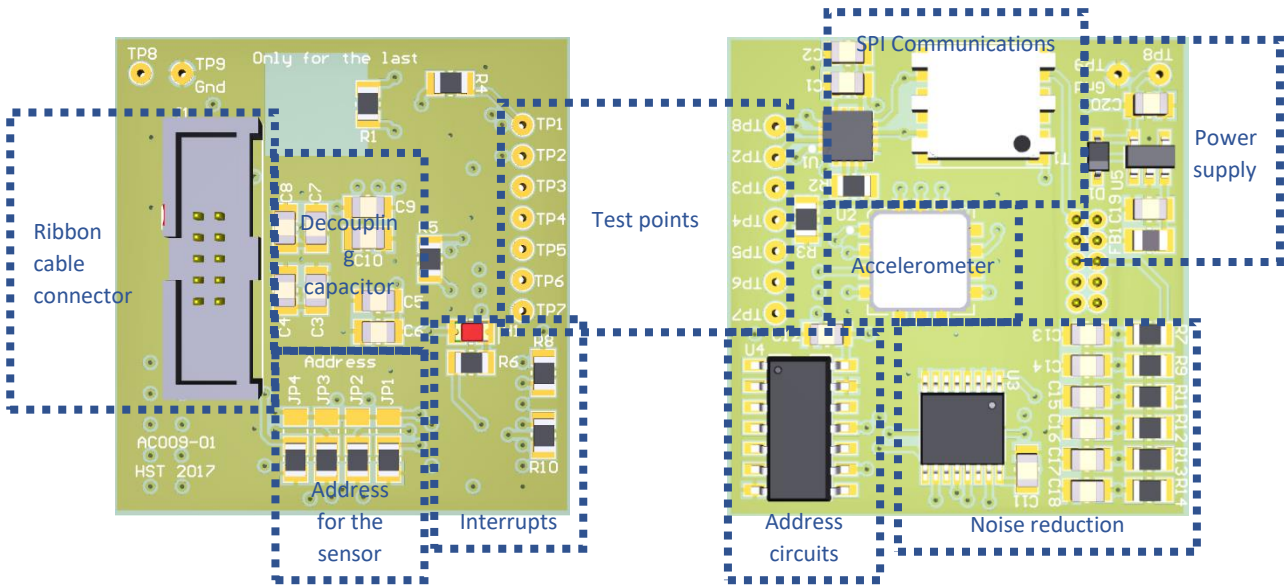


Figure 26 The electrical circuits for the Synchronous sampling block of the Sensors.

In case the INT2 and DRDY pins of the ADXL355 is programmed as an output, instead of the needed input function used for the synchronized sampling feature, a current limiting resistor is applied at the terminals of 1k. This limits any faulty current to 3.3 mA, well below the 10 mA current limit of the ADXL355 terminals.

Since this way of synchronizing the sensors depends on a decimation filter sampled at 64 times higher than the sampling frequency. This would mean the precision of synchronicity within the sensors, at 1 kHz sampling rate, would be at least  $\pm 16 \mu s$ .

### 8.1.2. DRAWING THE PCB



Due to a minor error during PCB drawing the component U1, responsible for transferring the SPI communication across the ribbon cable was mirror. This was first found out after assembling of the sensors was complete. Due to the relative high price of the accelerometer, a second PCB was designed and soldered onto the sensors PCB to replace the mirror component, as illustrated by Figure 27.

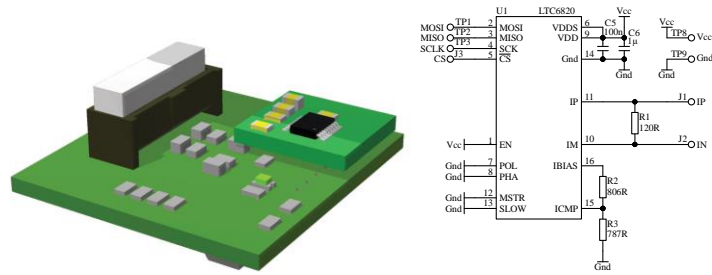
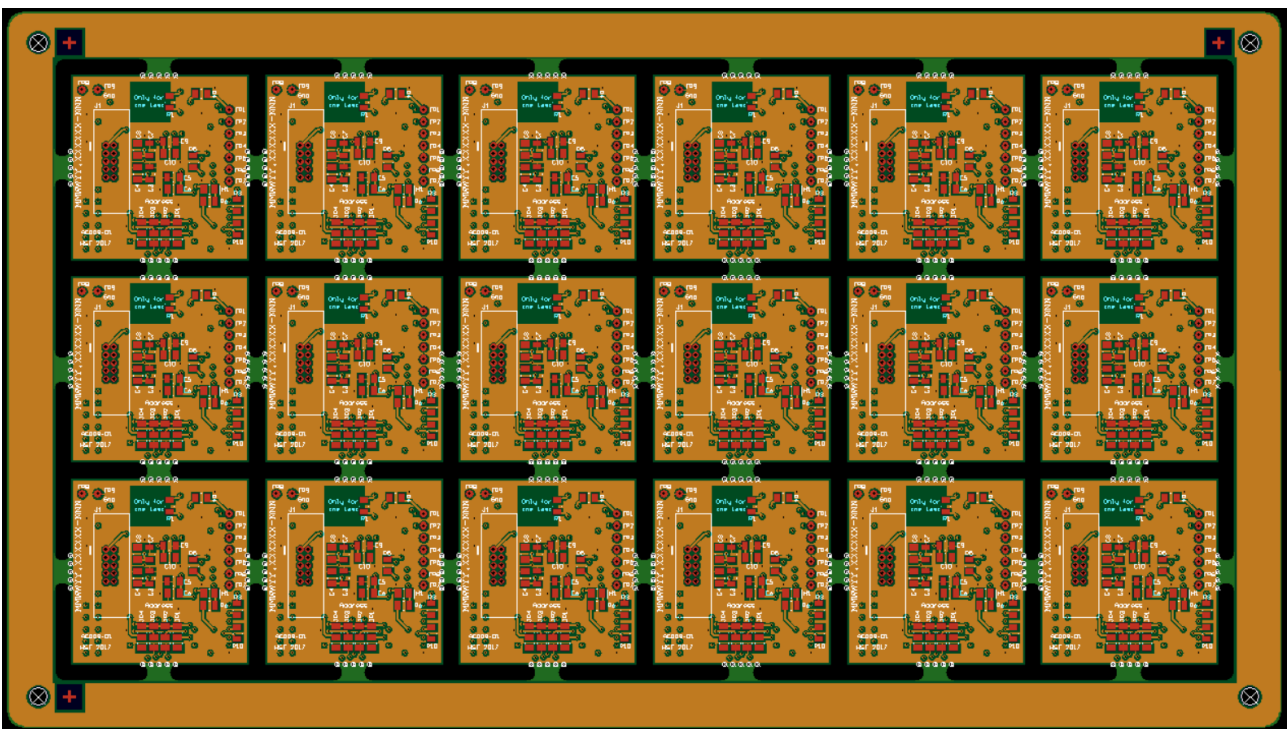


Figure 27 To the left is an animation of the sensor PCB with including the replacement PCB for the mirror LTC6820. To the right is the electrical circuits for the replacement board of the LTC6820.

### 8.1.3. ORDERING PCB PANELS AND SOLDER COMPONENTS



### 8.1.4. DRAWING AND ORDERING 3D PRINTED CASING



### Cables and connections

### 8.1.5. PROGRAMMING THE SENSOR



Before starting a measurement with the accelerometers, the different features of the ADXL355 had to be programmed by writing the address of the program register and the byte to be written into the register, as illustrated by Figure 28.

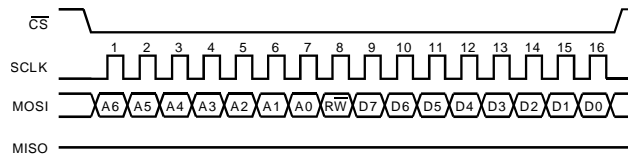


Figure 28 SPI protocol for writing a single byte to the ADXL355. A6-A0 is the register address and D7-D0 is the byte to write to the register

Before any further communications all sensors were reset by writing 0x52 to register 0x2F.

After the reset 6 registers would have to be written to stop any measuring, clearing potential interrupt flags and programming features, as listed by Table 14.

Table 14 List of SPI writes used to program the ADXL355 in accordance with the design. 0x## mean that the ## number was a hex value

Function	Register address	Byte to write	Description
<b>Stop</b>	0x2D	0x01	Stops any data conversion and clears FIFO buffer of the ADXL355
<b>Synchronization</b>	0x2B	0x06	Programs the ADXL355 to sample by the interpolation filter which included a SYNC pulse and a External clock source
<b>Sampling rate</b>	0x28	0x02	Sets the low pass filter of the ADXL355 at 250 Hz and no high pass filter
<b>Interrupt mapping</b>	0x2A	0x04	Sets the interrupt 1 pin as high when the FIFO buffer is full
<b>Range</b>	0x2C	0x41	Sets the range to $\pm 2g$ and the interrupt as active high
<b>Clear interrupt flags</b>	0x04	0xFF	Clears any interrupt flags

After programming the features of the ADXL355 it was also necessary to determine on what addresses a sensor was connected, starting data conversion, reading how many samples were written to the ADXL355 FIFO buffer and reading the data from the FIFO buffer. This was done similar to the programming of the initial features, however some of the address registers would be accessed with a read command, as listed by Table 15.

Table 15 List of SPI commands used for collecting data from the sensors. 0x## mean that the ## number was a hex value

Function	Register address	Byte to write/read	Write or read	Description
<b>Device identification</b>	0x00	0xAD	Read	When reading the device id of the ADXL355, 0xAD should always be returned
<b>Start</b>	0x2D	0x00	Write	Starts a conversion of data on every SYNC pulse
<b>FIFO entries</b>	0x05	0 to 96	Read	Returns the number of samples converted and stored in the ADXL355 FIFO buffer

<b>FIFO data</b>	0x011	Multiple bytes	Read	Reads x number of samples from the buffer dependent on number of samples read
------------------	-------	----------------	------	---

The last command, FIFO data, uses an SPI protocol where multiple samples can be read simultaneously in order to increase the transfer rate across the SPI. The multiple read protocol is illustrated by Figure 29.

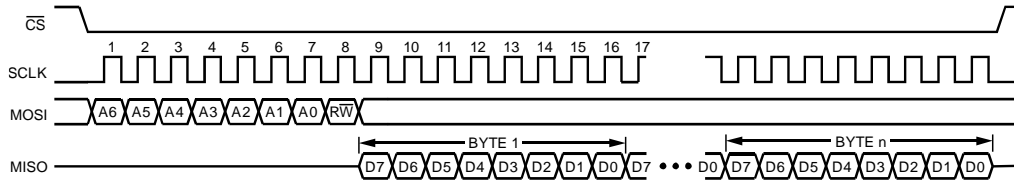
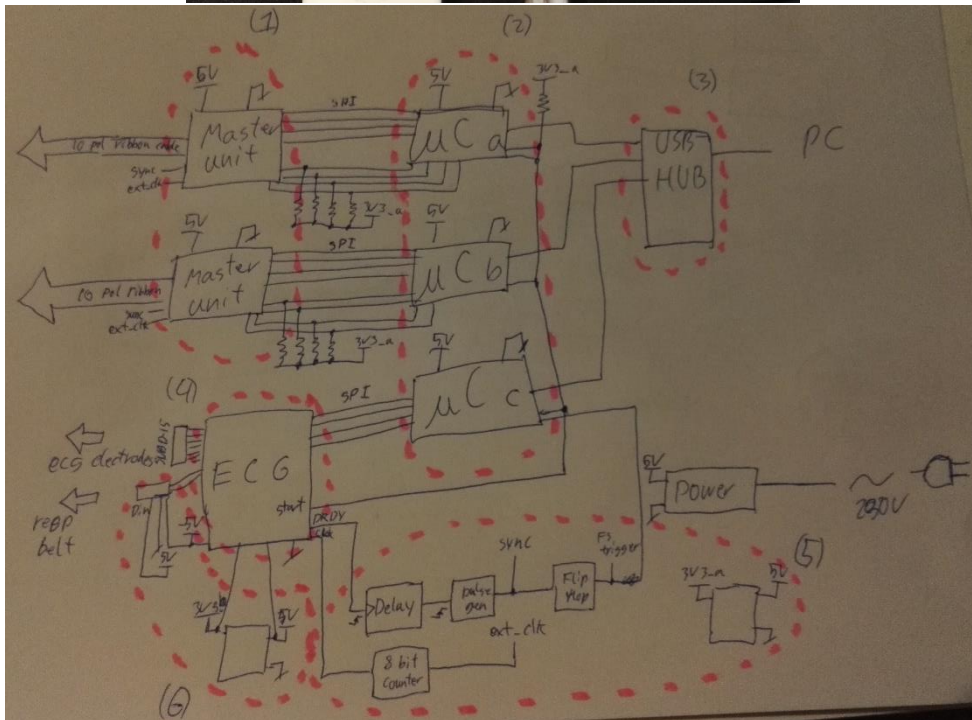
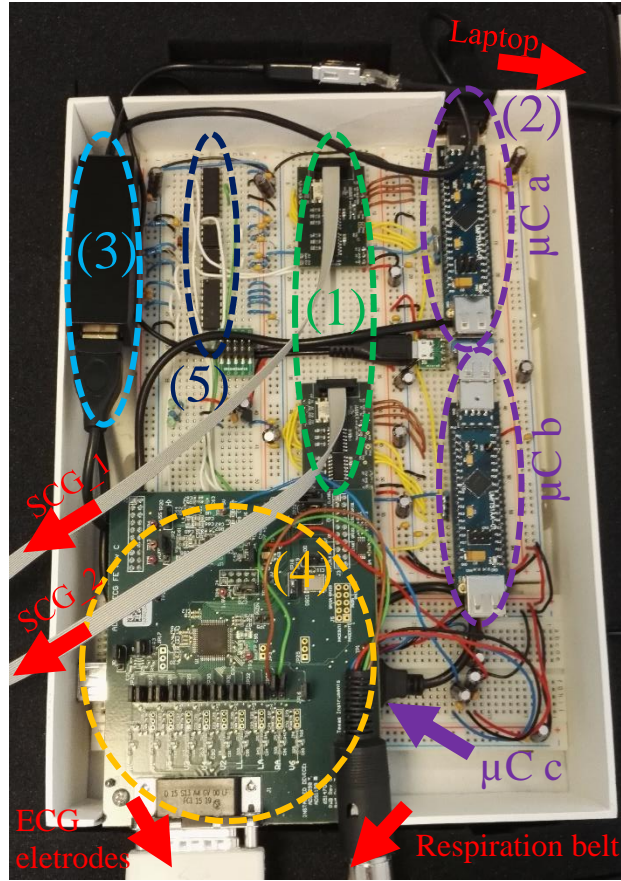


Figure 29 SPI protocol for reading multiple bytes from the ADXL355. A6-A0 is the register address and D7-D0 is each byte to read from the register

### 8.1. IMPLEMENTATION OF CENTRAL UNIT



### 8.1.1. MASTER UNIT

The master unit was designed to be the bridge between any micro controller that followed the SPI protocol and the sensors. The master unit includes a low noise power supply, SPI communication and the digital logic for the synchronize sampling and addressing of the sensors, as illustrated by Figure 30.

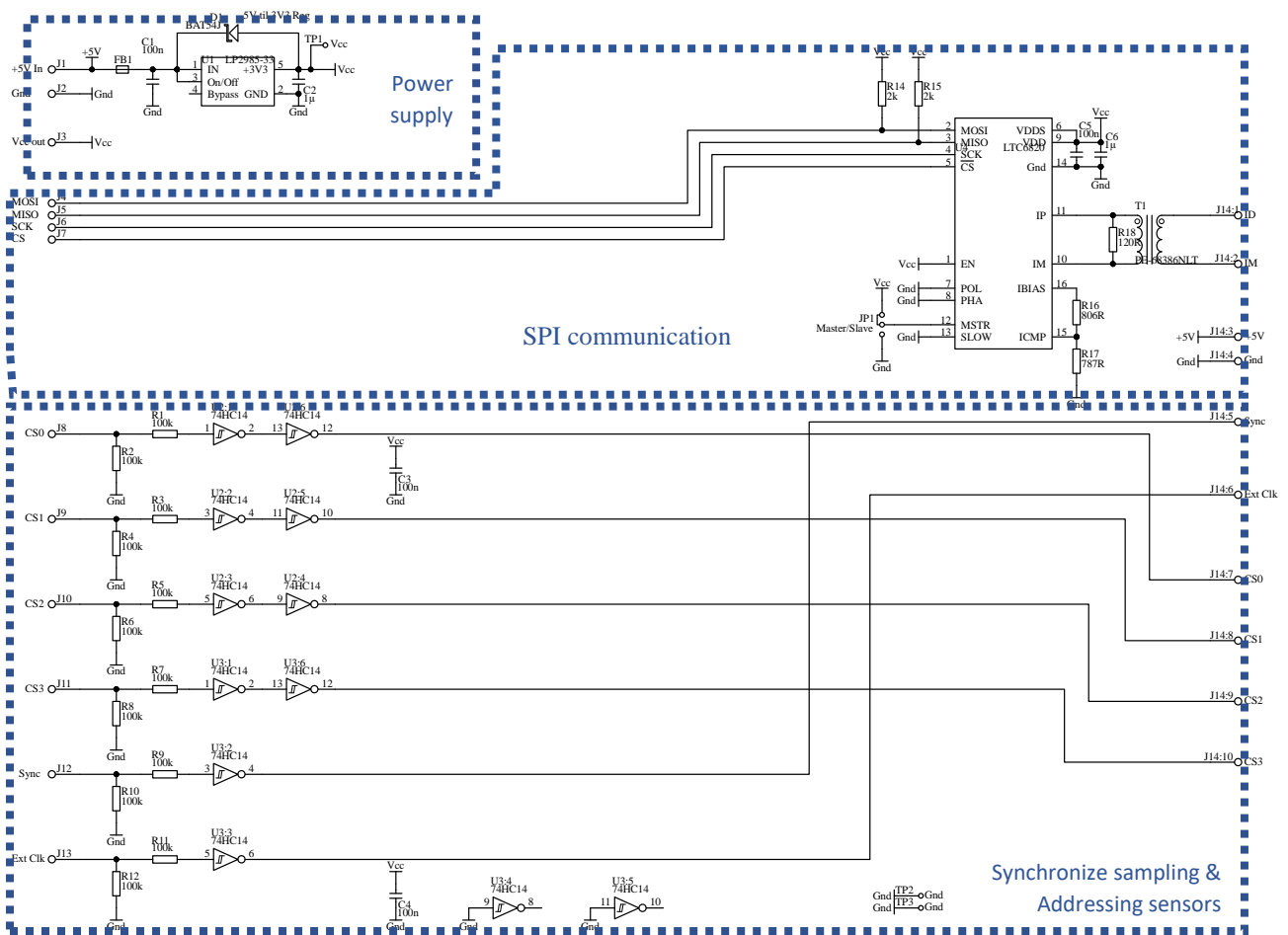


Figure 30 Circuit diagram of the Master unit with the three blocks of the design highlighted.

The Master unit was designed for use with a breadboard where each block was connected to their set of pin connectors and a ribbon cable socket for connection with the sensors. A 3D model of the Master unit board with connector marked are illustrated in Figure 31.

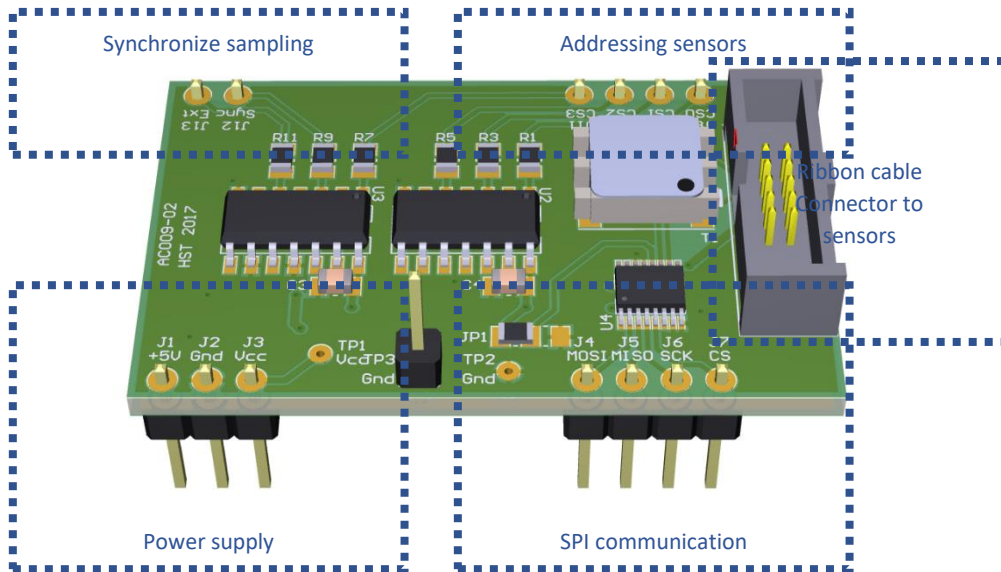


Figure 31 3D model of the Master unit along with marked board connection belonging to the blocks or the ribbon cable socket.

### Master unit debugging

Like the Sensors the Master unit also was designed with some debugging features. Among these features are test points and a method to switch between master and slave mode. By switching between modes, two Master unit could be used together without the sensors which made it possible to test the Master unit separately. However, in such a test setup only pin 1 and 2 of the ribbon cable would be connected between the two Master units.

### 8.1.2. $\mu\text{C}$ ELECTRICAL IMPLEMENTATION

The following 4  $\mu\text{C}$  connections were implemented on all the  $\mu\text{C}$  and the fifth connection was only implemented on the  $\mu\text{C}$  communicating with the ECG signal.

1. Power supply  
A 5V supply from a USB charger where used to power all the circuits including the  $\mu\text{C}$ . The reason for not using a direct power supply from the USB connected to the computer is due to a maximum initial load of 100 mA before the USB connection has been established. Circuits could have prevented powering of other devices than the  $\mu\text{C}$  before a connection would have been established, but this would also require additional programming time.
2. SPI communications connections to the master unit / ECG  
So that the  $\mu\text{C}$  would be able to program and collect data from the sensors and ECG, the 4-wire SPI connections were connected to the  $\mu\text{C}$  programmed to the corresponding leads (Chip Select, Source clock, Master In Slave Out, and Master Out Slave In).
3. Address select and pull up resistors to the master unit  
To be able to select which sensors to communicate with, the desired CS-address had to be selected by a 4-binary encoded signal. This was done by programming the pin connectors as digital output that could be set by the program and by adding pull up resistors on each pin.
4. The start signal triggering all  $\mu\text{C}$  in the system  
When a SCPI command starts measurements, it was important that all  $\mu\text{C}$  started collecting data. This was done by  $\mu\text{C}$ -a receiving the command and setting a digital output high, which in turn stated to all the  $\mu\text{C}$  that they would have to start the measuring of data. The ADS1298ECGFE-PDK also had a START pin that when set high would start converting samples, which also fitted the solution.

### 5. New ECG sample ready feedback to $\mu$ C

After the START pin of the ADS1298ECGFE-PDK was set high a data ready pulse would be send each time a new sample had been converted. By using this signal to trigger a flip flop, the system could determine if a new sample was ready for reading if the signal had changed.

Below is seen the code used for connecting the pin outside the  $\mu$ C with its internal functions:

```
void iomux(void) {
    IOMUX_RESET;
    IOMUX_ENABLE;
    IOMUX_CONFIG(IOMUX_CONFIG_x);
    // SPI Ma// 4-wire SPI
    IOMUX_OUTPUT(DIO_0, IOMUX_OUT_SPI_MASTER_SS_N_0); // CS
    IOMUX_OUTPUT(DIO_1, IOMUX_OUT_SPI_MASTER_SCLK); // SCLK
    IOMUX_INPUT(DIO_2, IOMUX_IN_SPI_MASTER_MISO); // MISO
    IOMUX_OUTPUT(DIO_3, IOMUX_OUT_SPI_MASTER_MOSI); // MOSI

    //CS addressing bits
    IOMUX_OUTPUT(DIO_8, IOMUX_OUT_PORT1_0); // CS_0
    IOMUX_OUTPUT(DIO_9, IOMUX_OUT_PORT1_1); // CS_1
    IOMUX_OUTPUT(DIO_10, IOMUX_OUT_PORT1_2); // CS_2
    IOMUX_OUTPUT(DIO_11, IOMUX_OUT_PORT1_3); // CS_3

    // Common  $\mu$ C start/stop signal
    IOMUX_OUTPUT(DIO_12, IOMUX_OUT_PORT3_4); // Start signal out
    IOMUX_INPUT(DIO_13, IOMUX_IN_PORT3_5); // Start signal in

    // New ECG sampler ready trigger
    IOMUX_INPUT(DIO_14, IOMUX_IN_PORT3_6); // FS trigger signal
}
```

### 8.1.3. USB HUB IMPLEMENTATION

One reason for selecting the UMFT51AA  $\mu$ C developer board was that they had a build in USB HUB. This meant that they could potentially be linked to gather as a chain reducing spaced needed and the complicity. However, due to some driver issues the  $\mu$ C could not be programmed as a USB HUB and still connect with the used Windows 10 computers. To solve this a separate USB HUB was used connect all the  $\mu$ C USB communication into one USB cable.

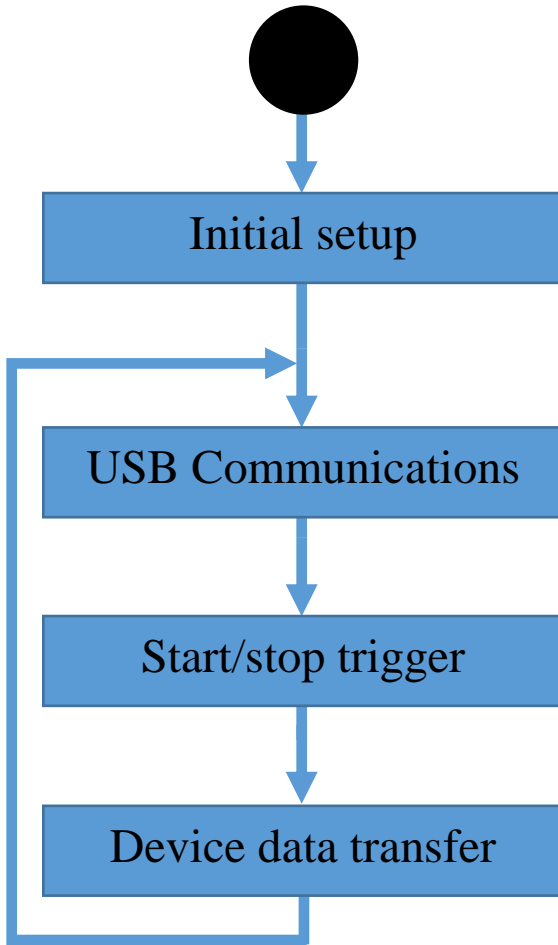
### 8.1.4. IMPLEMENTATION OF THE ADS1298ECGFE-PDK

The ECG developer board ADS1298ECGFE-PDK was implemented with the following four connections:

1. SPI communication to  $\mu$ C-c  
As mentioned before a 4-wire SPI protocol was used for communication between the ECG and  $\mu$ C-c.
2. START signal from  $\mu$ C-a  
The START signal that triggers a data collection on the  $\mu$ C, also starts the conversion of samples on the ADS1298ECGFE-PDK.
3. Data ready signal to trigger  $\mu$ C-c read of data and sensors converting a new sample  
Common on many SPI systems are the DRDY signal that is used for telling a  $\mu$ C that a new sample has been converted. This signal is used for both indicating to  $\mu$ C-c that a new sample is ready but also the trigger a conversion of samples on the sensors with a SYNC signal.
4. An external clock out used for synchronizing the Sensors



## 8.2. IMPLEMENTATION OF THE $\mu$ C PROGRAM



```
void select_CS_address(const int8_t CS) {  
    if (CS < 16) {  
        P1 = CS;  
    }  
    else{  
        P1 = 15;  
    }  
}
```

```

void ms_delay(int8_t delay) {
    uint16_t j, k;
    for (j = 0; j < delay; j++) {
        for (k = 0; k < 290; k++) {
            int volatile t = 120 * j + k;
            t = t + 5;
        }
    }
}

```

```

void main(void) {
    uint16_t j = 0; // used in for loops
    device_initialise(); // Initialize FT51A
    START_OFF();
    iomux(); // Setup the IOMUX to route signals to pins
    usb_setup(); // Initialize USB function
    SPI_setup(); // Initialize FT51A
    ms_delay(2); // Wait for 2ms to setup to complete
    for (j = 0; j < buffer_height; j++) {
        select_CS_address(j);
        meas_reset(); // Reset all sensors
    }
    ms_delay(50); // Wait for 50ms to reset to complete
    for (j = 0; j < buffer_height; j++) {
        select_CS_address(j);
        meas_setup(); // Program all the sensors
        // Make list of connected sensors
        scg_connected |= meas_find_connect() << j;
        pointer[j] = 2; // Clear buffer pointers
    }
    running = 0;
while (1) {

```

```

void main(void) {
    uint16_t j = 0; // used in for loops
    device_initialise(); // Initialize FT51A
    START_OFF();
    iomux(); // Setup the IOMUX to route signals to pins
    usb_setup(); // Initialize USB function
    SPI_setup(); // Initialize FT51A
    ms_delay(2); // Wait for 2ms to setup to complete
    ms_delay(100); // Wait for 150ms to let the ADS1298 startup
    meas_reset(); // Reset the ECG setup
    ms_delay(50); // Wait for 50ms to reset to complete
    meas_setup(); // Program the ECG
    running = 0;
while (1) {

```

```

do{
    USB_process(); // USB protocols and connections
    if (USB_get_state() == CONFIGURED) { // If USB connected
        tmc_process(); // Recive SCPI command or send data on request
    }
}while((cmdRespLen!=0)); // Continue in a loop until all requested data is send

```

```

do{
    USB_process(); // USB protocols and connections
    if (USB_get_state() == CONFIGURED) { // If USB connected
        tmc_process(); // Recive SCPI command or send data on request
    }
}while((cmdRespLen!=0) && (P3_6 != last_FS)); // Continue in a loop until all
requested data is send or a new ECG sample is ready

```

```

if (P3_5 && (running == 0)) { // First time START is set to high
    // Reset all relevant variables
    running = 1;
    bytes_read = 0;
    cmdRespLen = 0;
    DMA_ready = 1;
    DMA_active = 0;
    for (j = 0; j < buffer_height; j++) {
        pointer[j] = 2;
        select_CS_address(j);
        meas_start(); // Start measuring on all sensors
    }
    selected_scg = 0;
    select_CS_address(selected_scg);
} else if (!P3_5 && (running == 1)) { // First time START is set to low
    // Reset all relevant variables
    running = 0;
    bytes_read = 0;
    cmdRespLen = 0;
    while(DMA_ready==0);
    DMA_active = 0; //
    DMA_ready = 1;
    for (j = 0; j < buffer_height; j++) {
        select_CS_address(j);
        meas_stop(); // Stop measuring on all sensors
    }
}

```

```

if (P3_5 && (running == 0)) { // First time START is set to high
    // Reset all relevant variables
    running = 1;
    bytes_read = 0;
    cmdRespLen = 0;
    pointer = 2;
    last_FS = !P3_6;

} else if (!P3_5 && (running == 1)) { // First time START is set to low
    // Reset all relevant variables
    running = 0;
    bytes_read = 0;
    cmdRespLen = 0;
}

```

```

if ((P3_6 == last_FS) && (running == 1)) { // If there has been a sampling pulse
    bytes_read = meas_read(tempData); // Collect data from the ECG
    last_FS ^= 1; // Prepare to identify next new sample
    if (pointer < (buffer_size - bytes_read - 2)) { // If buffer is not full
        // Save collected data from ECG to the buffer
        memcopy(&dataBuffer[pointer], &tempData[3], bytes_read);
        pointer += bytes_read; // Update buffer pointer
    }
}

```

```

INT0_ISR(); // Check if the DMA is ready
if (running && DMA_ready && scg_connected) { // If the DMA is ready and a sensor
is connected
    if (bytes_read != 0) { // If data was collected during last
        memmove(&dataBuffer[selected_scg*buffer_width +
pointer[selected_scg]-1-bytes_read], &tempData[0], 1); // Paste wrongly
overwritten data
    }
    do { // Select the next sensor address that is connected
        selected_scg++;
        if (selected_scg == (buffer_height)) {
            selected_scg = 0;
        }
    } while ((scg_connected & (1 << selected_scg)) == 0);
    select_CS_address(selected_scg);

    DMA_active = 0; // Clear the DMA active register
    // If the buffer is not full
    if ( (pointer[selected_scg]) <= (buffer_width - maxBytesToTrans + 2) ) {
        memmove(&tempData[0], &dataBuffer[selected_scg*buffer_width
+ pointer[selected_scg]-1], 1); // Copy wrongly overwritten data
        bytes_read =
meas_read(&dataBuffer[selected_scg*buffer_width + pointer[selected_scg]-1] ); //
Collect data if more than 15 samples are ready
        if (bytes_read != 0) { // If data is being collected
            // Set the DMA active register
            DMA_active |= !DMA_ready << selected_scg;
            // Update the buffer pointer
            pointer[selected_scg] += bytes_read;
        }
    } else { // If buffer is full

```

```

uint16_t meas_read(char *buf) {
    uint16_t data_length;
    uint8_t t = 0;
    // Check how many samples are ready
    SPIM_transceive_ints(get_entries, din, 2);
    // Convert samples to number of bytes
    data_length = ((uint16_t)din[1]/3) * 3 * 3;
    if (data_length >= maxBytesToTrans){ // If more then 15 samples ready
        data_length = maxBytesToTrans;
        // Collect the 15 samples of SCG measurments
        SPIM_transceive_DMA(get_FIFO_first, buf, data_length+1);
    }else{
        data_length=0;
    }
    return data_length;
}

```

```

void scpi_cmd_measure(char * pBuffer) {
    unsigned char temp_byte;

    // Get channel data to send number from the SPCI command
    meas_channel = atoi(&pBuffer[6]);
    Resp_pointer = 0; // Clear BULK slice buffer pointer
    // if buffer is not empty and the DMA is not currentlty writing to it
    if ( (pointer[meas_channel]!=2) &&
        ((DMA_active & (1 << meas_channel) ) == 0)){
        cmdRespLen = pointer[meas_channel]; // Get buffer size
        pointer[meas_channel] = 2; // Clear the buffer

        // Write size of buffer into message uint16_t
        // Conver byte order from LSB to MSB
        temp_byte = (unsigned char) (cmdRespLen / 256);
        memcpy(&dataBuffer[meas_channel*buffer_width+0],
&temp_byte, sizeof(temp_byte));
        temp_byte = (unsigned char) (cmdRespLen % 256);
        memcpy(&dataBuffer[meas_channel*buffer_width+1],
&temp_byte, sizeof(temp_byte));
    }else{ // The buffer was empty or DMA was currently writing to the
buffer, send nothing
        cmdRespLen = 0;
    }
}

```

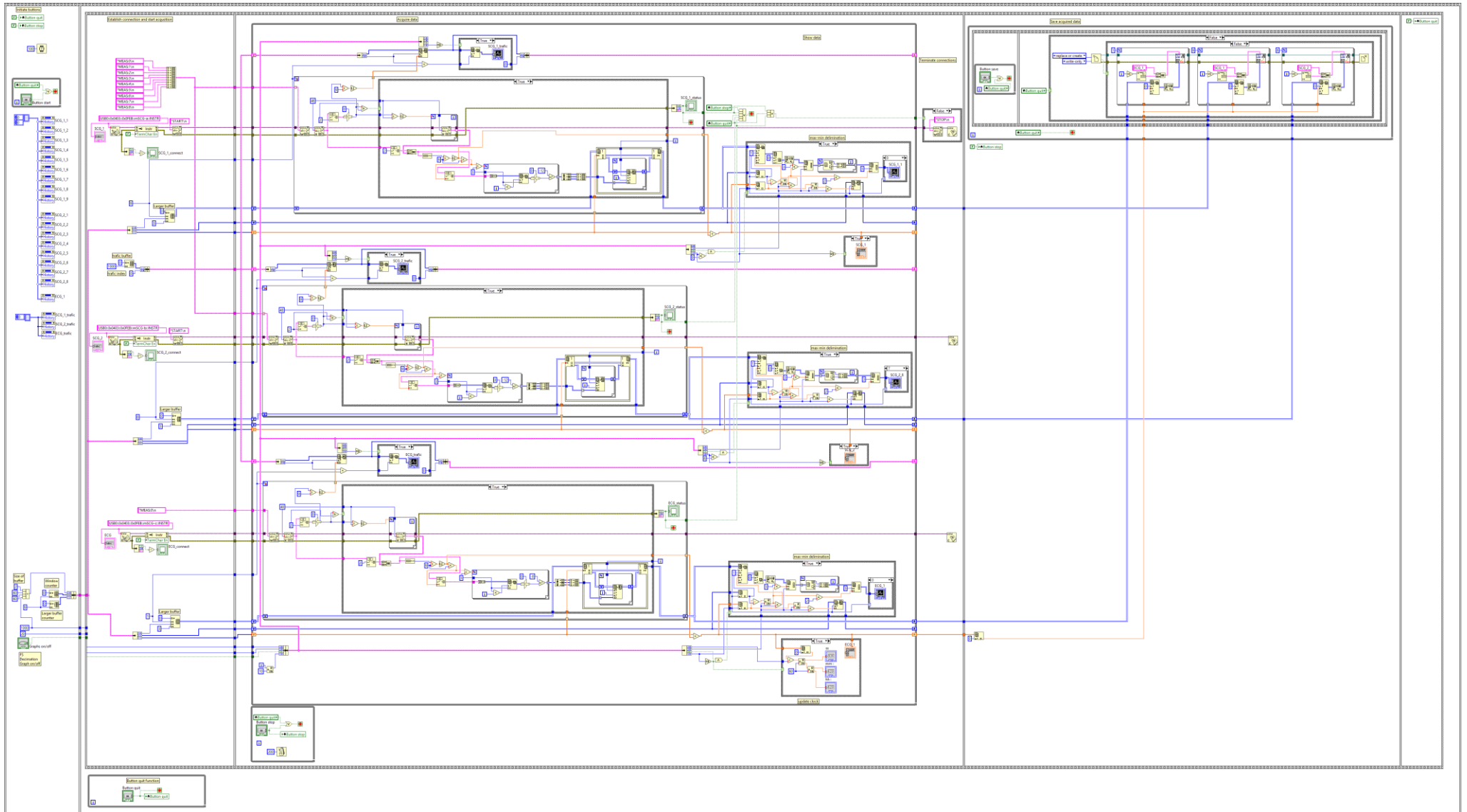
```

uint8_t tmc_response_cb(char *response) {
    uint8_t len;
    if (cmdRespLen > BulkDataSize) { // If there is more data than a BULK
        len = BulkDataSize; // Only send a BULK data slice
        cmdRespLen -= BulkDataSize;
    } else {
        len = cmdRespLen; // Else send the residual message
        cmdRespLen = 0;
    }
    // Copy the BULK data slice from the buffer into the USB endpoint
    memcpy(response, &dataBuffer[meas_channel*buffer_width+Resp_pointer],
len);
    Resp_pointer += BulkDataSize; // Update the BULK slice buffer pointer
    return len; // Return length of the message
}

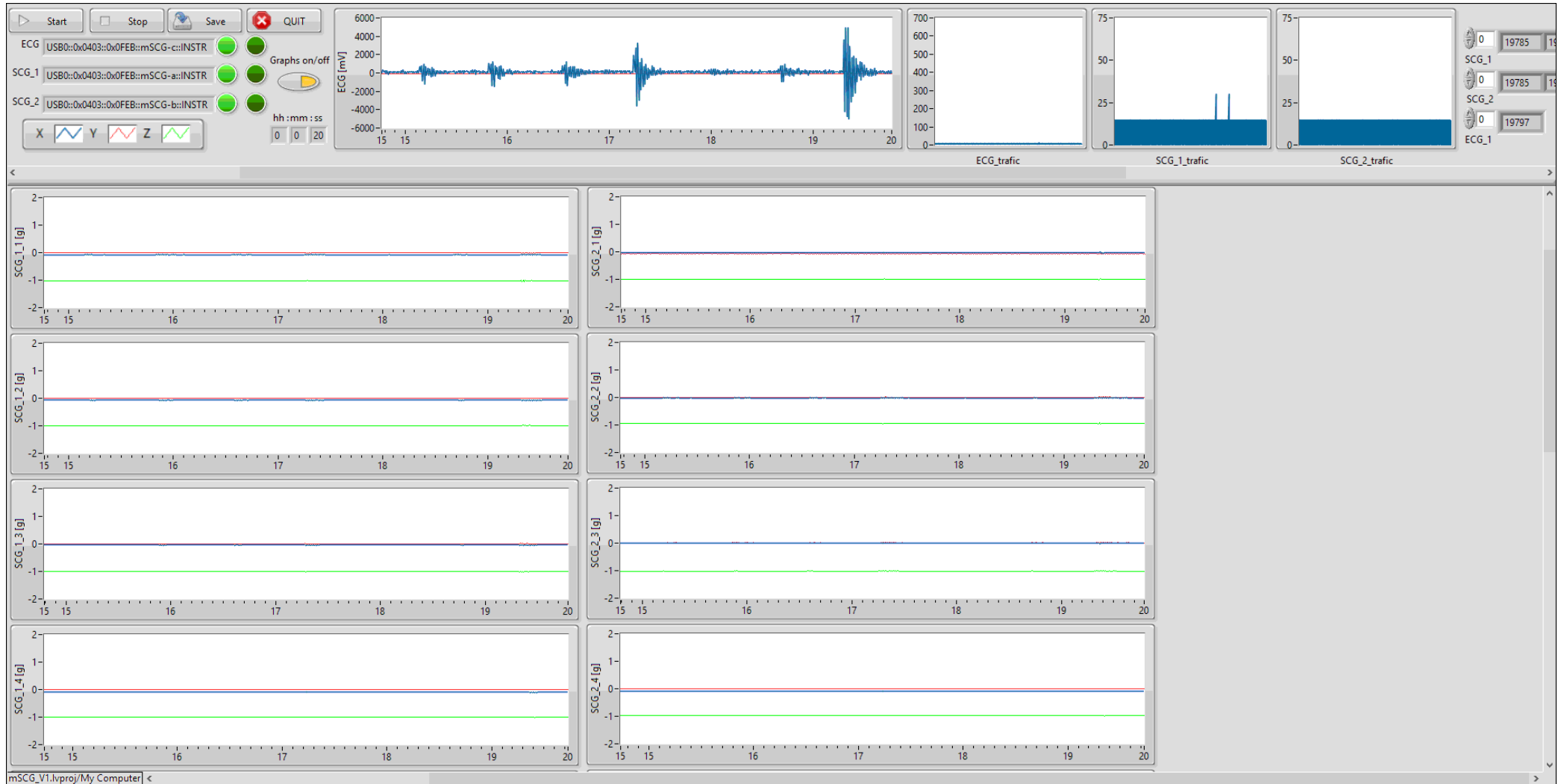
```

### 8.3. IMPLEMENTATION OF THE ACQUISITION SOFTWARE

DEVELOPMENT OF BODY SURFACE KINETIC MAPPING TECHNIC



CHAPTER 8 IMPLEMENTATION



## CHAPTER 9. TEST PROTOCOL

To test the equipment performance two test where conducted:

- Synchronization experiment
  - To test for the synchronization between sensors and between sensors and the ECG
- Signal characteristics investigation
  - To compare previous used accelerometers for SCG was the new design

### 9.1. SYNCHRONIZATION EXPERIMENT

It is important that each sensor, the ECG signal, and the respiration belt are sampled synchronous as described by the system specification. As described in Chapter 6, the two main reasons for proper synchronization of simultaneous sampled biological signals are: Alignment of signals during longer time periods and mapping of timed events.

In order to test the synchronization between the individual sensors and between the sensors, the ECG, and the respiration signal an experiment was designed, as illustrated by Figure 32.

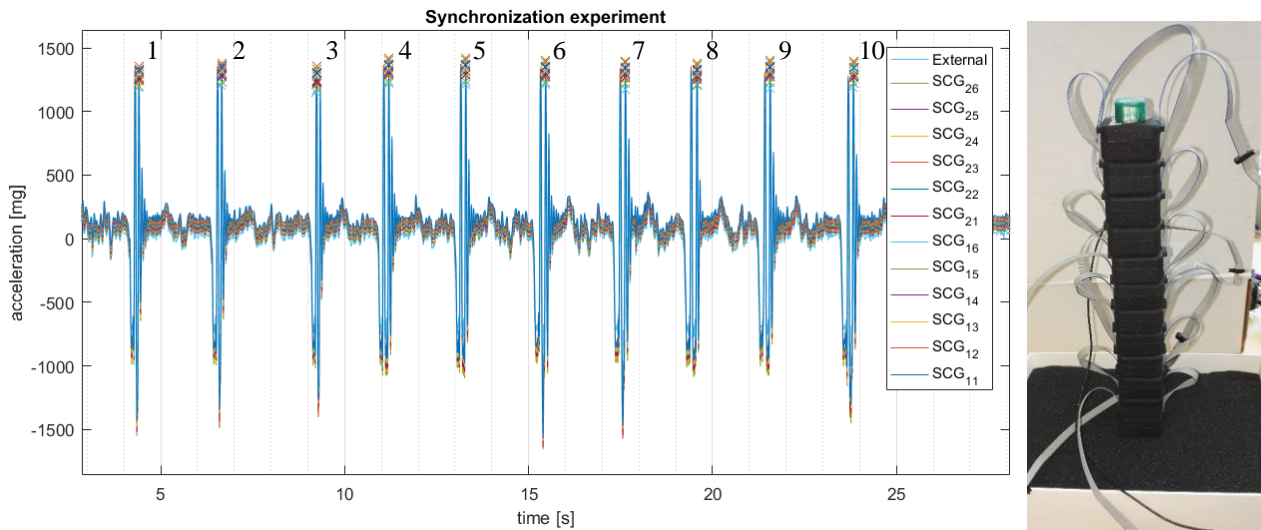


Figure 32 The graph illustrates measurements gathered during the equipment test experiments with the peaks of the ten times the accelerometers where dropped, detected, and numerated for future reference. The illustration on the right where the experimental setup, where sensors and external accelerometer where in the same order as the legend to the left

Each of the 12 sensors where stacked upon each other. To test for synchronicity between sensors and ECG an external accelerometer was connected to the ECG input and the sensors was put on the top of the stack. By dropping the stack of sensors and accelerometer from 10 cm down onto a foam pad, 10 times over a period of 25 seconds, the signals measured should the align if all the signals where properly aligned.

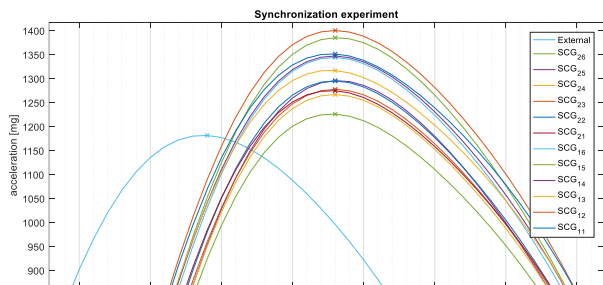


Figure 33 Illustration of a spike generated by the falling of a stack of sensors and an external accelerometer, along with the detected peaks

For each of the acceleration spikes, generated when the stack hit the foam pad, a corresponding peak where detected, as illustrated by Figure 33. To measure how well the sensors where synchronized the standard deviation of the time of each peak was calculated, in Figure 33 this would give  $\pm 0$  ms.

To investigate the alignment of the external accelerometer, and thereby the ECG signal, the difference between the average sensor and the external accelerometer where

calculated for each detected peak, in Figure 33 this would give -9 ms.

## **9.2. SIGNAL CHARACTERISTICS INVESTIGATION**

To compare the performance of the designed SCG sensors, a similar analysis of the PSD of the pilot study, where conducted. By comparing the PSD of a SCG signal measured with the designed equipment, and the measurements from the control and CRT group, the relationship between the signal strength and background noise levels can be computed. Both the control, CRT and equipment SCG signals compared where measured at the xiphoid process.

That data used in the pilot study and compared with here was gathered from a previous study (Jensen et al. 2014).

However, since these signals where not collected from the same persons and due to the small subject group measured on by the designed equipment, this would not be an ideal comparison but more a general picture of the conditions.

To best compare the signals an average PSD was computed by segmenting the signal into 60 segments of 10 seconds each. Similar as the pilot study calculated the average PSD of segmented beats.

In the results chapter the PSD of each of the three subjects were presented along with their average PSD and a comparison of the control group, CRT group, and experiments average PSD.

## CHAPTER 10. STUDY DESIGN

To answer the problem formulation a study was designed that would include the designed and implemented mSCG equipment and measurements conducted on healthy control subjects and CRT patients. The study protocol was approved by the local ethical committee (N-20170008). The protocol is attached in Appendix C.

Due to time limitations of this project the study in the study was conducted using fewer accelerometers and included three healthy subjects.

### 10.1. PURPOSE

The main objective was to investigate the potential of mSCG and how it relates to the mechanical function of the heart. The hypotheses were that by investigating the amount of additional information mSCG could contribute with about the mechanical function of the heart.

### 10.2. SUBJECTS

For this study healthy control group were desirable that meet with the following:

Inclusion criteria:

- Male
- 20 to 80 years of age

Exclusion criteria:

- Known cardiovascular diseases including subjects receiving cardiovascular-related medications such as medication for hypertension and hyperlipidemia
- Lack of ability to cooperate

### 10.3. DESIGN AND METHODS

The study was conducted as follows:

- Equipment setup
- Relaxation period (10 minutes)
- Relaxed (5 minutes)
- Removing equipment

For the equipment setup, the SCG sensors were placed in a grid formation relative to the xiphoid process. The grid was 3 by 4 sensors and placement of SCG sensors, ECG electrodes and respiration belt was illustrated by Figure 34.

Photographs of how SCG sensors, ECG electrodes, respiration belt and wires were connected for all three subjects was illustrated by Figure 35.

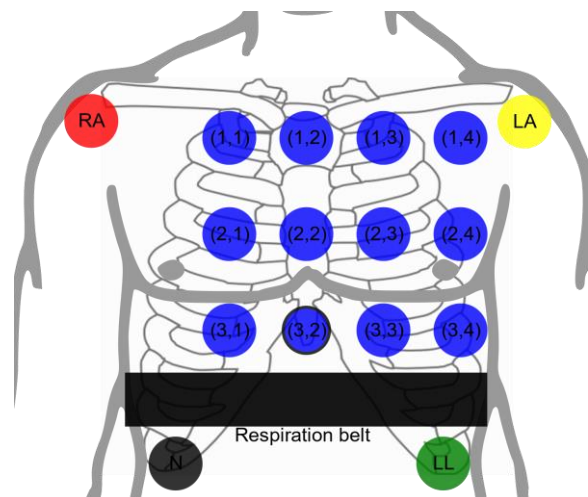
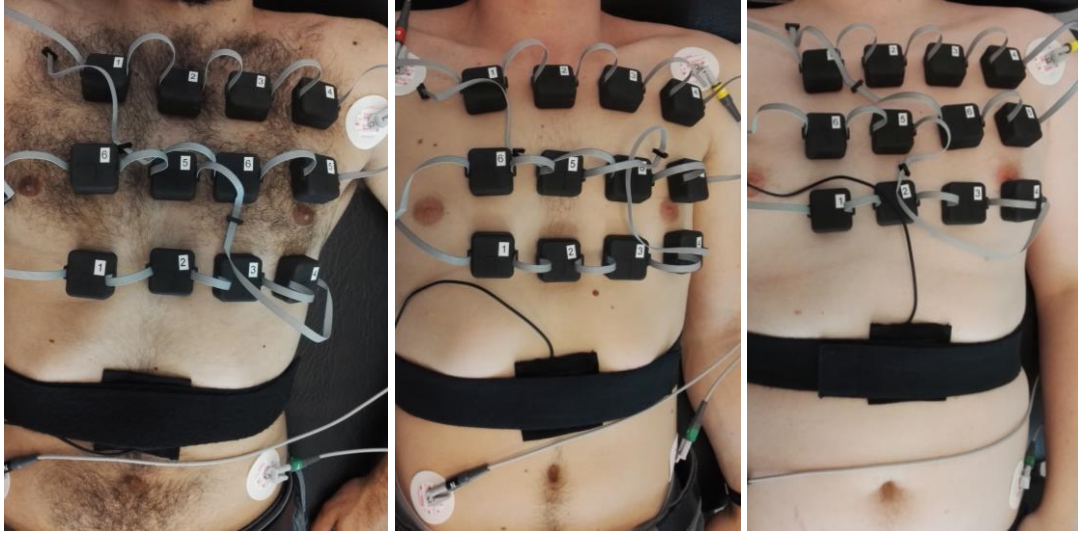


Figure 34 Illustration of the placement of accelerometers, ECG electrodes and respiration belt. This illustration relates to the graphs and maps in results



*Figure 35 Photographic illustration of study setup with the 3 included subject, starting with subject 1 to the left, subject 2 in the middle and subject 3 to the right. Illustration documents the placement of individual sensors and respiration belt*

## CHAPTER 11. DATA PROCESSING

As described by the study protocol, the hypotheses were that “by investigating the amount of additional information mSCG could contribute with about the mechanical function of the heart.”. To answer the hypotheses the following data process was applied to data from the three subjects.

The process used to analyze the 10 minutes of data from 12 single axis accelerometers, two lead ECG and respiration belt is illustrated on Figure 36. First a 45 Hz low pass filter was applied to the ECG signals where only lead II was included for further signal processing. For the heart sound signals the mSCG was all band pass filtered at 20 to 250 Hz. For the force signals the mSCG was all band pass filtered at 0.5 to 30 Hz. Then through visual inspection all signals of 10 minutes were segmented into one segment of approximately 5 heart beats.

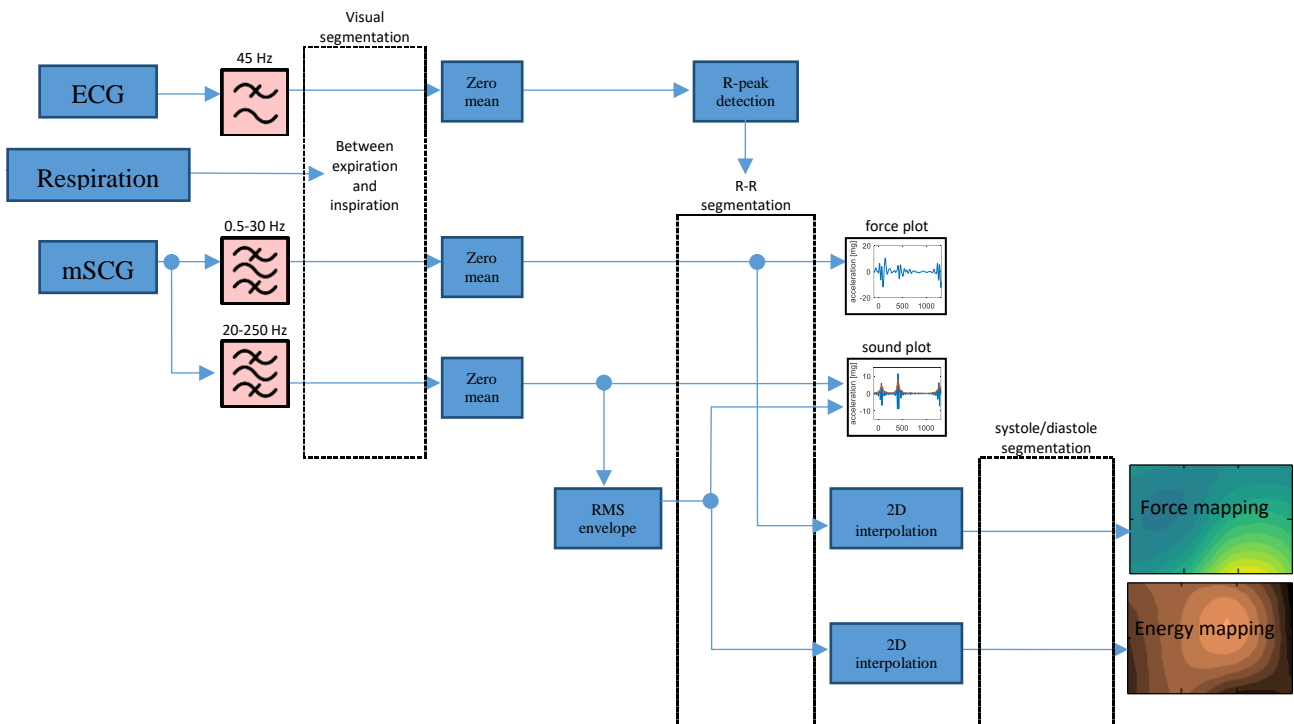


Figure 36 Blockdiagram illustrating the data processing of data collected in the study design by the developed novel method for multichannel seismocardiography

The mean was subtracted from all the signals for better comparison and the R-peak was detected with the Pan Tompkins algorithm. From the band pass filtered signal an envelope RMS was calculated to represent the energy of the heart sounds. The R-peak detection were then used to further segment and to define a time line of a single heart cycle. Signals from the 20 to 250 Hz signals along with the energy of the signal and the ECG is presented in results 12.2.

Signals from the 0,5 to 30 Hz signal was illustrated as the forces involved in a heart cycle in along with the ECG and the heart sounds measured at the xiphoid process and the energy of the heart sound, was presented in results 12.3.

To further investigate these signal, the Body Surface Kinetic Maps were composed from the mSCG signal. The BSKM were images derived from information in all the mSCG signals at specific time point relative to the R-peak. In the process of composing the BSKM, the mSCG were interpolated by a 2D interpolation method based on cubic to improve the resolution of these images, so that there would be 315 pixels instead of the original 12 pixels. A complete set of BSKM for each subject was presented in Appendix D. To better investigate the BSKM, they were further segmented into systole and diastole, due to an amplitude difference of the two episodes.

Two types of maps were used for mapping the low frequency signals and the higher frequency signals.

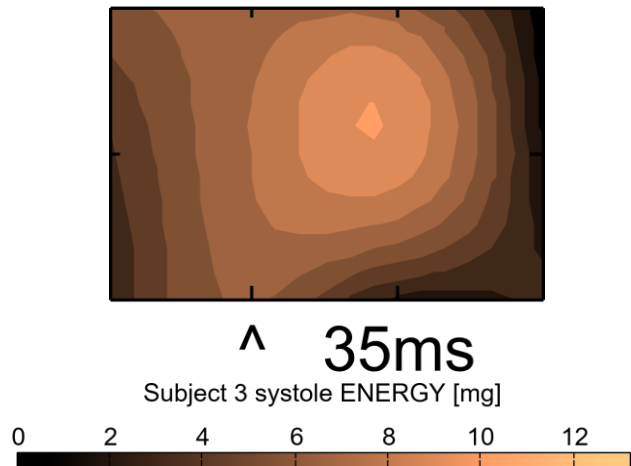
- Energy mapping
- Force mapping

### 11.1. ENERGY MAPPING

For representing how the energy of the heart sounds was distributed at different time points a copper colormap was selected. Each of the tick marks and the corners represent the original measuring sites, along with the intersecting two tick lines in the middle of the maps.

For the energy maps 11 levels was selected for the representation of the magnitudes. The last level represented the maximum energy within the currently represented segment. The marking of “^” defines where the xiphoid process is in the measurements, due to its more common measuring site by the literature.

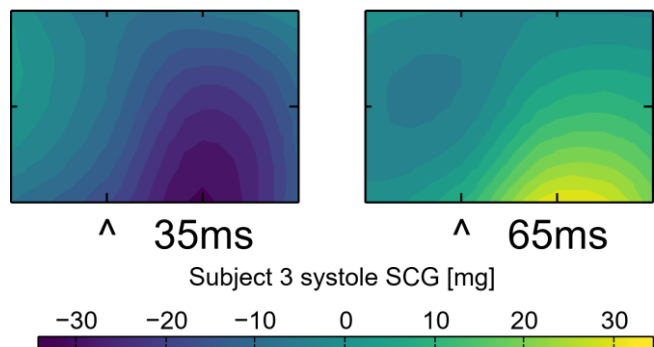
For each map, the specific time relative to the R-peak noted, next to the “^” symbol.



### 11.2. FORCE MAPPING

The force maps follows the same principal of markings and notations as the energy maps. However, since these signals can be of a negative nature the colormap “viridis” was selected.

For the force maps 21 levels were selected for the representation of the magnitudes, meaning one represented close to zero values and then 10 levels in each direction represented the magnitudes. Here the maximum absolute value of the current segment was the highest level of the maps.



## CHAPTER 12. RESULTS

In the following chapter, results from the equipment experiments and the designed study is presented. The equipment experiments include a test to investigate the equipment ability to synchronize the acquired signals. The equipment experiments also include an analysis of the sensors performance that may be compared to the similar pilot study on signal specifications.

The results from the designed study where presented in two sub sections. The first section focuses on the higher frequency heart sounds and how their energies would be distributed over time onto the chest.

The last results where the mapping of the forces applied to the chest by the heart in respect to time.

### 12.1. RESULTS FROM THE SYNCHRONIZATION EXPERIMENT

According to the design of the sensors, in section 7.1, this design should give a synchronization between sensors of less than  $\pm 16 \mu\text{s}$ . However, the test showed a precision of  $\pm 140 \mu\text{s}$ , as illustrated by Table 16.

The lag between sensors and ECG channel was consistent over the full test period, as illustrated by Table 16. The 9 ms lag between sensors and ECG was accounted for in any further results.

*Table 16 The results from the equipment test experiment for each individual detected peak, numerated by Figure 32, and the collective results*

<b>Numerated peaks</b>	<b>Standard deviation of lag between sensors</b>	<b>Lag between average sensors to the ECG channel accelerometer</b>
<b>1</b>	$\pm 0 \text{ ms}$	9 ms
<b>2</b>	$\pm 0 \text{ ms}$	9 ms
<b>3</b>	$\pm 0.85 \text{ ms}$	5.7 ms
<b>4</b>	$\pm 0 \text{ ms}$	8 ms
<b>5</b>	$\pm 0 \text{ ms}$	9 ms
<b>6</b>	$\pm 0.28 \text{ ms}$	8.1 ms
<b>7</b>	$\pm 0.37 \text{ ms}$	8.8 ms
<b>8</b>	$\pm 0.37 \text{ ms}$	8.2 ms
<b>9</b>	$\pm 0 \text{ ms}$	9 ms
<b>10</b>	$\pm 0.28 \text{ ms}$	8.9 ms
<b>Median</b>	$\pm 0.14 \text{ ms}$	8.9 ms

### 12.1. RESULT FROM SIGNAL CHARACTERISTICS INVESTIGATION

Three subjects were included in this study where measurements from the most typical measuring site of SCG, at the xiphoid process, was compared by their PSD with SCG signals acquired by different equipment from a control and CRT group. The PSD and average PSD of subject 1, 2, and 3 were illustrated by Figure 37, Figure 38, and Figure 39, along with a sample of the SCG signal.

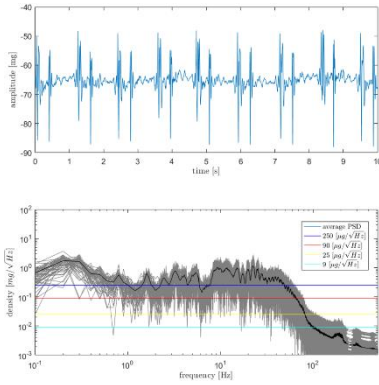


Figure 37 A raw SCG segment signal at the top and the Power Spectral Density (PSD) of individual segments of 10 seconds each and their average PSD, measured with a sensor on subject 1's xiphoid process

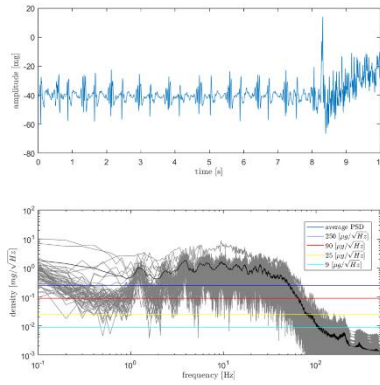


Figure 38 A raw SCG segment signal at the top and the Power Spectral Density (PSD) of individual segments of 10 seconds each and their average PSD, measured with a sensor on subject 2's xiphoid process

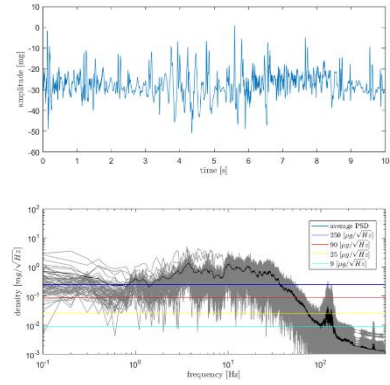


Figure 39 A raw SCG segment signal at the top and the Power Spectral Density (PSD) of individual segments of 10 seconds each and their average PSD, measured with a sensor on subject 3's xiphoid process

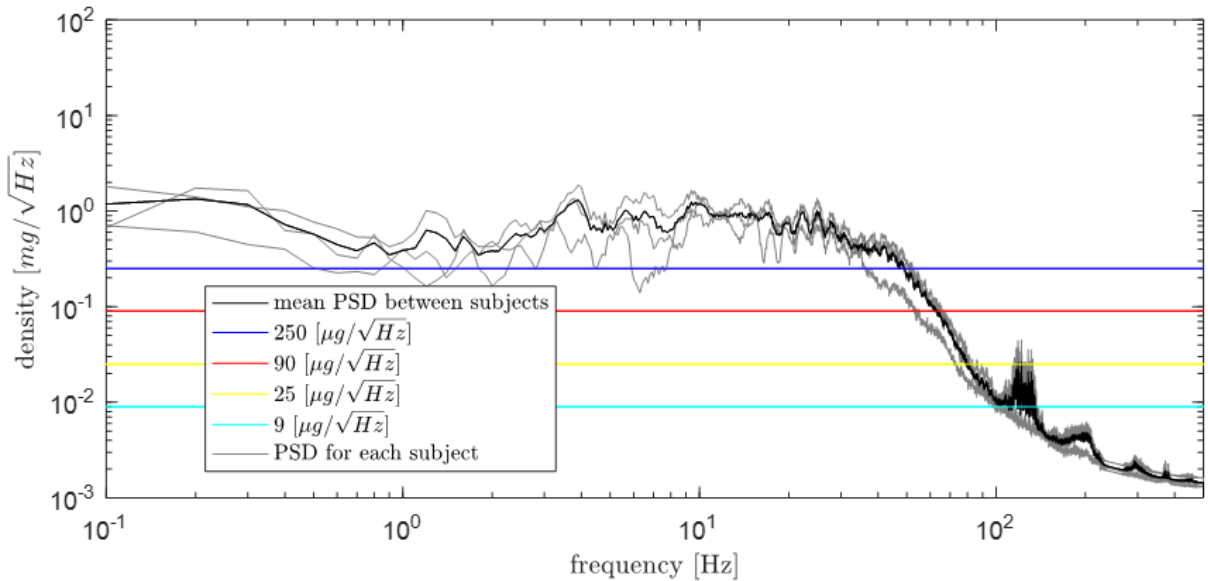


Figure 40 The average Power Spectrum Density for each subject in the study along with the average between all subjects and markers for the different noise levels investigated by the pilot study

One of the features of the PSD for all the subjects where the built in 250 Hz low pass filter of the sensors and a signal density above  $90 \mu\text{g}/\sqrt{\text{Hz}}$ .

When comparing the average PSD between subject in Figure 41, one large difference is that the pilot study groups did not have a built in 250 Hz low pass filter, but that some of the similar signal attributes were present above this frequency on all groups. Signal densities were closely related to that of the pilot study control group and the noise floor was not clearly present due to the 250 Hz low pass filter. However, some indications point to a less noise SCG signal than that of the previous equipment.

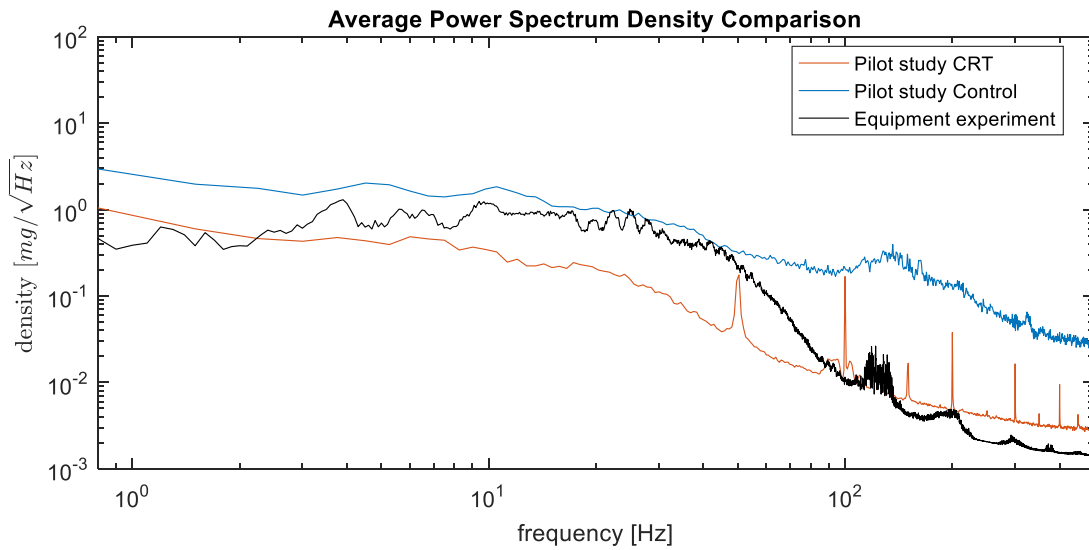


Figure 41 The average Power Spectrum Density between subjects of SCG signals from the study group, pilot study control group, and pilot study CRT group

## 12.2. HEART SOUND SIGNALS

When investigating the SCG signals from each measuring sites, filtered to only reveal the heart sounds certain differences and resemblance appears between the subjects. These signals are presented by Figure 42, Figure 43, and Figure 44 along with the ECG signal.

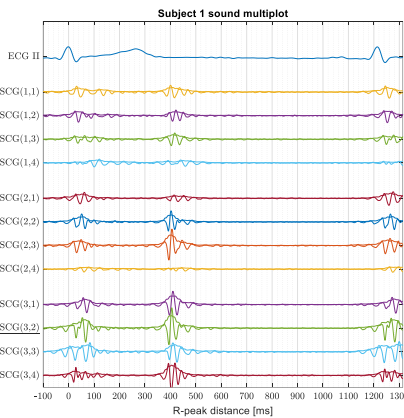


Figure 42 One heart cycle of the ECG signal and all SCG measurements from subject 1, bandpass filteret at 20 to 250 Hz

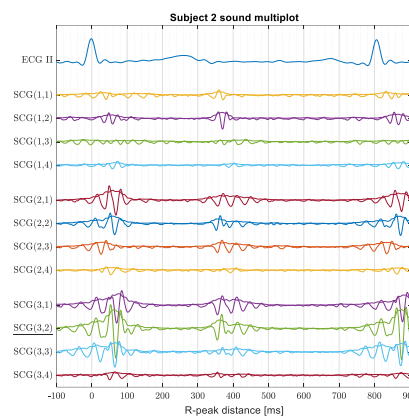


Figure 43 One heart cycle of the ECG signal and all SCG measurements from subject 2, bandpass filteret at 20 to 250 Hz

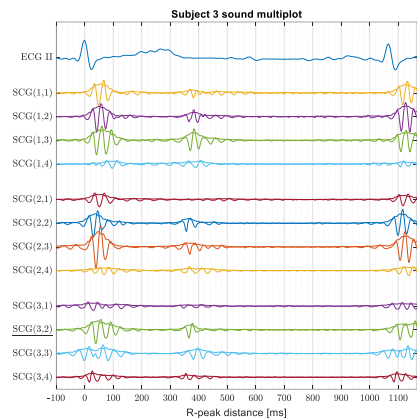


Figure 44 One heart cycle of the ECG signal and all SCG measurements from subject 3, bandpass filteret at 20 to 250 Hz

### 12.2.1. ENERGY MAPPING DURING SYSTOLE

Maps of the energy of the S1 heart sound during systole was illustrated for subject 1, 2, and 3 by Figure 45, Figure 46, and Figure 47, respectively.

Similar for all the heart sound energy maps where that the first signs of a S1 appears near 45 ms before the R-peak. For subject 1 and 2 this origin of the S1 appears on the lower sensors and close to the xiphoid process. For subject 3 the origin of S1 appears a little higher and a little to the left of the sternum. Shortly after the R-peak, the energy of S1 distributes more across the chest area for all subjects. After this the energy of S1 dissipates, but is kept for a longer period at the sensors at the edge of the sensor grid. Similar for all subject where that the site of the first sign of energy in S1 would also be close to the peak energy of S1.

Complete sequence of heart sound energy maps for each subject can be found in Appendix D, without the segmentation of systole and diastole.

Subject 2 should be the one where the tricuspid and mitral valves heart sound should be the easers the distingue, due to a slightly visible S1 split. From frames a 0 ms to 35 ms, in Figure 43, it would seem that two sources could be present. One left of sternum and the other right of sternum, most clear on the sensors (2,1) and (2,3) respectively.

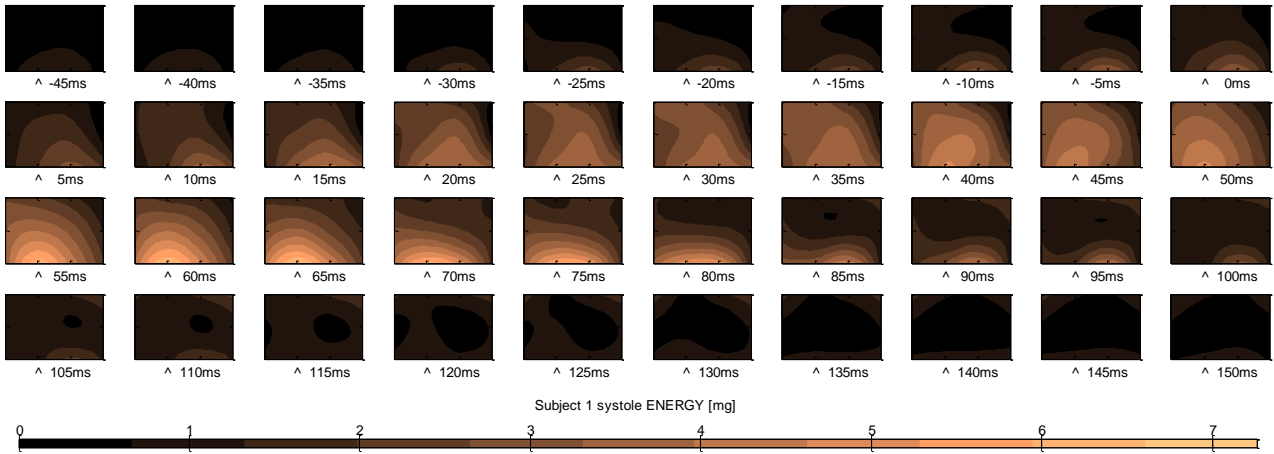


Figure 45 Energy maps of the heart sounds bandpass filteret at 20 to 250 Hz durring the systole of the heart cycle. Maps are a representation of the multi channel SCG signals from subject 1 of this study

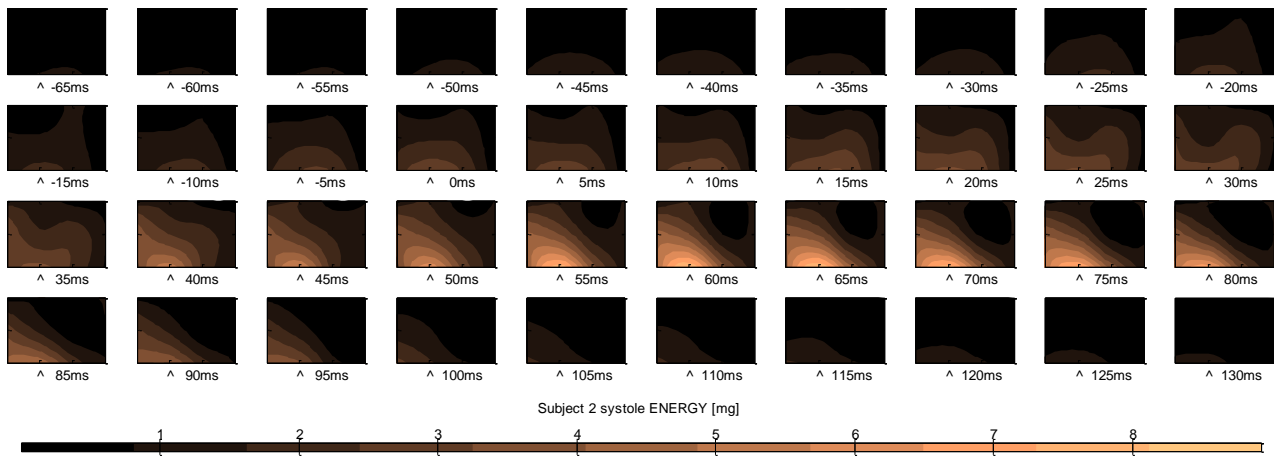


Figure 46 Energy maps of the heart sounds bandpass filteret at 20 to 250 Hz durring the systole of the heart cycle. Maps are a representation of the multi channel SCG signals from subject 2 of this study

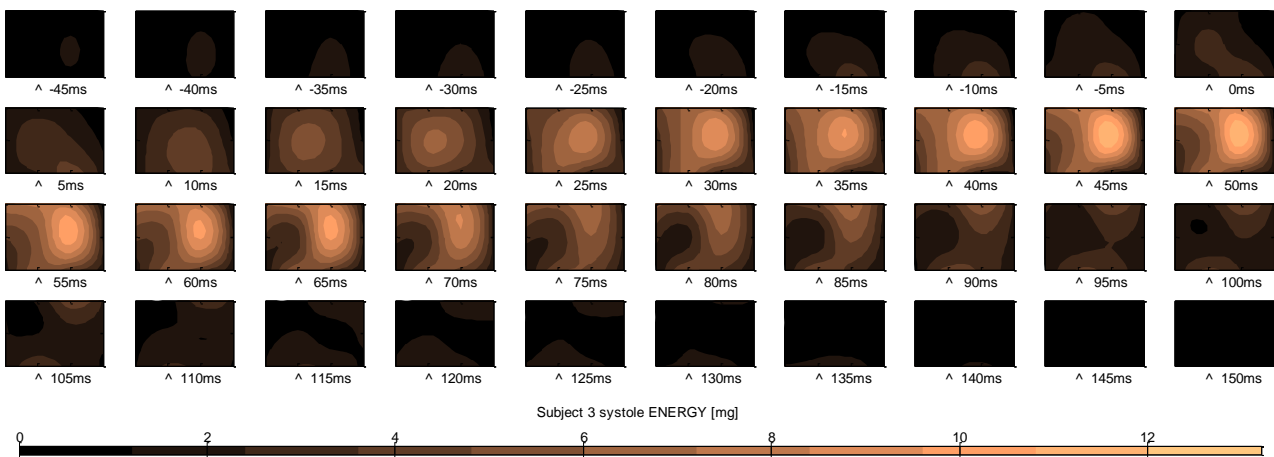


Figure 47 Energy maps of the heart sounds bandpass filteret at 20 to 250 Hz durring the systole of the heart cycle. Maps are a representation of the multi channel SCG signals from subject 3 of this study

### 12.2.2. ENERGY MAPPING DURING DIASTOLE

Maps of the energy of the S2 heart sound during diastole was illustrated for subject 1, 2, and 3 by Figure 48, Figure 49, and Figure 50.

Similar for all the heart sound energy maps where that two sources of the S2 heart sound appears to be visible on the maps. For all the subjects, one of the sources of S2 appears to be located near the xiphoid process. For subject 2 and 3 the second source of S2 appears near the highest row of sensors and for subject 1 it seems to be closer to the mid row of sensors. After this the energy of S2 dissipates, but is kept for a longer period at the sensors at the edge of the sensor grid, like that of S1.

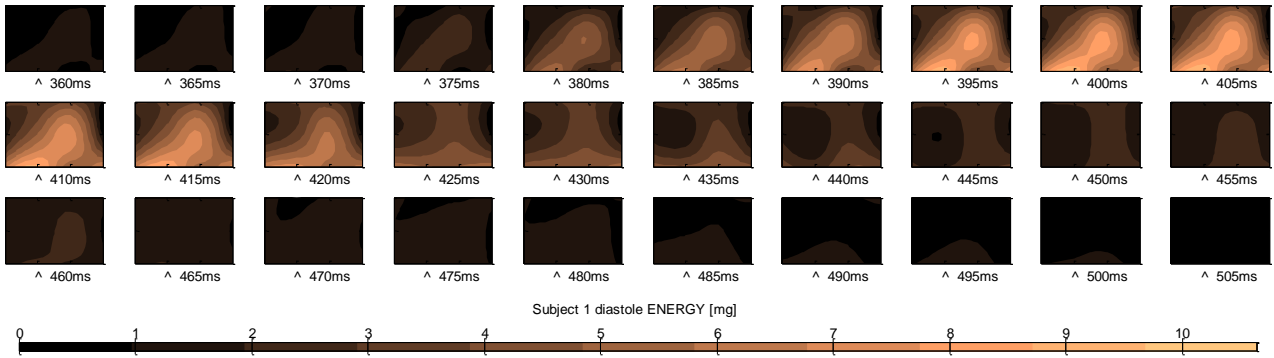


Figure 48 Energy maps of the heart sounds bandpass filteret at 20 to 250 Hz durring the diastole of the heart cycle. Maps are a representation of the multi channel SCG signals from subject 1 of this study

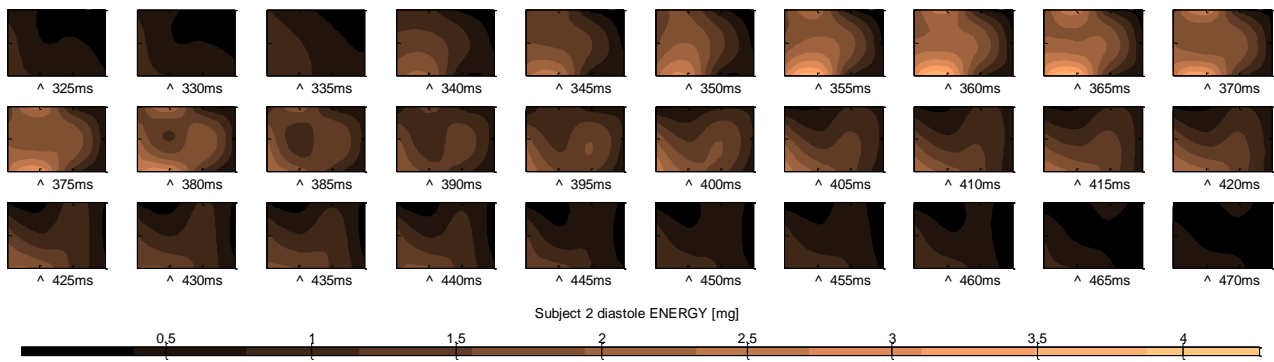


Figure 49 Energy maps of the heart sounds bandpass filteret at 20 to 250 Hz durring the diastole of the heart cycle. Maps are a representation of the multi channel SCG signals from subject 2 of this study

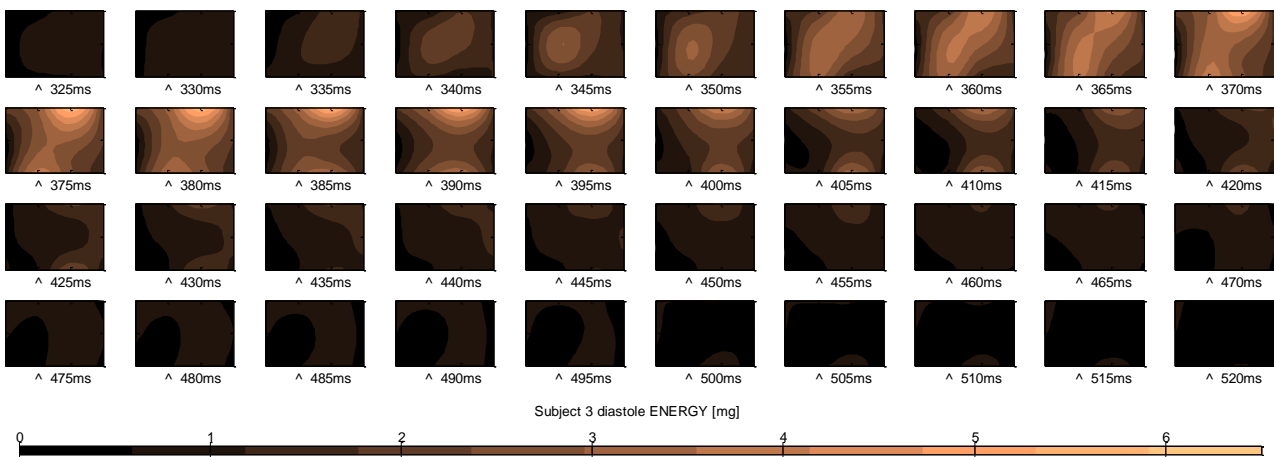
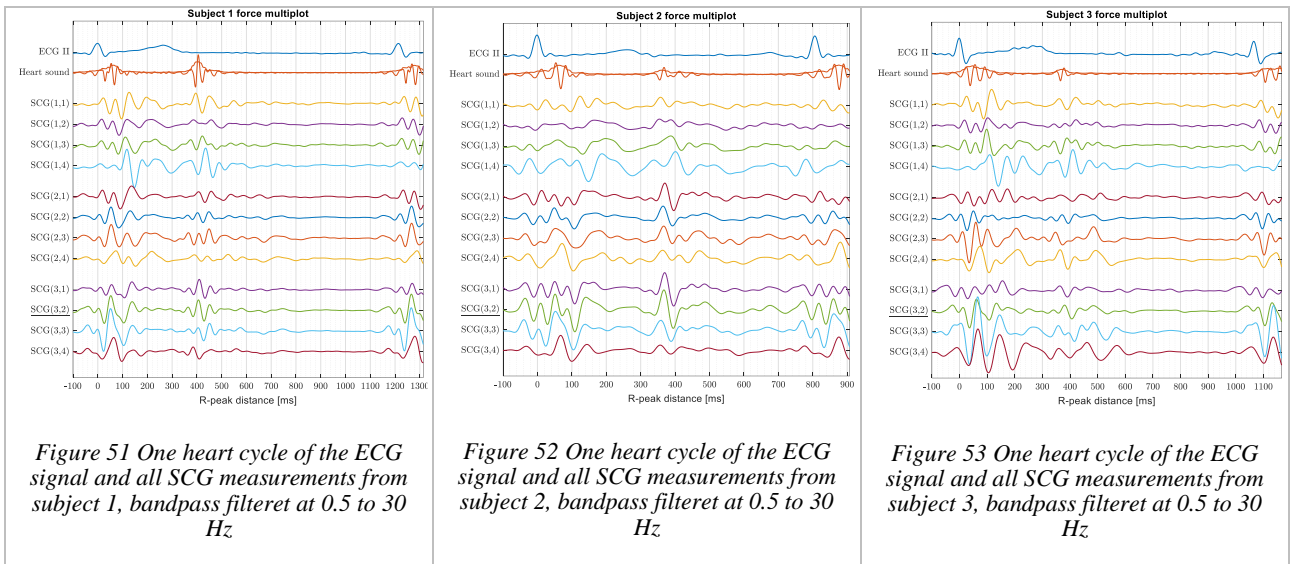


Figure 50 Energy maps of the heart sounds bandpass filteret at 20 to 250 Hz durring the diastole of the heart cycle. Maps are a representation of the multi channel SCG signals from subject 3 of this study

### 12.3. SCG SIGNALS

When investigating the SCG signals from each measuring sites, filtered to only reveal the low frequency forces, certain differences and resemblance appears between the subjects. These signals were presented by Figure 51, Figure 52, and Figure 53 along with the ECG signal.

For all subject two distinct patterns were present. One during the first part of the signals (systole) and one at the same time as the S2 heart sound.



All force signals at the xiphoid process seems to follow the same pattern during the systole, as illustrated by Figure 54. According to the pattern the period before the R-peak would consist of two minor waves. Right after the R-peak would be followed by a strong negative force going inwards followed by a strong and long outgoing force at approximately 50 ms. The strong outgoing force would be followed by a small ingoing force, at 100 ms, then outgoing force, at 150 ms, and at 200 ms the oscillations would dissipate.

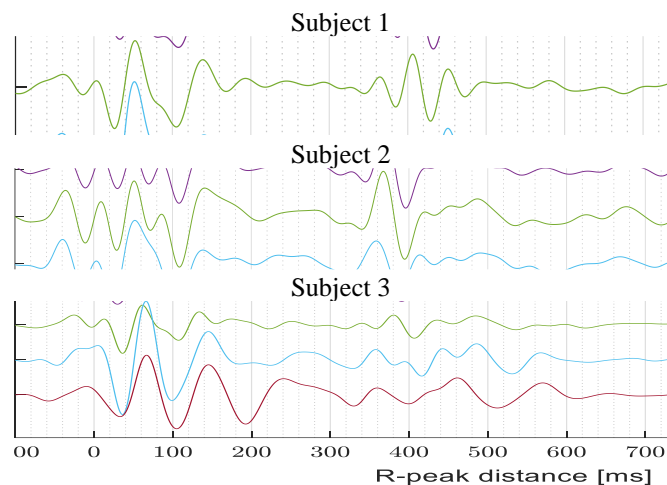


Figure 54 The three graphs shows the SCG signals measured at the xiphoid process, as the green line. Each graph are for each subject and their time axis where aligned for better comparison

Complete sequence of force maps for each subject can be found in Appendix D, without the segmentation of systole and diastole.

### 12.3.1. FORCE MAPPING DURING SYSTOLE

Similar for all the force maps during the systole of the SCG signal where that they shared a common pattern. The pattern is listed below and marked by numbers on Figure 55, Figure 56, and Figure 57, that represent the force maps for each subject during the systole.

1. Neutral state
2. Posterior force near sternum
3. Short neutral state
4. Anterior force near sternum
5. Two new opposite forces (opposite forces 1)
6. Short neutral state
7. Two new opposite forces (opposite forces 2)
8. Neutral state

Two features were of significant interest since this was only apparent once multiple sites were measured simultaneously. These features were when the forces of the signals at different sites were opposite each other. The direction of these opposite forces was also marked on Figure 55, Figure 56, and Figure 57.

For the first opposite forces, both subject 1 and 2 had a direction going from left to right. However, this first opposite force change for subject 1 to a down going direction like that of subject 3.

The second opposite forces, both subject 1 and 2 had a direction going from lower right to upper left. Subject 3, however, experienced a force direction going upwards on the left side of the maps.

Similar for all subjects were that the beginning direction of the first opposite forces were in the reverse direction of the second opposite forces.

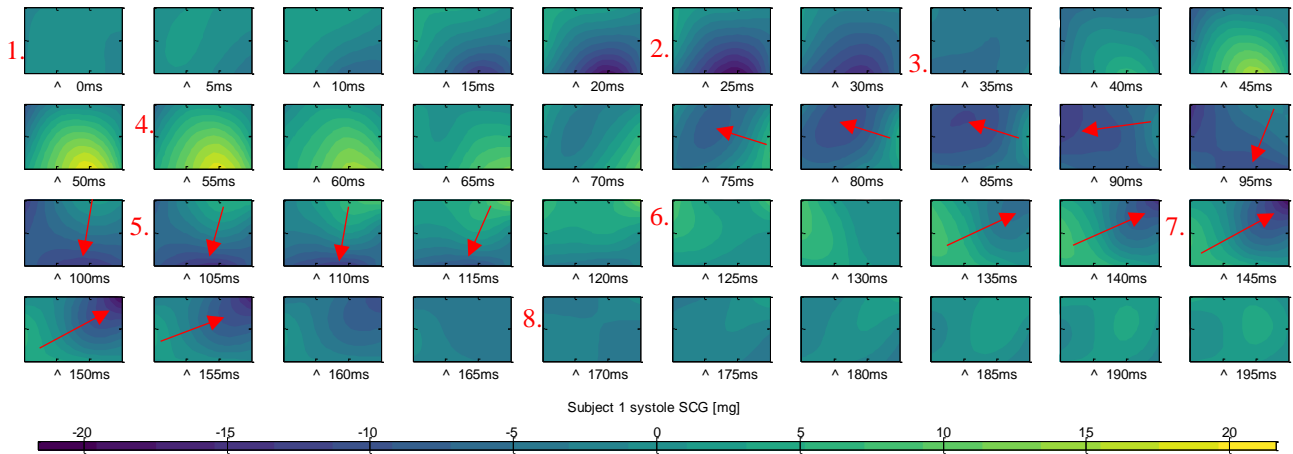


Figure 55 Force maps of the SCG signals bandpass filteret at 0.5 to 30 Hz durring the systole of the heart cycle. Maps are a representation of the multi channel SCG signals from subject 1 of this study. Numbered markings are identified features of the maps sequence and arrows notes the opposite forces direction

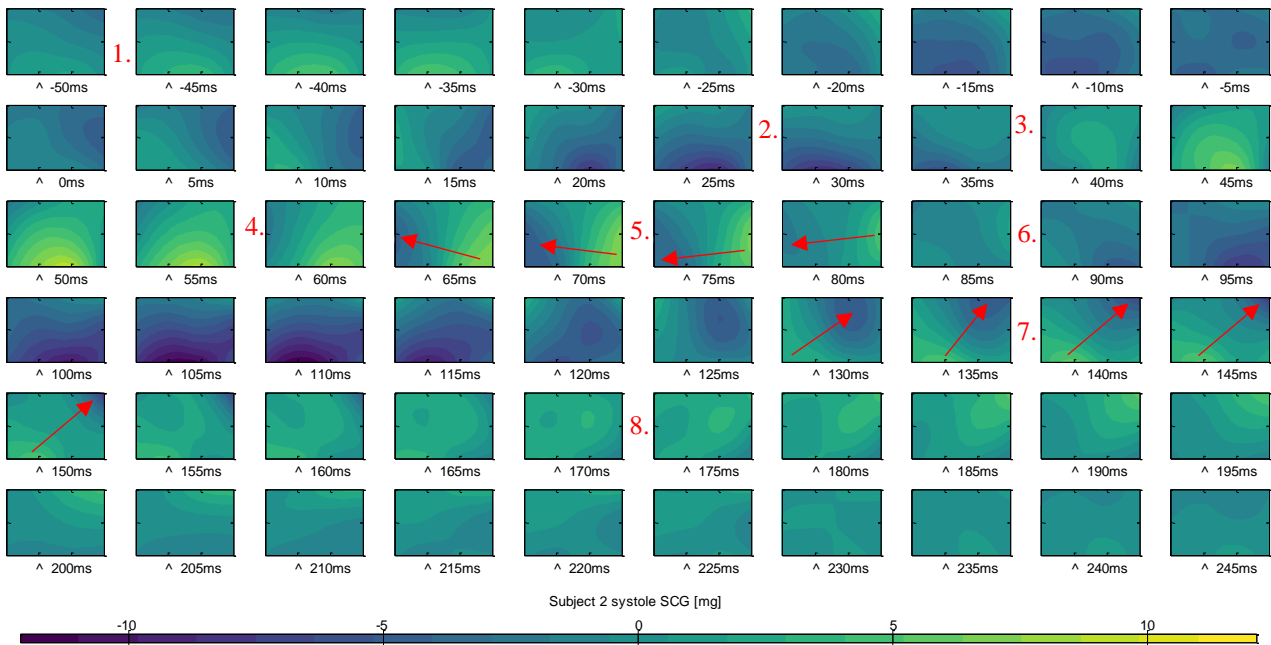


Figure 56 Force maps of the SCG signals bandpass filteret at 0.5 to 30 Hz durring the systole of the heart cycle. Maps are a representation of the multi channel SCG signals from subject 2 of this study. Numbered markings are identified features of the maps sequence and arrows notes the opposite forces direction

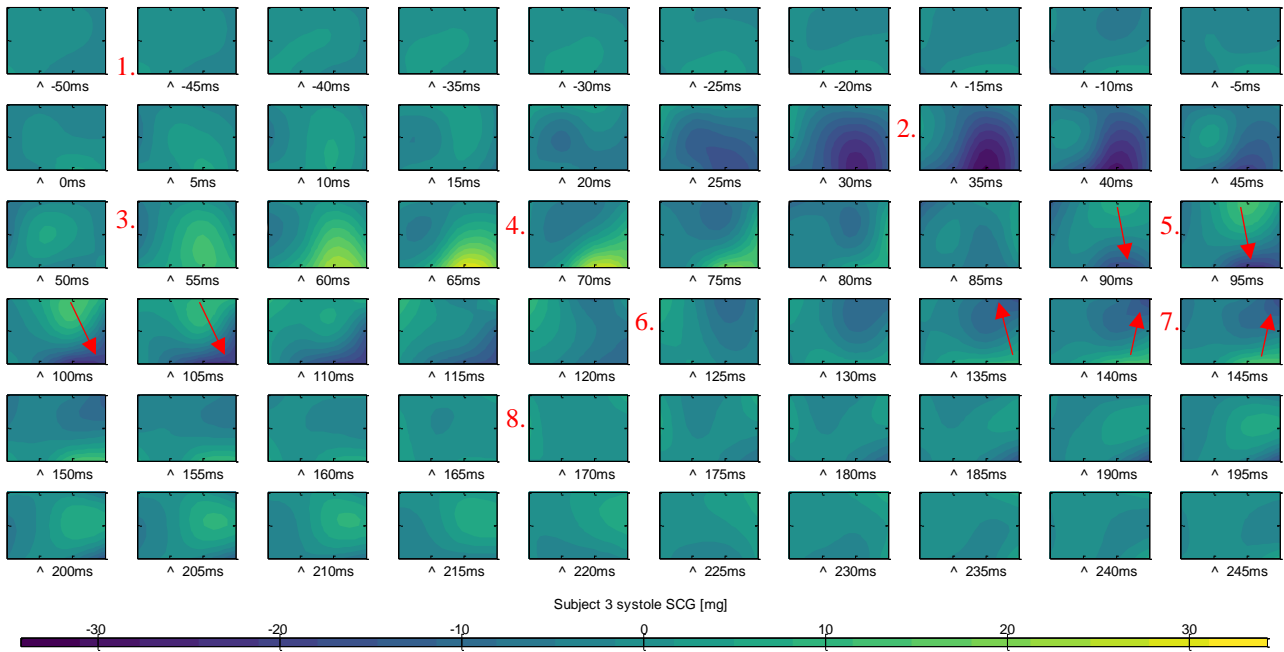


Figure 57 Force maps of the SCG signals bandpass filteret at 0.5 to 30 Hz durring the systole of the heart cycle. Maps are a representation of the multi channel SCG signals from subject 3 of this study. Numbered markings are identified features of the maps sequence and arrows notes the opposite forces direction

### 12.3.2. FORCE MAPPING DURING DIASTOLE

Like the force maps of the systole, also two opposite force were identified for all subject. However, oppose to the systole cycle, these opposite forces share the same direction going from the upper left corner to the lower right, for all subjects. These force maps and the direction of the opposite faces and frames of location of these where illustrated by Figure 58, Figure 59, and Figure 60.

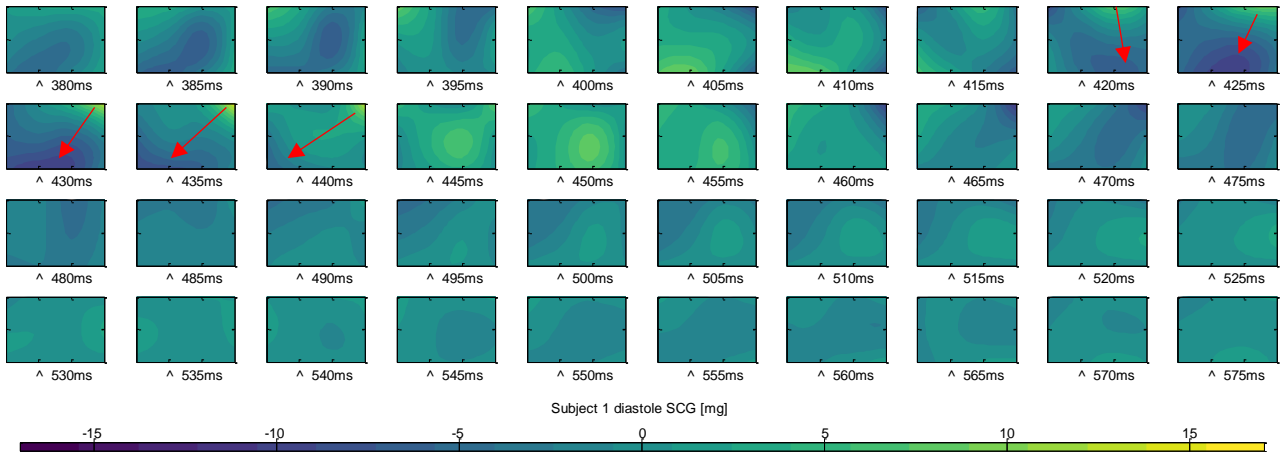


Figure 58 Force maps of the SCG signals bandpass filteret at 0.5 to 30 Hz durring the diastole of the heart cycle. Maps are a representation of the multi channel SCG signals from subject 1 of this study. Arrows notes the opposite forces direction

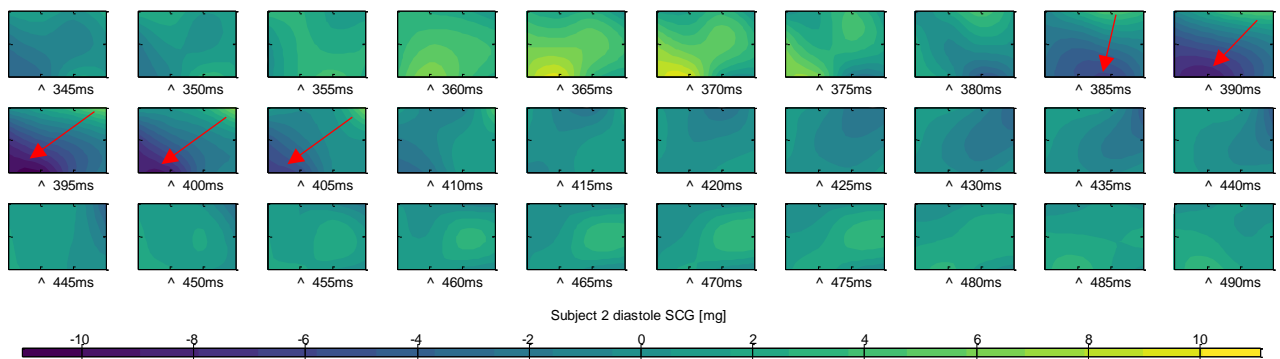


Figure 59 Force maps of the SCG signals bandpass filteret at 0.5 to 30 Hz durring the diastole of the heart cycle. Maps are a representation of the multi channel SCG signals from subject 1 of this study. Arrows notes the opposite forces direction

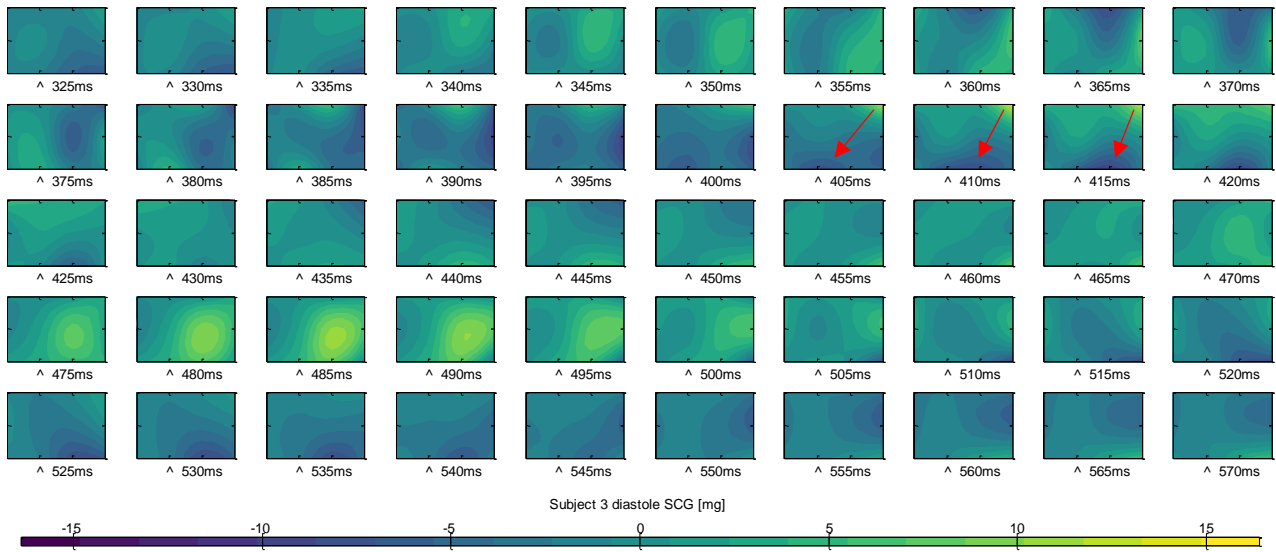


Figure 60 Force maps of the SCG signals bandpass filteret at 0.5 to 30 Hz durring the diastole of the heart cycle. Maps are a representation of the multi channel SCG signals from subject 1 of this study. Arrows notes the opposite forces direction

## CHAPTER 13. DISCUSSION

The discussion was divided into the chapters following the method in the master thesis:

### **Pilot study**

In addition to the pilot study, a placement study was designed to investigate how far apart SCG sites could be without losing any information. However, due to some issues with one of the accelerometers and a placement distance between sites of too much, the results could not give any conclusive information. For future works a similar study should be designed with a shorter distance of approximately 2 cm, to properly investigate the placement distance influence the maps.

Due to concerns regarding how the size and weight of SCG sensors might impact the mapping result, a pilot study should be designed to investigate how these characteristics might have an impact on the measured SCG.

### **Equipment design**

For the system to function with all the 17 sensors, additional changes to the structure of the  $\mu$ C storage of data and methods for transferring data. Here a constant streaming protocol should be incorporated, rather than the send data on request currently implemented. The storage procedure should be based on one large “First In Last Out” buffer rather than the currently implemented individual sensor storage as when read clear.

With some minor initiating changes to the system requirement, a similar system could have been designed with a more adaptable design for the possibilities to change accelerometer or sensor type for different modality mapping, such as gyroscopes.

During the period of the system design, a similar study was published where mSCG was used to measure on healthy subjects. For this approach, less SCG channels were used and analog MEMS accelerometers were implemented. Apart from this the equipment had some of the same designs, and the study also included synchronous ECG and echocardiography. (Lin et al. 2016)

### **Test of equipment**

Further testing of the sensors characteristics would be a good idea. By using a calibrated vibration block, better controlled conditions and longer periods to test for synchronicity would be best. With this method, specific frequencies could also be selected and the frequency response along with background noise of the sensors could be better determined. This method of testing could also be setup to test for any cross-cable contamination due to any concern of related to the ribbon cables.

A comparison of the sensors accuracy should also be tested, along with the robustness of the system after any the optimization procedures described earlier.

### **Study design**

By implementing the optimization procedures described earlier, 17 sensors could be incorporated in the study design. Based on the preliminary results from the three subjects, and results from Munck et al. 2016; Struijk et al. 2016, the additional row of sensors should be placed lower on the subjects chest. This is because of the peaks of the maps typically being close to this boarder.

To better determine if the markers would indicate a good CRT response, simultaneous echocardiography with Tissue Doppler imaging should be included in the study design, at least for the CRT group of the study.

### Future data processing

To improve on interpolation method of the mapping process a 3D interpolation method should be used that also incorporates the temporal domain information into the estimates. This might help improve the accuracy of the interpolated points.

For better understanding, how the heart sounds are distributed additional maps and analysis should be conducted. A doppler shift analysis of the heart sounds may reveal in with direction the heart is moving at the point of the heart valves closing, and similar information might be gained by conducting a phase analysis of the signals possibly by implementing the Hilbert transform.

By investigating the derivatives of the SCG, such as velocity and displacement, information about how the respiration relates to the respiration belt measurements.

One of the stronger features by measuring multiple sites of the same modality is the potential for solving the inverse problem. The two heart sounds, S1 and S2, are really four heart sounds that can be source detected by for example applying an independence component analysis.

Only a third of the SCG information have been analyzed, since each sensor were able to measure in three axes. Further work in understanding how these axes relate to each.

### Results

When investigating the SCG signals measured on the three subjects xiphoid process and comparing them to the description of the SCG in the problem analysis, similar patterns are clear.

During the systole similar features was present in the maps generated from the SCG signals compared to the Laser Doppler Vibrometer (LDV) signal from Munck et al. 2016. Here also the maximum was present after the R-peak, followed by two opposite forces, and ending with a minimum force. However, the individual SCG signal and maps seemed to include more information than the LDV signals.

The opposite forces from the energy maps could be explained by newtons third law of motion: *“To every action there is always opposed and equal reaction”*. By this is meant, that if a force is applied by the heart moving to the left in the chest, an opposite force would then fill the void left by the heart. In addition, when examining the systole maps this apparent movement of the heart is followed by the heart moving back in the opposite direction.

When investigating the energy maps during the systole and diastole, the results show that the S2 heart sound energy is located higher than the S1 heart sound energy. It is consistent when the prior knowledge of auscultatory areas (Pelech 2004), and previous mapping studies that have mapped the heart sounds energy (Struijk et al. 2016; Kompis & Pasterkamp 2001).

## CHAPTER 14. CONCLUSION

Ventricular dyssynchrony commonly leads to heart failure and there is a need for a better marker to predict, if these heart failure patients would benefit from Cardiac Resynchronization Therapy (CRT). Since seismocardiography (SCG) is a measurement of the resulting forces from contraction of the ventricles projected into the chest, it was speculated that SCG would be a good candidate for such a marker. However, the literature lacks knowledge about how on different sites on multiple sites simultaneously would improve the information of the SCG. This led to the problem formulation:

To develop, implement, and study a novel method for investigating multichannel seismocardiography (mSCG) as a marker for ventricular dyssynchrony in heart failure patients.

To investigate mSCG as a marker a study was designed where a novel method needed to be developed and built, that could collect a mSCG of healthy subjects and CRT patients. Before designing the equipment, additional knowledge about the characteristics of the signals to measure would be necessary, and therefore a pilot study was conducted on the basis of pre-acquired SCG from a control and CRT group. Based on the pilot study, literature found in the problem analysis and with the study design center, system specifications were defined, based on the actors involved in the study's points of view, and priorities.

This led to the design of a complete solution to collect the mSCG that involved designing the sensors for SCG, ECG and respiration and designing a system that could quantify the measurements and transfer them to the designed data acquisition software. This involved selecting a brand-new MEMS accelerometer that would meet with the requirements, and designing electrical circuits necessary for optimal functioning of the complete system.

Based on the design a 12 channel SCG equipment with ECG, respiration belt utilities, and accurate alignment of the modalities. The implementation involved applying for resources at the "*Siemens fonden*", were granted. The implementation also involved drawing electrical circuit boards, mounting of the components by external expert resources, 3D printing housing, programming of the microcontroller, and programming of the data acquisition tool on the computer.

A test of the implemented equipment was designed and performed to investigate if it could meet with some of the system requirements that were the basis for the implemented equipment. The equipment responded satisfyingly in the two tests conducted in the experiment.

The study design was announced to the ethics committee, and got approved in the first try. To investigate if mSCG could be useful as a marker for the CRT response an initiating three healthy subjects were included in this master thesis with future respect including CRT patients and additional control subjects.

To understand the behavior of the mSCG signal, the collected data was signal processed to present the forces and heart sound energies by mapping how they would be distributed over the chest at specific time points.

In the resulting maps from the three subjects, similar patterns were found both in the signal SCG but in addition opposite force and energy location of the heart sounds that was possible due to the additional information found by investigating the novel method of mSCG.

Further work should include optimization to 17 channel SCG and further testing of the implemented equipment performance. Only a small amount of the information available has been drawn out from the mSCG by the signal process, and future works should focus on solving the inverse problem, including all 3-axis SCG, and include data from the CRT group.

The current study only involving healthy subjects would not be able to answer the problem formulation conclusively, but the investigated features were related to the contraction of the ventricles and may prove to be better markers as CRT patients are included in the study.

## BIBLIOGRAPHY

- Abraham, W.T. et al., 2002. Cardiac Resynchronization in Chronic Heart Failure. *The New England journal of medicine*, 346(24), pp.1845–1853.
- Acar, C. & Shkel, A.M., 2003. Experimental evaluation and comparative analysis of commercial variable-capacitance MEMS accelerometers. *Journal of Micromechanics and Microengineering*, 13(5), pp.634–645.
- Aliverti, A. et al., 1998. Respiratory kinematics by optoelectronic analysis of chest wall motion and ultrasonic imaging of the diaphragm. *Medical Imaging 1998: Physiology and Function from Multidimensional Images*, 3337(February), pp.52–62.
- American Heart Association, 2014. About Arrhythmia. Available at: [http://www.heart.org/HEARTORG/Conditions/Arrhythmia/AboutArrhythmia/About-Arrhythmia\\_UCM\\_002010\\_Article.jsp#.WafxaiSTOg4](http://www.heart.org/HEARTORG/Conditions/Arrhythmia/AboutArrhythmia/About-Arrhythmia_UCM_002010_Article.jsp#.WafxaiSTOg4) [Accessed October 20, 2016].
- Analog Devices, 2016a. Digital Output MEMS Accelerometer ADXL362.
- Analog Devices, 2016b. Low Noise, Low Drift, Low Power, 3-Axis MEMS Accelerometers ADXL354/ADXL355. , pp.1–42.
- Andrejašič, M. & Poberaj, I., 2008. Mems Accelerometers. *University of Ljubljana*, pp.1–17.
- Bleeker, G.B. et al., 2006. Left ventricular dyssynchrony in patients with heart failure: pathophysiology, diagnosis and treatment. *Nature Publishing Group*, 3(4), pp.213–219.
- Bleeker, G.B. et al., 2004. Relationship Between QRS Duration and Left Ventricular Dyssynchrony in Patients with End-Stage Heart Failure. *J Cardiovasc Electrophysiol*, 15, pp.544–549.
- Bleeker, G.B. et al., 2005. Tissue Doppler imaging to assess left ventricular dyssynchrony and resynchronization therapy \*. , pp.382–384.
- BOZHENKO, B.S., 1961. [Seismocardiography--a new method in the study of functional conditions of the heart]. *Terapevticheskii arkhiv*, 33, pp.55–64. Available at: <http://www.ncbi.nlm.nih.gov/pubmed/13872234>.
- Burri, H. et al., 2006. Optimization of Device Programming for Cardiac Resynchronization Therapy. *PACE*, 29, pp.1416–1425.
- Castiglioni, P. et al., 2007. Wearable seismocardiography. *Annual International Conference of the IEEE Engineering in Medicine and Biology - Proceedings*, pp.3954–3957.
- Chung, E.S. et al., 2008. Results of the Predictors of Response to CRT ( PROSPECT ) Trial. , pp.2608–2617.
- Cozic, M., Durand, L.G. & Guardo, R., 1998. Development of a cardiac acoustic mapping system. *Medical and Biological Engineering and Computing*, 36(4), pp.431–437.
- Dansk Cardiologisk Selskab, 2007. *Hjerteinsufficiens*,
- DeMaria, A.N. & Blanchard, D.G., 2008. Echocardiography. In *The Heart*. Poole-Wilson, pp. 359–466.
- Erdmann, E. et al., 2005. The Effect of Cardiac Resynchronization on Morbidity and Mortality in Heart Failure. *The New England journal of medicine*, pp.1539–1549.
- Inan, O.T. et al., 2015. Ballistocardiography and Seismocardiography: A Review of Recent Advances. *IEEE Journal of Biomedical and Health Informatics*, 19(4), pp.1414–1427.
- Jafari Tadi, M. et al., 2014b. Accelerometer-based method for extracting respiratory and cardiac gating information for dual gating during nuclear medicine imaging. *International Journal of Biomedical Imaging*, 2014.
- Jafari Tadi, M. et al., 2014a. Accelerometer-based method for extracting respiratory and cardiac gating information for dual gating during nuclear medicine imaging. *International Journal of Biomedical Imaging*, 2014.

- Jain, P.K., Tiwari, A.K. & Chourasia, V.S., 2016. Performance analysis of seismocardiography for heart sound signal recording in noisy scenarios. *Journal of Medical Engineering & Technology*, 1902(February), pp.1–13. Available at: <http://www.tandfonline.com/doi/full/10.3109/03091902.2016.1139203>.
- Jensen, A.S. et al., 2014. Effects of Cardiac Resynchronization Therapy on the First Heart Sound Energy. *Computers in Cardiology 2014*, 41, pp.29–32.
- John G. Webster, 2010. *Medical instrumentation, application and design* 4th ed., Malloy Inc.
- Kajbaf, H. & Ghassemian, H., 2009. Acoustic Imaging of Heart Using Microphone Arrays. *ICBME Proceedings*, 23, pp.738–741.
- Kaminska, B. et al., 2007. Prevention and Risk Reduction in Heart Health. *NSTI-Nanotech*, 2, pp.531–534.
- Kompis, H.M. & Pasterkamp, G.R.W., 2001. Acoustic imaging of the human chest. *CHEST*, 120, pp.1309–1321.
- Krueger, S. et al., 2004. Cardiac-Resynchronization Therapy with or without an Implantable Defibrillator in Advanced Chronic Heart Failure. *The New England journal of medicine*, pp.2140–2150.
- Kaajakari, V., 2004. MEMS Tutorial : Mechanical noise in microelectromechanical systems. <http://www.kaajakari.net>. Available at: [http://www.kaajakari.net/~ville/research/tutorials/mech\\_noise\\_tutorial.pdf](http://www.kaajakari.net/~ville/research/tutorials/mech_noise_tutorial.pdf).
- Laurin, A. et al., 2016. Accurate and consistent automatic seismocardiogram annotation without concurrent ECG. *Computing in Cardiology*, 42, pp.25–28. Available at: <http://dx.doi.org/10.1088/0967-3334/37/9/1588>.
- Lin, W. et al., 2016. Identification of Location Specific Feature Points in a Cardiac Cycle Using a Novel Seismocardiogram Spectrum System. , 2194(c).
- Linear Technology Corporation, 2012. LTC6820 - isoSPI Isolated Communications Interface. , pp.1–30.
- Munck, K. et al., 2016. Body Surface Mapping of the Mechanical Cardiac Activity. , 43.
- Nagueh, S.F., 2008. Mechanical Dyssynchrony in Congestive Heart Failure. Diagnostic and Therapeutic Implications. *Journal of the American College of Cardiology*, 51(1), pp.18–22.
- Nguyen, H., Zhang, J. & Nam, Y.H., 2012. Timing detection and seismocardiography waveform extraction. *Proceedings of the Annual International Conference of the IEEE Engineering in Medicine and Biology Society, EMBS*, pp.3553–3556.
- O'Reilly, R., Khenkin, A. & Harney, K., 2009. Sonic Nirvana: Using MEMS Accelerometers as Acoustic Pickups in Musical Instruments. *analog-dialogue*, 43. Available at: <http://www.analog.com/en/analog-dialogue/articles/mems-accelerometers-as-acoustic-pickups.html>.
- Olsen, N.T. et al., 2009. Predicting Response to Cardiac Resynchronization Therapy with Cross-Correlation Analysis of Myocardial Systolic Acceleration: A New Approach to Echocardiographic Dyssynchrony Evaluation. *Journal of the American Society of Echocardiography*, 22(6), pp.657–664. Available at: <http://dx.doi.org/10.1016/j.echo.2009.03.017>.
- Pandia, K. et al., 2012. Extracting respiratory information from seismocardiogram signals acquired on the chest using a miniature accelerometer. *Physiological measurement*, 33(10), pp.1643–60. Available at: <http://www.ncbi.nlm.nih.gov/pubmed/22986375>.
- Paper, C., 2016. Methods and results in characterizing electronic stethoscopes Methods and Results in Characterizing Electronic Stethoscopes. , 29.
- Paukkunen, M. et al., 2016. Beat-by-Beat Quantification of Cardiac Cycle Events Detected From Three-Dimensional Precordial Acceleration Signals. *IEEE Journal of Biomedical and Health Informatics*, 20(2), pp.435–439.
- Paukkunen, M., 2014. *Seismocardiography: Practical implementation and feasibility*,
- Pelech, A.N., 2004. The physiology of cardiac auscultation. *Pediatric Clinics of North America*, 51(6 SPEC. ISS.), pp.1515–1535.
- Ramos-castro, J. et al., 2012. Heart rate variability analysis using a seismocardiogram signal. *Conference proceedings :*

- ... *Annual International Conference of the IEEE Engineering in Medicine and Biology Society. IEEE Engineering in Medicine and Biology Society. Annual Conference*, 2012, pp.5642–5. Available at: <http://www.ncbi.nlm.nih.gov/pubmed/23367209>.
- Rendón, D.B. et al., 2007. Mapping the human body for vibrations using an accelerometer. *Conference proceedings : ... Annual International Conference of the IEEE Engineering in Medicine and Biology Society. IEEE Engineering in Medicine and Biology Society. Annual Conference*, 2007, pp.1671–4. Available at: <http://www.ncbi.nlm.nih.gov/pubmed/18002295>.
- Di Rienzo, M. et al., 2013. Wearable seismocardiography: Towards a beat-by-beat assessment of cardiac mechanics in ambulant subjects. *Autonomic Neuroscience: Basic and Clinical*, 178(1–2), pp.50–59. Available at: <http://dx.doi.org/10.1016/j.autneu.2013.04.005>.
- Risum, N. et al., 2012. Simple regional strain pattern analysis to predict response to cardiac resynchronization therapy: Rationale, initial results, and advantages. *American Heart Journal*, 163(4), pp.697–704. Available at: <http://dx.doi.org/10.1016/j.ahj.2012.01.025>.
- Salerno, D.M. et al., 1991. Seismocardiographic changes associated with obstruction of coronary blood flow during balloon angioplasty. *The American Journal of Cardiology*, 68(2), pp.201–207.
- Schmidt, S.E. et al., 2016. Temporal Alignment of Asynchronously Sampled Biomedical Signals Pre-processing. , 43, pp.10–13.
- Schmidt, S.E. et al., 2014. Three-dimensional Apex-seismocardiography. *Computers in Cardiology*, 41(October 2016), pp.1105–1108.
- Struijk, J.J. et al., 2016. Heart-valve Sounds Obtained with a Laser Doppler Vibrometer. , 43.
- Tavakolian, K. et al., 2013. Precordial acceleration signals improve the performance of diastolic timed vibrations. *Medical Engineering and Physics*, 35(8), pp.1133–1140. Available at: <http://dx.doi.org/10.1016/j.medengphy.2012.12.001>.
- Ted Rogers Centre for Heart Research, 2017. Cardiac Resynchronization Therapy (CRT). Available at: <http://tedrogersheartfunction.ca/treatments/device-therapies/cardiac-resynchronization-therapy-crt/> [Accessed June 6, 2017].
- Walter, P.L., 2007. The History of the Accelerometer. *Sound and Vibration*, (January), p.9. Available at: [www.SandV.com](http://www.SandV.com).
- Wick, C.A. et al., 2015. Relationship between cardiac quiescent periods derived from seismocardiography and echocardiography. *Proceedings of the Annual International Conference of the IEEE Engineering in Medicine and Biology Society, EMBS*, 2015–Novem, pp.687–690.
- Wick, C.A. et al., 2012. A system for seismocardiography-based identification of quiescent heart phases: Implications for cardiac imaging. *IEEE Transactions on Information Technology in Biomedicine*, 16(5), pp.869–877.
- Yu, C. et al., 2003. High prevalence of left ventricular systolic and diastolic asynchrony in patients with congestive heart failure and normal QRS duration. *Heart*, (89), pp.54–60.
- Zanetti, J.M. & Tavakolian, K., 2013. Seismocardiography: past, present and future. *Conference proceedings : ... Annual International Conference of the IEEE Engineering in Medicine and Biology Society. IEEE Engineering in Medicine and Biology Society. Annual Conference*, 2013, pp.7004–7007.

# APPENDICE

<b><u>APPENDIX A. MICRO ELECTRO-MECHANICAL SYSTEMS ACCELEROMETERS.....</u></b>	<b>96</b>
HOW MEMS WORKS.....	96
MEMS PARAMETERS.....	97
FREQUENCY RESPONSE .....	98
<b><u>APPENDIX B. APPLICATION FOR FUNDING FROM SIEMENS FONDEN.....</u></b>	<b>100</b>
PROJEKT BESKRIVELSE:.....	100
BUDGET:.....	101
<b><u>APPENDIX C. APPLICATION FOR THE ETHICS COMMITTEE (EXPERIMENTAL PROTOCOL).....</u></b>	<b>102</b>
BACKGROUND .....	102
STRATEGY FOR LITERATURE SEARCH .....	102
PURPOSE.....	102
SUBJECTS .....	103
DESIGN AND METHODS .....	104
RISKS, SIDE EFFECTS AND DISADVANTAGES.....	106
STATISTICS.....	106
ETHICAL CONSIDERATIONS .....	107
INSURANCE.....	107
PERSONAL DATA .....	107
INFORMATION FROM MEDICAL CHARTS.....	107
PROJECT ECONOMY .....	107
PUBLISHING OF RESULTS.....	107
TIME SCHEDULE .....	108
GUIDELINES FOR ORAL INFORMATION AND INFORMED CONSENT .....	108
<b><u>APPENDIX D. ADDITION RESULT ILLUSTRATIONS.....</u></b>	<b>110</b>
SUBJECT 1 MSCG MAPS.....	110
SUBJECT 1 SOUND MAPS .....	111
SUBJECT 1 SOUND ENERGY MAPS .....	112
SUBJECT 2 MSCG MAPS.....	113
SUBJECT 2 SOUND MAPS .....	114
SUBJECT 2 SOUND ENERGY MAPS .....	115
SUBJECT 3 MSCG MAPS.....	116
SUBJECT 3 SOUND MAPS .....	117
SUBJECT 3 SOUND ENERGY MAPS .....	118

## Appendix A. Micro Electro-Mechanical Systems accelerometers

An accelerometer is a device capable of measuring the forces applied to a free mass, which implies that an acceleration had occurred. The first type of commercial available accelerometer was a resistance-bridge-type accelerometer that was released 1923. However, these early accelerometers had a low resonance frequency making them bad at measuring higher frequencies above 200 Hz. In the 1940's to 1950's a lot of new piezoelectric accelerometers was developed that was capable of measuring frequencies up to 10 kHz. (Walter 2007) Piezoelectric accelerometers had dominated the market of accelerometers for a long period, however, there was still some issues with this technology. Piezoelectric accelerometers were expensive, energy consuming, large and their mass damped low energy vibrations. By the development of the first MEMS accelerometers, in the 1990's, a more energy sufficient, mass production friendly, smaller and lighter type of accelerometer was commercially available.

### How MEMS works

MEMS are silicon technologies like that of the electronic microchip, but instead of the removing and adding silicon was used for designing electronic circuits it was also used its mechanical attributes (Walter 2007).

MEMS comes in many different types for measuring different things such as; pressure, optical MEMS, and inertia sensor. Among the inertia sensors are gyroscopes, magnetometers and accelerometers. The accelerometer is one of the simplest but also most applicable MEMS. (Andrejašič & Poberaj 2008)

A simple MEMS accelerometer is composed of three parts; a mass, a spring and movable/fixed capacitor plates, as illustrated by Figure 14-1. When an acceleration of an object goes in on direction an equal and opposite reaction occurs, making the mass move dependent on the acceleration and opposing force by the springs. When the mass moves the distance between the three capacitor plates change, with in tern changes the capacity between the two-fixed point and the mass, as described by equation (2).

$$C = \frac{A}{d} \quad (2)$$

As illustrated by the electron micro scan of a MEMS accelerometer illustrated in Figure 14-2, one mass is combined with many capacitor plates and as illustrated by Figure 14-3 many masses are combined in a single accelerometer to measure the acceleration. (O'Reilly et al. 2009)

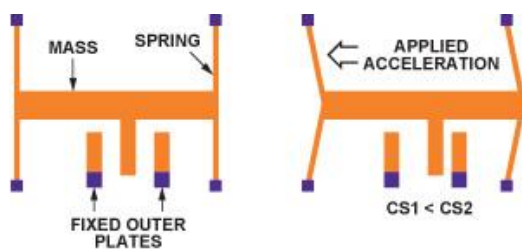


Figure 14-1 The concept of MEMS accelerometers, where the purple squares are fixed point and a capacity is measurable between the two fixed outer plates and the mass are measurable. The figure on the left has no acceleration and the right figure those have an acceleration going left. (O'Reilly et al. 2009)

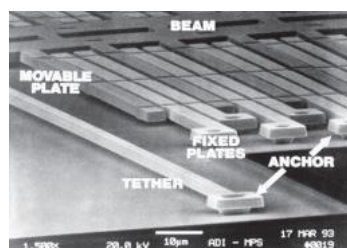


Figure 14-2 A closeup electron microscope image of a MEMS accelerometer. Where the Tether is the spring, the Beam is the mass, and the fixed plates are the capacitors. (O'Reilly et al. 2009)

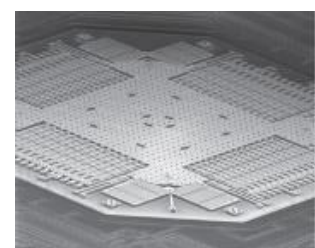


Figure 14-3 An electron microscope image of a MEMS accelerometer with multiple sets of mass, springs and capacitors. (O'Reilly et al. 2009)

All similar sets of capacitors are connected in parallel. Combining the capacitors are necessary for detecting the small variations in capacity. The displacement of the mass can then be described by equation (3). Where  $x$  is the displacement,  $c_0$  is the initial capacity of both capacitors,  $c_1$  and  $c_2$  are the capacity of each capacitor. (Andrejašič & Poberaj 2008)

$$x = d \frac{c_1 - c_2}{c_0} \quad (3)$$

Per Hook's law and Newton's second law the relationship between the displacement of a mass in a spring system and the acceleration the mass is being applied by can be described by equation (4). Where  $k$  is the spring constant,  $m$  is the mass and  $a$  is the acceleration. (Andrejašič & Poberaj 2008)

$$a = \frac{k}{m} x \quad (4)$$

To measure the capacity of the two capacitors an oscillator is connected to the two capacitors as a voltage divider. When an acceleration occurs the capacitors change values in opposing directions and thereby the voltage output of the voltage divider changes accordingly, as illustrated by Figure 14-4.

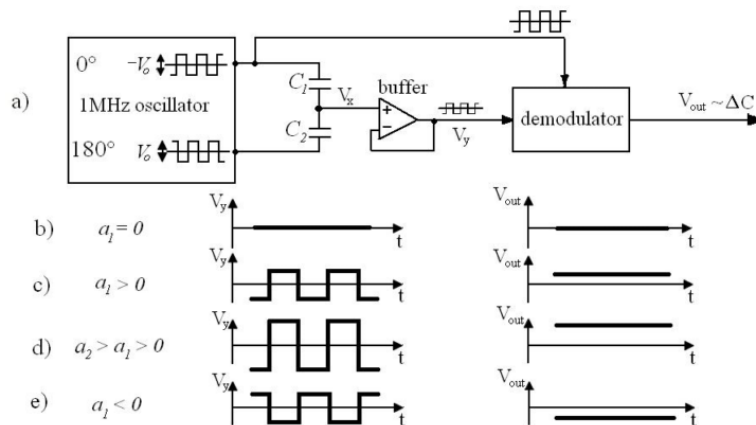


Figure 14-4 Electronic circuit used for measuring change of capacity between the two capacitors and thereby the acceleration of an MEMS (Andrejašič & Poberaj 2008).

## MEMS Parameters

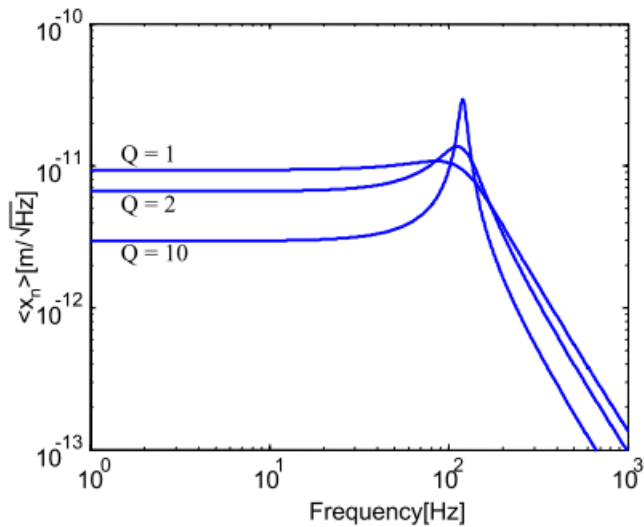
When a MEMS accelerometer is design, certain attributes are specified dependent on the use attended for the accelerometer. Some of these parameters are if the accelerometer should deliver an analog output or if the unit should include an Analog to Digital Conversion (ADC) of the measurements. There were also the number of axis in the accelerometer and their measuring range. (Andrejašič & Poberaj 2008) Typically ranges of  $\pm 2$  g was used for weak SCG signals. Last there are the precision, frequency bandwidth and noise density, which depend on each other.

There are three sources of noise in a MEMS; mechanical vibrations, electronic circuits and from the measurement. In an SCG signal when measuring on a subject noise such as movement and soundwaves absorbed by the body would be understood as noise. (Andrejašič & Poberaj 2008) Operational amplifiers would add some additional noise to any system, but are necessary for filtering, amplification and ADC. However, the maybe large source of noise comes from the mechanical vibrations of the MEMS.

The mechanical noise in MEMS accelerometers is caused by the fact that it's an oscillator and the thermal energy.

The MEMS accelerometer is a free mass connected to a spring, which is essentially on oscillator. An oscillator has a resonance frequency  $w_0 = k \cdot m$  and quality factor  $Q = w_0 \cdot m/\gamma$ . At the resonance frequency, some ringing occurs that limits the bandwidth of accelerometer. If the purpose of the accelerometer was to measure higher frequencies above 1 kHz a pizelectric accelerometer would therefore be more applicable. Apart from the oscillator noise their also occurs some noise do the thermal energy stored in the system. The signal to noise ratio becomes lower when the size of the MEMS are

reduced. (Kaajakari 2004) As illustrated by figure ## the power spectrum density noise can be describe by the thermal and oscillators contribution to noise.



Since higher frequencies means that the accelerometer would have to update the measurements faster, for achieving the same precision, higher oscillator frequency would also be necessary (Andrejašič & Poberaj 2008).

Typically noise densities of  $500 \mu\text{g}/\sqrt{\text{Hz}}$  and  $200 \mu\text{g}/\sqrt{\text{Hz}}$  are used (Andrejašič & Poberaj 2008). However, newer nitrogen damped MEMS accelerometer have noise level as low as  $5 \mu\text{g}/\sqrt{\text{Hz}}$  (Schmidt et al. 2014).

### Frequency response

Comparing the frequency response of the traditional accusation method for heart sounds, PCG, with the MEMS accelerometer method, the advantages and disadvantages are better revealed.

PCG is measured using high quality microphones that can measure these low frequency signals, below 1 kHz, so that they may be filtered and amplified for the physicians to better diagnose from them. When investigating the frequency response of these electronic PCG devices, the results indicate that the frequency response was very poor compared to an accelerometer (Paper 2016). The evaluated electronic PCG devices was also not able to measure the ultra-low frequencies, below 5 Hz very well, as illustrated by Figure 1.

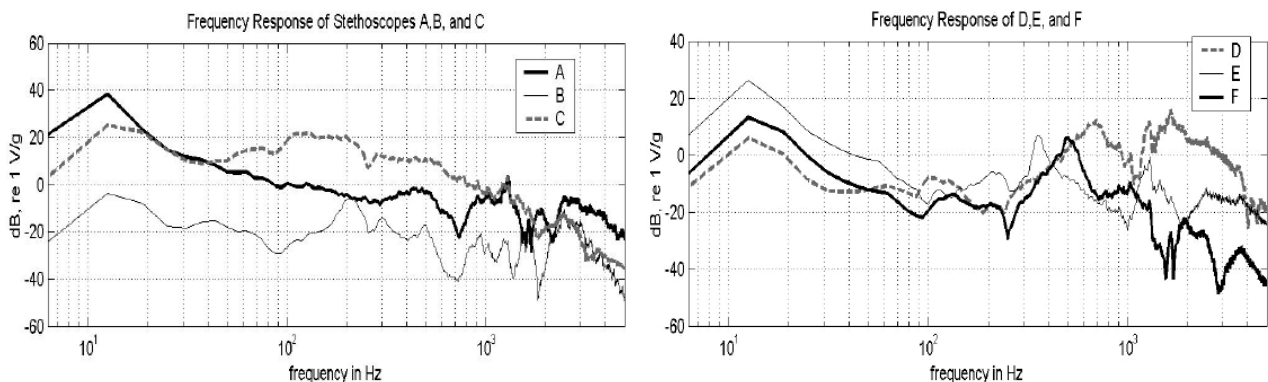


Figure 1 Frequency response of six types of electronic stethoscopes, going from 5 Hz to 200 Hz, compared to an accelerometer measurement. A and D are Force Gage transducer types and B, C, E and F are electret transducer type electronic stethoscopes. (Paper 2016)

However, when considering the MEMS accelerometer, they have a flat frequency response capable of measuring much lower frequencies than the PCG devices, as illustrated by the Figure 3 (Acar & Shkel 2003). The downside of MEMS accelerometers is that they were not able to measure higher frequencies above 200 Hz as good as the electronic PCG devices, without adding additional noise and that the accelerometers were not as noise robust as PCG devices.

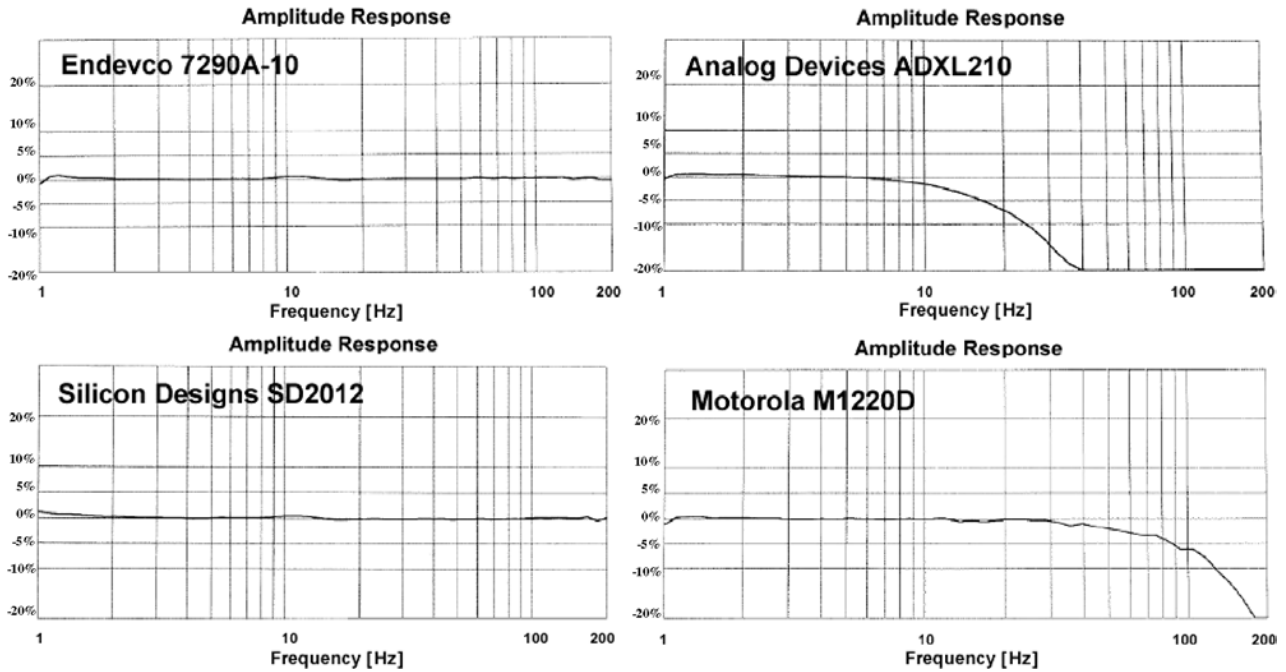


Figure 2 Frequency responses of four different accelerometers. (Acar & Shkel 2003)

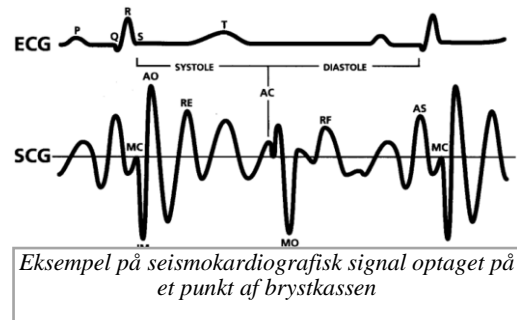
## Appendix B. Application for funding from Siemens Fonden

Kim Munck Jeppesen  
Aalborg Universitet  
Sundhedsteknologi 3. + 4. semester master  
e-mail: [kkj@hst.aau.dk](mailto:kkj@hst.aau.dk)

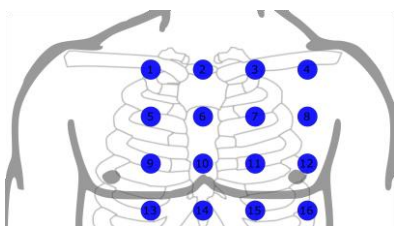
# Multikanals Seismokardiografi til Forbedret Indstilling af Biventrikulær Pacemaker samt dens Diagnostiske Egenskaber

### Projekt beskrivelse:

Formålet med projektet er at øge forståelsen af målemetode seismokardiografi (SCG), for fremtidigt at kunne give en bedre forståelse af hjertets aktiviteter og bedre diagnose hjerte dysfunktioner. Seismokardiografi er målingen af acceleration på brystkasse grundet bevægelser fra hjertet. Seismokardiografi er, sammenlignet med elektrokardiografi (ECG), et signal der udtrykker hjertets mekaniske aktivitet fremfor dens elektriske signal. Selvom interessen for seismokardiografi inden for de sidste 10 år er øget er der stadigvæk en manglende forståelse af signalets kilde og anvendeligheden af målemetoden.



Projektet ønsker at øge forståelsen af seismokardiografi ved at optage multikanals seismokardiografi, på henholdsvis raske forsøgspersoner og hjertesvigts patienter med dysfunktionel hjerteaktivitet. Ved at optage multikanals seismokardiografi på raske forsøgspersoner kan vi øge forståelsen af kilden for seismokardiografi signalet. Dysfunktionel hjerteaktivitet behandles i mange tilfælde ved kardial resynkroniseringsterapi som foregår ved hjælp af en biventrikulær pacemaker. Den biventrikulær pacemaker skal indstilles korrekt ved hjælp af ultralyd scanninger af hjertets mekaniske aktivitet, for at kunne give den forbedrede pumpe effektivitet. Indstillingen af den biventrikulær pacemaker er en besværlig og dyr proces som vil kunne resultere i et længere patient forløb. Ved at optage multikanals seismokardiografi på hjertesvigts patienter som får kardial resynkroniseringsterapi, vil vi kunne udvikle en algoritme der forsimples indstillingen af den biventrikulær pacemaker og derved forbedre patientens behandlingsforløb samt mindske behandlingsomkostninger. Desuden vil optagelsen af multikanals seismokardiografi fra henholdsvis kontrol gruppen og hjertesvigts gruppen kunne bidrage til videre udviklingen af kardiologisk diagnose redskaber.



Eksempel på placering af accelerometer ved multikanals seismokardiografi

De ansøgte midler på 27 500 kr. går til udviklingen og implementering af udstyr til optagelse af et multikanals (16 kanaler) seismokardiogram. Dette udstyr vil desuden i fremtidige studier få tilføjet yderligere modaliteter, til øget forståelse af sammenhængen mellem multikanals seismokardiografi og disse modaliteter. Udover at denne nye målemetode kan anvendes til

undersøgelse af hjertets aktivitet, vil det også kunne anvendes i fremtidige projekter som også kan involvere kortlægning af respiration.

### Budget:

I budgettet er uddybet de elementer som udgør det samlede udstyr til optagelse af multikanals seismokardiografi samt udstyr til tilføjelse en ekstra modalitet i form af et elektrokardiogram (ECG).

Igennem pilotstudier er der fundet et behov for 16 accelerometer med specifikationer som ADXL355/ADXL354 opfylder. Da der er et ønske om en digital løsning hvor hvert accelerometer har deres egen indbygget ADC anvendes ADXL355. For at kunne downloade disse digitale måling fra accelerometer hurtigt nok er der et behov for et digital data acquisition tool som NI USB-8452 opfylder specifikationerne til. Derudover er der et behov for simultan synkrone optaget elektrokardiogram, hvor ADS1298ECGFE-PDK er kompatibel med den foreslået løsning. For et kunne implementer denne løsning er der derudover udgifter til print layout, kabler, støj reducerende kredsløb og 3D printet etui til accelerometer.

Beskrivelse	Budgettering	Detaljer
ADXL355 accelerometer	8 000,-	16 lav støj og høj sensitive accelerometer til 500,- per styk
NI USB-8452	5 500,-	Digital data acquisition tool til at indsamle data fra all accelerometer, ECG og indstilling af udstyr
Datalinje støjreducerende kredsløb	2 500,-	For at kunne anvende de indbyggede Communications protokoller over længere afstande, vil der være behov for dette.
Par snoet, skærmet og bløde kabler	2 000,-	Der er behov for kabler som er med til at reducere støjen og som samtidig har en lavere indflydelse på bevægelsen af de individuelle accelerometer
3D printet etui til accelerometer	3 000,-	Beskyttelse af høj g følsomme accelerometer, elektrisk adskillelse fra forsøgsperson og lav vægt påvirkning af accelerometer bevægelse
Print layout	5 000,-	For hvert accelerometer og i sammenhæng med NI USB-8452
ADS1298ECGFE-PDK	1 500,-	Digital ECG sampling udstyr som er compatible med kommunikations protokol fra accelerometer
Samlet budget:	27 500,-	

## Appendix C. Application for the ethics committee (Experimental Protocol)

### Background

The purpose of this explorative study is to evaluate the potential of multichannel seismocardiography (mSCG) for mapping movements of the chest, caused by the beating of the heart (Salerno et al. 1991). Similar technics of mapping on multiple sites of the chest have been investigated with other modalities such as phonocardiography to understand the potential of mapping these for better understanding the behaviour of the heart. However, the relations between the mapping and an unhealthy heart have never been fully established (Kajbaf & Ghassemian 2009; Rendón et al. 2007). The correct location for SCG measuring has never been fully established, and the current study setting would elucidate on this as well (Inan et al. 2015).

Cardiac resynchronization therapy (CRT) improves global left ventricle (LV) function as well as indices of timing in patients with activation induced heart failure. In general, CRT benefit is seen early after therapy is initiated, and it is maintained and further improved over the following years until a stable condition is reached (Risum et al. 2012). However, CRT only corrects the mechanical contractile function whereas the underlying conduction abnormality is still present even during the chronic stage of treatment. Thus, turning off the pacemaker will immediately impair the LV function. Biventricular pacemakers are commonly used in CRT when ventricular dyssynchrony has been diagnosed. When turning off the CRT, this ventricular dyssynchrony reappears and we expect to see these changes in mechanical contractile function on the mapping of the chest movements (Olsen et al. 2009).

### Strategy for literature search

The basis of the study has been found among peer-reviewed articles, publicly available material, and Aalborg University's own research. 91 articles were found and 7 references used (please see the section List of References) for this study which form the basis for the research within seismocardiographic and its relations to cardiac resynchronization therapy.

The literature has been found by reviewing of the search engine Scopus. The following search words were used in combinations for review of the literature: Seismocardiography or (Seismocardiography and cardiac resynchronization therapy or pacemaker).

Only studies with interest within human research have been used and the studies have been produced within the last 10 years.

### Purpose

The main objective is to investigate the potential of multichannel seismocardiography and how it relates to the mechanical contractile function of the heart. Then the main hypotheses are that by investigating groups with different mechanical contractile functions of the heart we would be able to assess mSCG potentials. This leads us to three sub-hypotheses where measurements across three conditions of different mechanical contractile functions of the heart would be investigated.

**Hypothesis of sub-project 1**

The hypothesis is that there is a difference between the mSCG mapping when the CRT is on and off that relates to a change in mechanical contractile function of the heart.

**Hypothesis of sub-project 2**

The hypothesis is that there is a smaller difference between the mSCG mapping of the healthy subjects and subjects that are undergoing CRT that relates to a change in mechanical contractile function of the heart.

**Hypothesis of sub-project 3**

The hypothesis is that there is a difference between the mSCG mapping of healthy subjects and subjects that have an activation-induced heart failure and have their CRT turned off that relates to a change in mechanical contractile function of the heart.

**Subjects**

For this study, we wish to recruit subjects for both a control group and a CRT group.

**Control group**

For the control group, we wish to recruit 30 healthy volunteers through notices at Aalborg University. The following inclusion and exclusion criteria will be used:

**Inclusion:**

- Male
- 20 to 80 years of age

**Exclusion:**

- Known cardiovascular disease including subjects receiving cardiovascular-related medications such as medication for hypertension and hyperlipidaemia
- Lack of ability to cooperate

**CRT group**

For the CRT group, we wish to recruit 20 volunteers through notices at the pacemaker outpatient clinic at Aalborg University Hospital. The following inclusion and exclusion criteria will be used:

**Inclusion:**

- Male
- 20 to 80 years of age
- Biventricular pacemaker implant more than 3 M ago
- Freedom from AFIB and frequent ectopic beats

**Exclusion:**

- Lack of ability to cooperate

## Design and methods

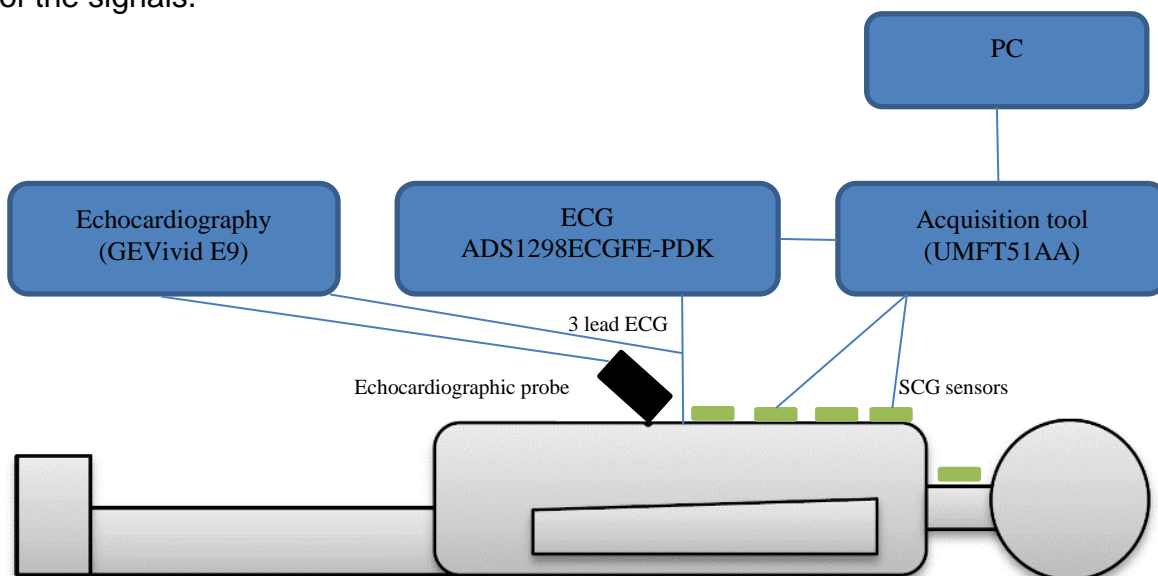
### Study procedures

Two study procedures are used for this study dependent on the subject group. The difference between the two procedures is turning the CRT device off and on and that the CRT group includes echocardiography recordings. During the entire experiment the subject will be in a supine position and measurements will be collected uninterruptedly.

Control group	CRT group
<ul style="list-style-type: none"> <li>• Equipment setup</li> <li>• Relaxation period (10 min)</li> <li>• Relaxed (5 min)</li> <li>• Removing equipment</li> </ul>	<ul style="list-style-type: none"> <li>• Equipment setup</li> <li>• Relaxation period (10 min)</li> <li>• CRT on with standard settings (5 min)</li> <li>• Echocardiogram</li> <li>• CRT off (2 min)</li> <li>• Echocardiogram</li> <li>• CRT on with standard settings (2 min)</li> <li>• Removing equipment</li> </ul>

### Data acquisition equipment

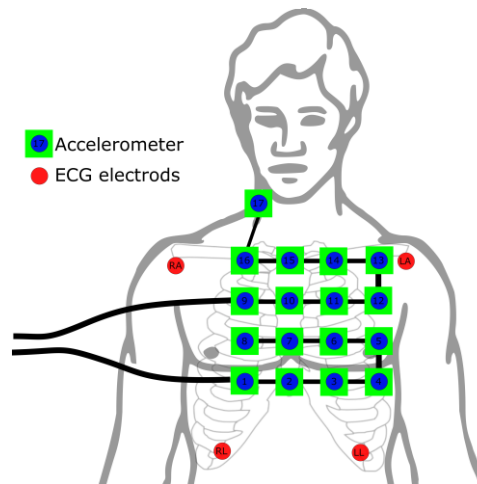
Central in the data acquisition tool is an acquisition setup based on the UMFT51AA (FTDI-chip). The acquisition tool is responsible for collecting measurements from the 17 accelerometers and the ECG signal from the ADS1298ECGFE-PDK (Texas Instrument). Further, it is responsible for ensuring that the signals are measured synchronously. The acquisition tool is connected to a PC running LabVIEW that is used for the data recording of the signals.



### The SCG sensors:

An ADXL355 from Analog Devices is used for acquiring the individual SCG signals. Each accelerometer is situated in an ABS plastic housing. Thereby the accelerometer is

shielded from any direct patient contact. The accelerometer is connected to a chain on the same wire and digital bus. Thereby the potential discomfort associated with multiple wires being connected to the subject is minimized. The accelerometers are powered by a 5 volt supply from the acquisition tool. The SCG sensors are attached to the skin using a double adhesive patch and shaving of the subject's chest hair might be necessary. Placement of the SCG sensors is done by projecting a map of the placement for consistency, and the SCG sensors are placed as illustrated. SCG sensors are placed as found common by the found literature.



#### ECG:

ECG is recorded using the ADS1298ECGFE-PDK (Texas Instrument) and for the CRT group ECG is also recorded simultaneously by the Echocardiograph. This is done to ensure synchronization between the modalities. All equivalent leads are connected to the same electrodes.

#### Echocardiograph:

The echocardiography is recorded using a Vivid E9 (GE Healthcare, Milwaukee) and is performed only for the CRT group.

#### Recordings

The mSCG and ECG are recorded continuously during the entire experiment.

The following echocardiography recordings will be obtained for the CRT group:

- Parasternal long-axis, 70 frames/s
- Parasternal long-axis with focus on the LVOT
- Parasternal short-axis at the level of the mitral valve, mid-ventricular and at the apex, 70 frames/s
- Apical 4, 2 and long-axis plus recordings of the same views including the left atrium
- Trans-mitral PW flow
- Annular PW TDI in the septal and lateral mitral annulus
- Aortic LVOT flow
- Five chamber LV in and out-flow by PW
- Apical 4, 2 and long-axis TDI > 160 frames/s

### Risks, side effects and disadvantages

There will be risks associated with manipulations of the biventricular pacemaker that could cause acute hemodynamic changes. The duration of which the pacemaker is turned off is too short for any clinical or symptomatic deterioration to occur even though acute hemodynamic changes can be observed. In addition, patients are carefully monitored by the Clinical Responsible with ECG and echocardiography and in the unlikely event that a significant deterioration is detected, the study protocol will be interrupted and standard pacing turned on.

Since no invasive procedures, no medications and no extensive physical activities will be conducted for the control group, we consider that there is no major risk or side effects for the control subjects. However, we will closely monitor the wellbeing of the subjects during the experiment and ask the subjects to report any side effects during and after the study. If any pathological conditions are recognized in the study, the subject will be encouraged to seek further medical consultation and the findings will be described orally and in text.

There is a minor risk that the subjects will experience skin irritation during and shortly after the experiment due to the way the accelerometers and electrodes are mounted to the subject. The accelerometers are electrically insulated by ABS housing to ensure patient safety. Being wired up too many wires could cause some psychological stress. However, by connecting most of these accelerometers in series the wire count and the potential psychological stress will be minimized.

### Statistics

Since this study is an explorative study where the primary point is to investigate which parameters would be useful for discriminating between healthy subjects, subjects undergoing CRT and subjects with their CRT turned off, we do not yet completely know which parameters to investigate. However, an example of these parameters could be the S1 heart sound energy, which has been investigated by a similar study (Jensen et al. 2014). This study used a similar population and approach with a single channel SCG. If it could be assumed that a change in energy would be similar with mSCG, the power calculations would be as follows:

### Power calculation

The number of subjects is based on the effect observed in (Jensen et al. 2014). This study was made at our department so we have the numbers for calculating the mean difference and standard deviation in the S1 energy. The study included 10 patients with a mean age of  $64 \pm 8.4$ .

For this study, we assume the same standard deviation and mean difference since the populations are similar in age and medical history. Mean difference was 6.19 dB and the standard deviation was 4.27 dB.

With a significance level of 0.05 and a power of 90%, 15 subjects are needed when using the following equation.

$$n = \frac{2\sigma^2(z_{1-\frac{\alpha}{2}} + z_{1-\beta})^2}{\Delta^2} = \frac{2 \cdot 2,47 \cdot (1,95996 + 1,281551)^2}{6,19} = 15$$

As a safety margin, we will include 20 subjects. We speculate that when comparing healthy subjects with subjects undergoing CRT the mean difference would be smaller and

therefor a ratio of 2 would be needed for achieving the same power. This would mean that a sample size of 30 subjects in the control group would be necessary.

#### **Ethical considerations**

As presented in the Risks section, we do not consider that the experiment contains a large risk for the subjects. Therefore, we consider the amount of time spent by the subjects reasonable compared to the benefits of the knowledge gained.

The subjects would not gain any direct benefit from participating in this experiment. However, knowledge gained through this research would potentially lead to an improved treatment process for the CRT group.

#### **Insurance**

The subjects are covered by the Danish Patient Compensation Association (Patient-erstatningen).

#### **Personal data**

Data will be stored after termination of the project. These data can only be used for the interpretation of this project and will therefore not be of interest to third party.

Data are stored in accordance with the stipulations in The Danish Personal Data Protection Act (Persondataloven) and other relevant Danish legislation.

The project is reported to The Danish Data Protection Agency through the Aalborg University umbrella agreement

#### **Information from medical charts**

To summon potential subjects for the CRT group, the clinical responsible doctor needs to validate that the potential subjects meet the inclusion criteria. Information accessed from the medical charts will not be stored within the project. This information includes: time of implantation, type of device implanted, and behaviour of implanted device.

#### **Project economy**

This project has been initialized by Samuel Emil Schmidt, Associate Professor, Medical Informatics Group, Department of Health Science and Technology, Aalborg University. The project is financed with DKK 4,500 by Aalborg University and with DKK 30,000 by a grant to Johannes Jan Struijk from Det Frie Forskningsråd, Forskningsråd for Teknologi og Produktion (FTP), project "Cardiac Excitation Contraction Coupling" (DFF no: 4184-00437).

Project participants Peter Søgaard, Johannes Struijk and Samuel Emil Schmidt are working together with AAU Innovation to commercialize seismocardiography.

#### **Compensation to subjects**

The subjects will not receive any compensation for their participation in the experiment.

#### **Publishing of results**

All results of the project will be published regardless of the outcome of the project.

**Time schedule**

The project is scheduled between 1 March 2017 and 1 March 2019.

**Guidelines for oral information and informed consent****Summoning potential subjects**

When potential subjects address the contact person, the following should be stated:

- That it is a request for participation in a scientific research project
- The purpose of the project
- That participation is voluntary and that the subject can withdraw from the project at any time without consequences
- That the potential subject has time to consider his/her participation before giving consent to participation in the project and that the potential subject is welcome to bring a family member or a friend to the information meeting. The potential volunteer will receive the leaflet "The Rights of a Trial Subject in a Health Scientific Research Project"/ "Forsøgspersonens rettigheder i et sundhedsvidenskabeligt forskningsprojekt" which includes information on confidentiality, right of access to documents and right to complain.
- That the material "Information for Participants"/"Deltagerinformation" will be forwarded by mail/e-mail to the potential subject in order for him/her to know more about the project before the information meeting.
- Finally, time for the information meeting is arranged

**The information meeting**

The information meeting is held in a quiet room where it is possible to have an uninterrupted conversation. Coffee/tea/soft drink may be served. The information meeting is held by the person responsible for the project or a senior researcher who has been authorized to do the information.

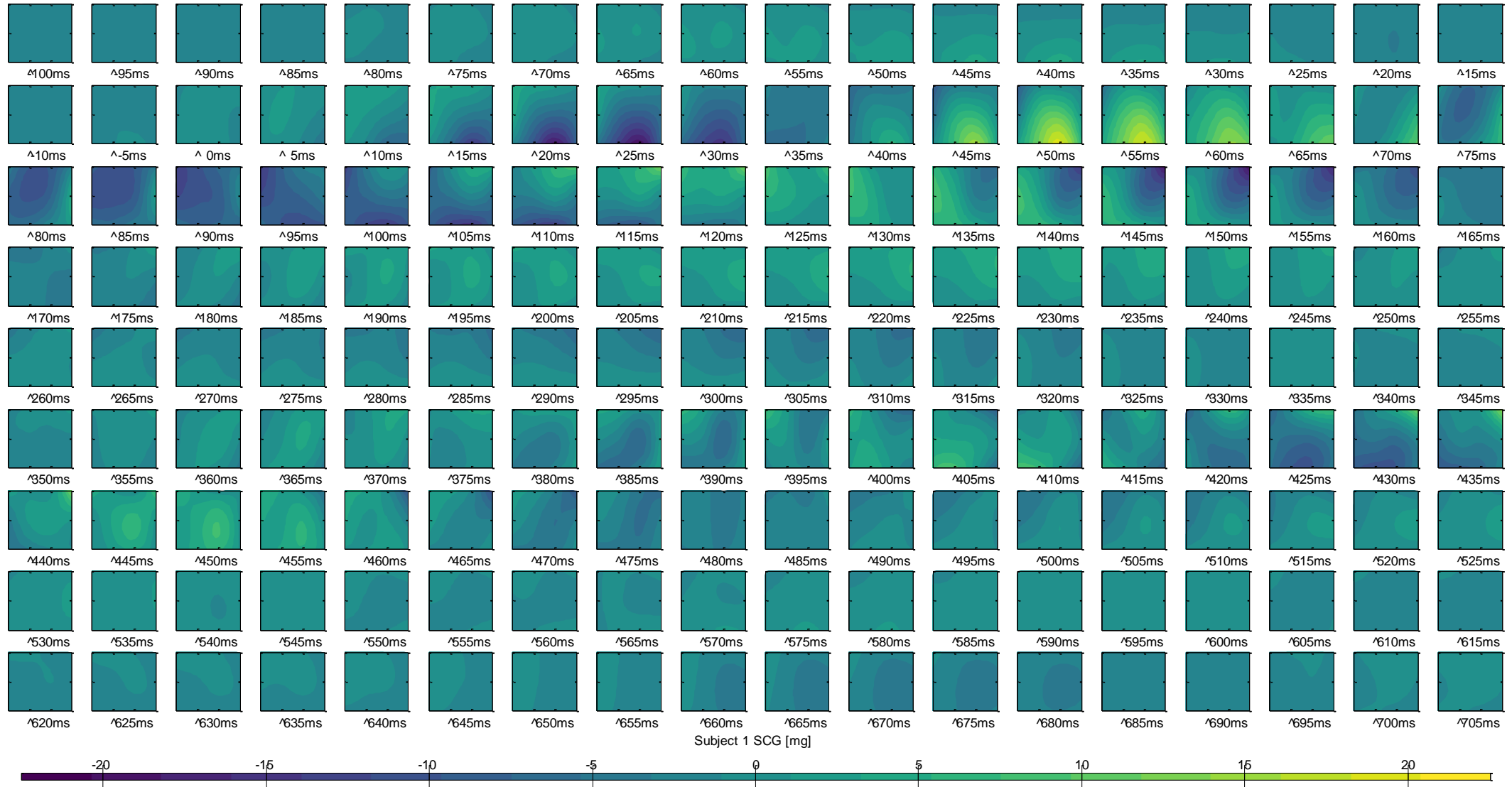
The meeting is to include the following information/questions:

- Participation is voluntary and the subject can withdraw from the project at any time without consequences
- The subject has time to consider his/her participation before giving consent to participation in the project, and the subject is welcome to bring a family member or a friend to the information meeting.
- The subject is asked whether he/she wants a family member/friend to be present at the meeting.
- The purpose of the experiment is presented, and it is explained how the experiment is performed. The "Information for Participants"/"Deltagerinformation", which has been sent to the potential subject in advance, is the starting point for the information meeting.
- The subject is asked if he/she is healthy or whether he/she has an infectious disease.
- The subject is asked whether he/she is a Danish citizen. If the answer is no, he/she is asked if he/she has a valid work permit.

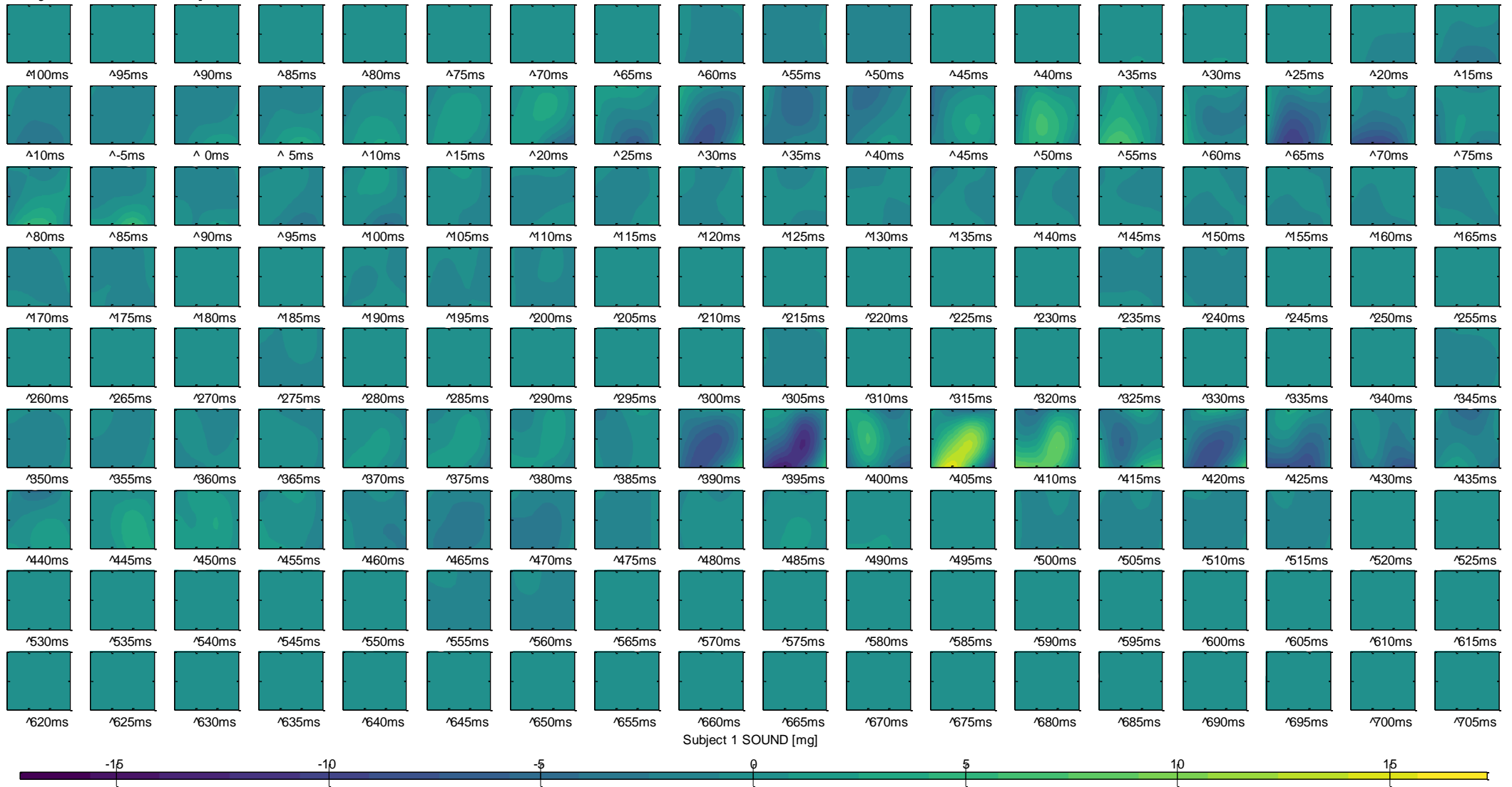
- The leaflet “The Rights of a Trial Subject in a Health Scientific Research Project”/ “Forsøgspersonens rettigheder i et sundhedsvidenskabeligt forskningsprojekt” is handed over. It is explained that it includes information on confidentiality, right of access to documents and right to complain.
- The subject is asked whether he/she has read “Information for Participants”/ “Deltagerinformation”. If this is not the case, we will ask the subject to read it.
- When it has been ensured that the subject has read the “Information for Participants”/“Deltagerinformation”, he/she is asked whether he/she has questions about the experiment.
- After this a demonstration is given in the lab; measuring equipment and its use is presented to the subject.
- It is underlined that participation is voluntary, and that the subject has time to consider his/her participation (please note that The National Committee on Health Research Ethics recommends 24 hours of deliberation time)
- Again it is underlined that participation is voluntary and that the subject can withdraw his/her consent at any time without consequences.
- The subject is informed that if he/she does not need time to consider the participation, the consent can be given at the information meeting.
- Time/place for the experiment is agreed.
- Finally, information about the contact person of the experiment is given (it is shown to the subject that the name and contact details appear from the “Information for Participants”/“Deltagerinformation”) and it is informed that this person can be contacted at any time if further questions should arise.

# Appendix D. Addition result illustrations

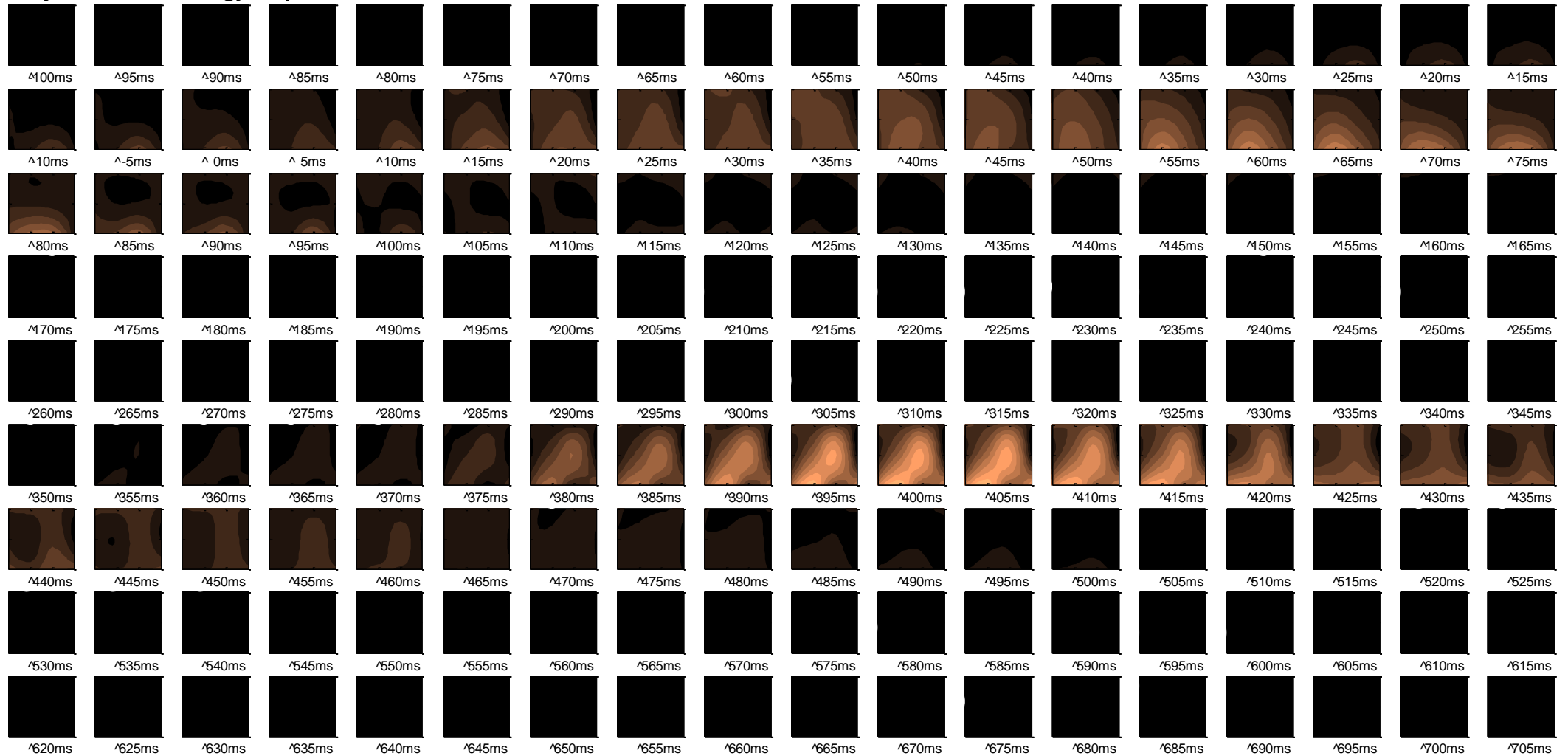
## Subject 1 mSCG maps



Subject 1 sound maps



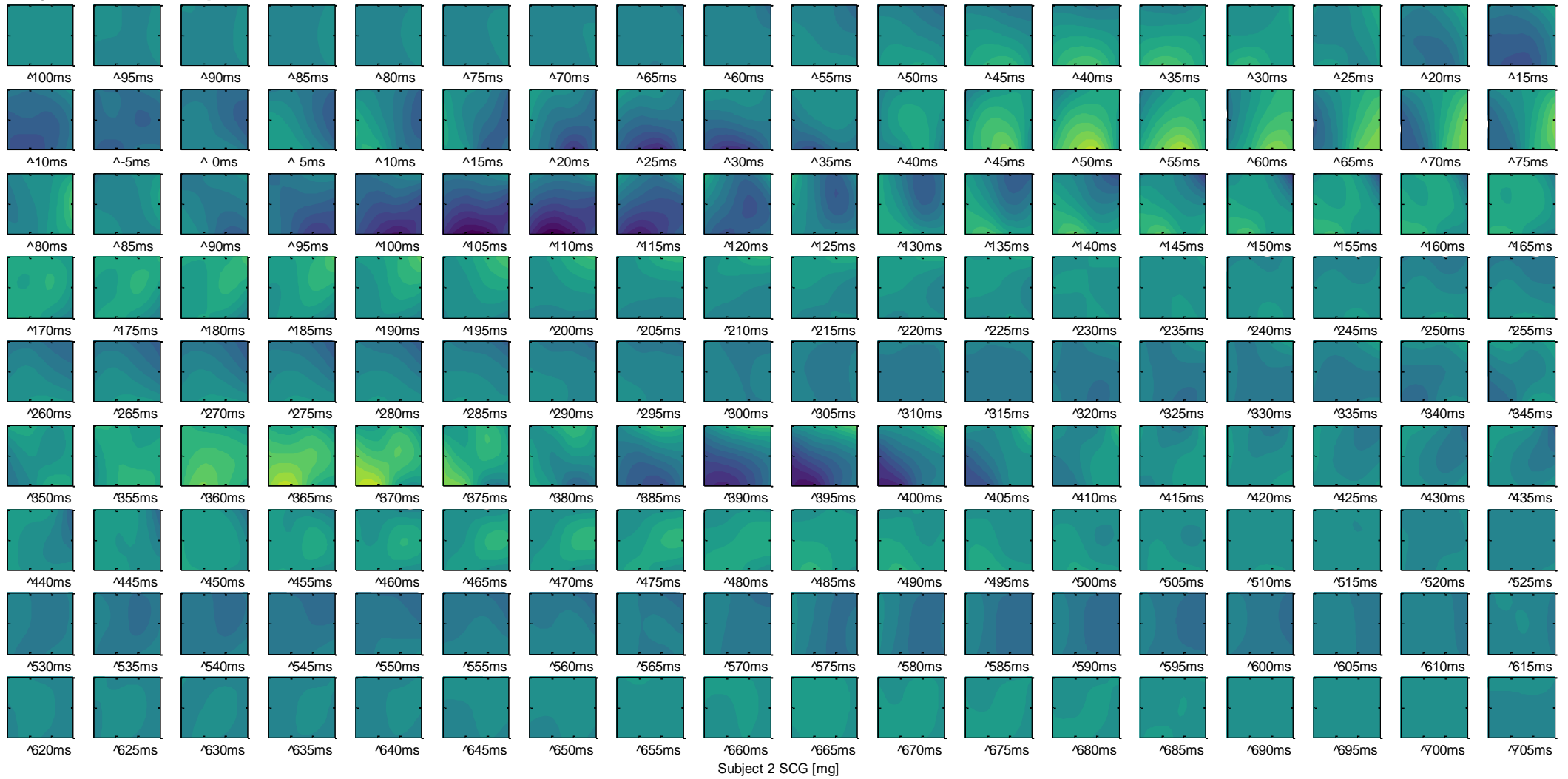
Subject 1 sound energy maps



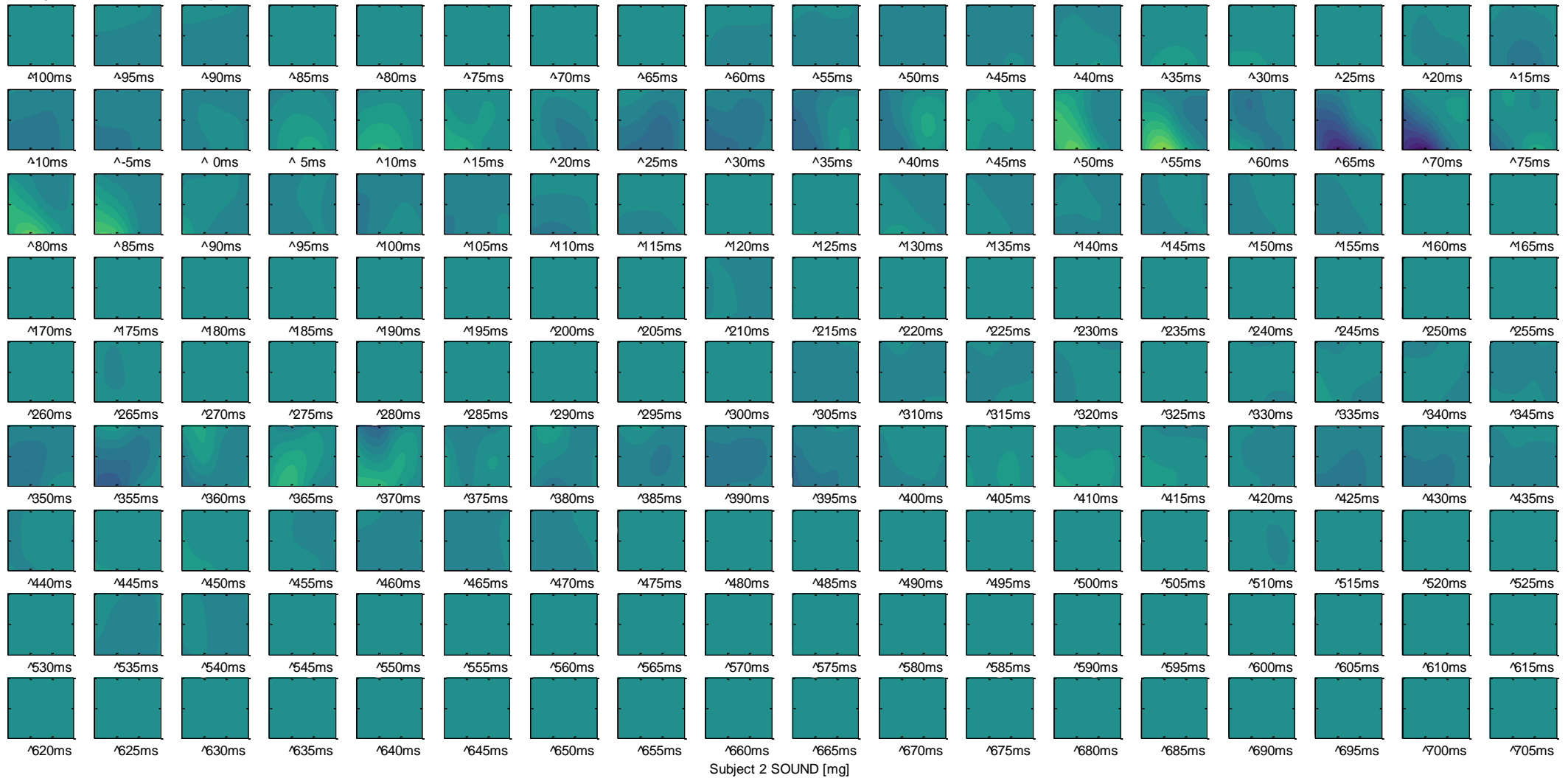
Subject 1 ENERGY [mg]



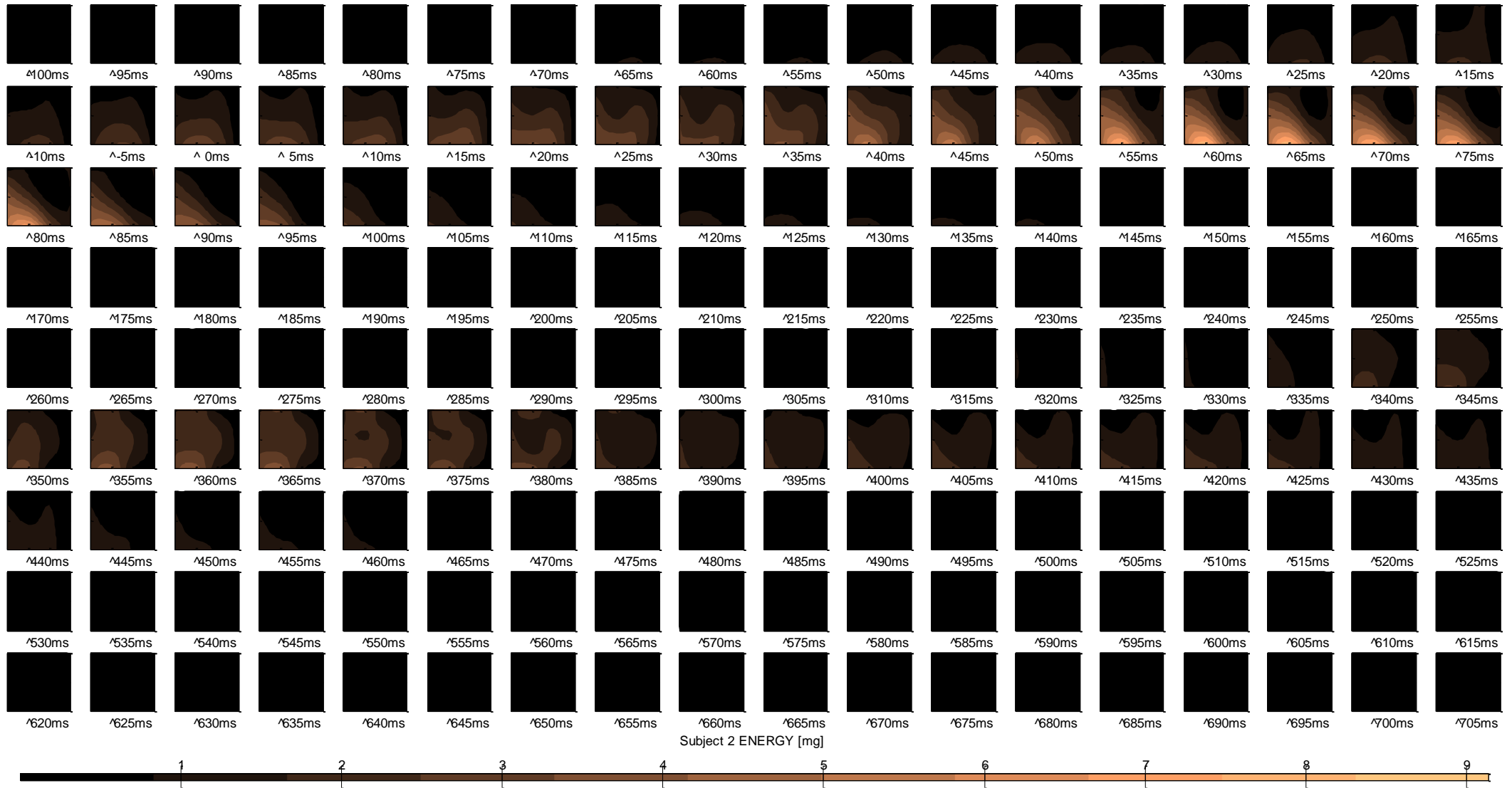
Subject 2 mSCG maps



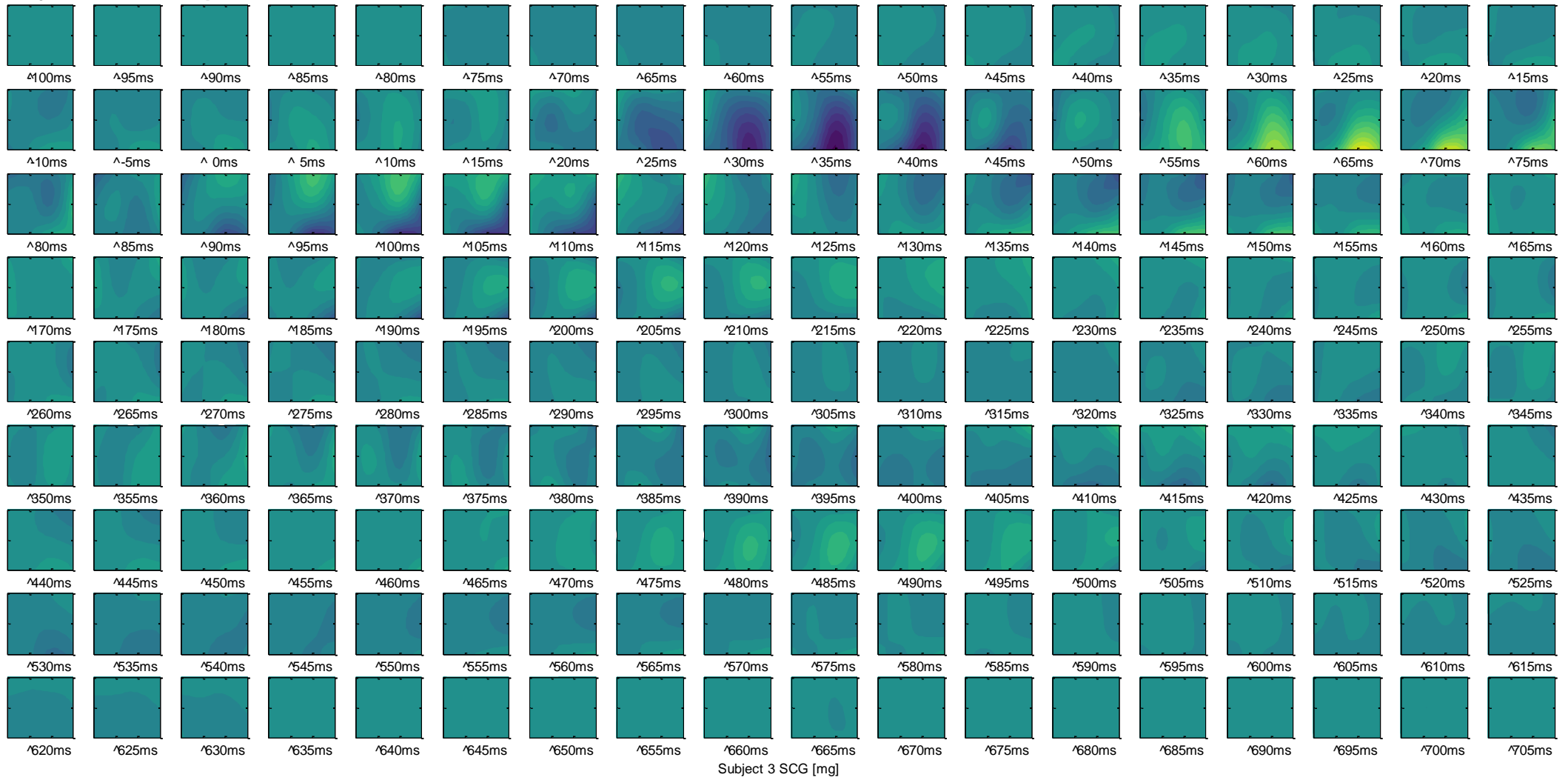
Subject 2 sound maps



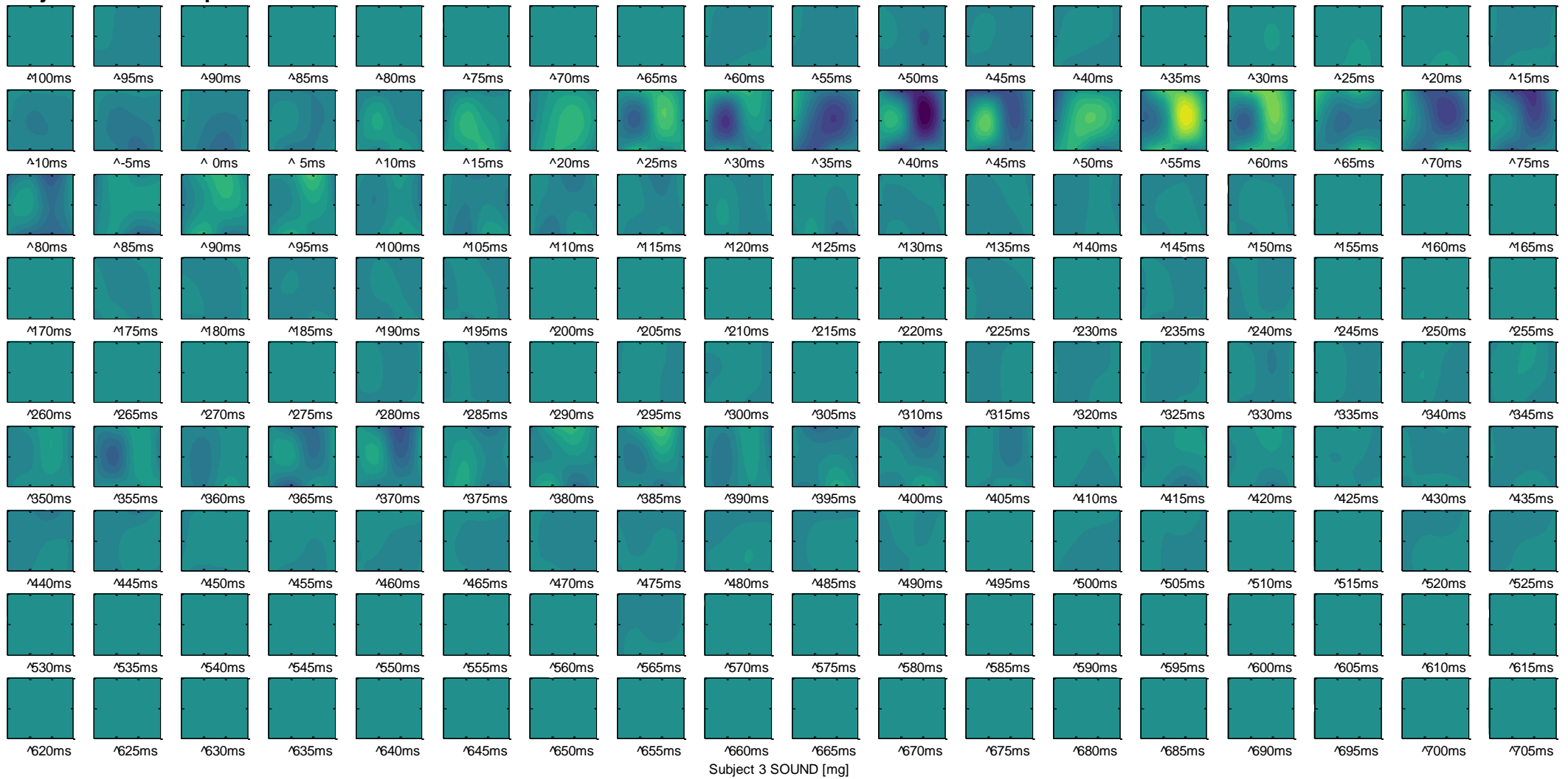
Subject 2 sound energy maps



Subject 3 mSCG maps



Subject 3 sound maps



Subject 3 sound energy maps

